Astronomy & Astrophysics manuscript no. alvesbrito13jan10
January 14, 2010

Chemical similarities between Galactic bulge and local thick disk red giants: O, Na, Mg, Al, Si, Ca and Ti

A. Alves-Brito[1,2], J. Meléndez[3], M. Asplund[4], I. Ramírez[4], and D. Yong[5]

[1] Universidade de São Paulo, IAG, Rua do Matão 1226, Cidade Universitária, São Paulo 05508-900, Brazil; e-mail: `abrito@astro.iag.usp.br`
[2] Centre for Astrophysics and Supercomputing, Swinburne University of Technology, Hawthorn, Victoria 3122, Australia
[3] Centro de Astrofísica da Universidade do Porto, Rua das Estrelas, 4150-762 Porto, Portugal; e-mail: `jorge@astro.up.pt`
[4] Max Planck Institut für Astrophysik, Postfach 1317, 85741 Garching, Germany
[5] Research School of Astronomy and Astrophysics, The Australian National University, Cotter Road, Weston, ACT 2611, Australia

Received: ; accepted:

ABSTRACT

Context. The formation and evolution of the Galactic bulge and its relationship with the other Galactic populations is still poorly understood.

Aims. To establish the chemical differences and similarities between the bulge and other stellar populations, we performed an elemental abundance analysis of α- (O, Mg, Si, Ca, and Ti) and Z-odd (Na and Al) elements of red giant stars in the bulge as well as of local thin disk, thick disk and halo giants.

Methods. We use high-resolution optical spectra of 25 bulge giants in Baade's window and 55 comparison giants (4 halo, 29 thin disk and 22 thick disk giants) in the solar neighborhood. All stars have similar stellar parameters but cover a broad range in metallicity ($-1.5 <$ [Fe/H] $< +0.5$). A standard 1D local thermodynamic equilibrium analysis using both Kurucz and MARCS models yielded the abundances of O, Na, Mg, Al, Si, Ca, Ti and Fe. Our homogeneous and differential analysis of the Galactic stellar populations ensured that systematic errors were minimized.

Results. We confirm the well-established differences for [α/Fe] at a given metallicity between the local thin and thick disks. For all the elements investigated, we find no chemical distinction between the bulge and the local thick disk, in agreement with our previous study of C, N and O but in contrast to other groups relying on literature values for nearby disk dwarf stars. For $-1.5 <$ [Fe/H] < -0.3 exactly the same trend is followed by both the bulge and thick disk stars, with a star-to-star scatter of only 0.03 dex. Furthermore, both populations share the location of the knee in the [α/Fe] vs [Fe/H] diagram. It still remains to be confirmed that the local thick disk extends to super-solar metallicities as is the case for the bulge. These are the most stringent constraints to date on the chemical similarity of these stellar populations.

Conclusions. Our findings suggest that the bulge and local thick disk stars experienced similar formation timescales, star formation rates and initial mass functions, confirming thus the main outcomes of our previous homogeneous analysis of [O/Fe] from infrared spectra for nearly the same sample. The identical α-enhancements of thick disk and bulge stars may reflect a rapid chemical evolution taking place before the bulge and thick disk structures we see today were formed, or it may reflect Galactic orbital migration of inner disk/bulge stars resulting in stars in the solar neighborhood with thick-disk kinematics.

Key words. Stars: abundances – Galaxy: abundances – Galaxy: bulge – Galaxy: disk – Galaxy: evolution

1. Introduction

The Galactic bulge is the least understood stellar population in the Milky Way, as even its classification (classical or pseudo-bulge; Kormendy & Kennicutt 2004) seems unclear. The Galactic bulge has signatures of an old (Ortolani et al. 1995; Zoccali et al. 2003) classical bulge formed rapidly during intensive star formation as reflected in the enhancement of α-elements (e.g. McWilliam & Rich 1994; Cunha & Smith 2006; Zoccali et al. 2006; Lecureur et al. 2007; Fulbright et al. 2007; Meléndez et al. 2008; Ryde et al. 2009a,b). On the other hand its boxy shape is consistent with a pseudo-bulge indicative of formation by secular evolution through dynamical instability of an already established inner disk.

Recently, Elmegreen et al. (2008) have shown that bulges formed by coalescence of giant clumps can have properties of both classical and pseudo-bulges, because secular evolution can take place in a very short timescale (< 1 Gyr). They suggest that our Galactic bulge (and many $z \sim 2$ early disk galaxies; Genzel et al. 2008) formed this way, and that the bulge and thick disk may have formed at the same time. Thus, the nature of our Galactic bulge can be unveiled by detailed chemical composition analysis and by careful comparisons with the thick disk.

Although all recent works agree in enhancements of the α-elements relative to solar abundances in bulge field K giants, the level of enhancement is currently under debate. Based on a comparison of bulge giant stars with thick disk dwarf stars, Zoccali et al. (2006), Lecureur et al. (2007) and Fulbright et al. (2007) suggested that the bulge and the thick disk have different chemical composition patterns, and that the α-elements are overabundant in the bulge compared with the thick disk. Therefore, they argued for a shorter formation timescale and higher star formation rate for the Galactic bulge than that for the thick disk. Ballero et al. (2007) also concluded that the initial mass functions must have been different between the two populations based on both the high [Mg/Fe] and metallicity distribution of the bulge (see also Cescutti et al. 2009). Nevertheless, those comparisons should be

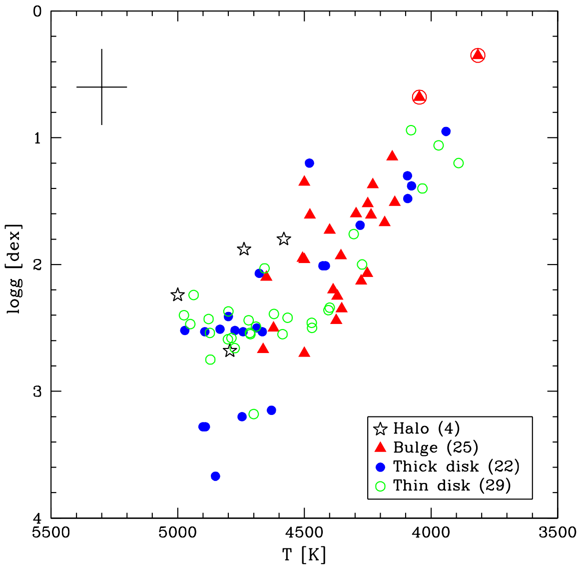

Fig. 1. H-R diagram showing our program stars. The symbols are described in the plot. The two most luminous stars (filled triangles enclosed by circles) are bulge giants which show abundance anomalies like O-deficiency and Na-enhancement similar to those observed in some globular cluster stars. A typical error bar in $T_{\rm eff}$ and $\log g$ is shown.

taken with care as systematic errors may be present due to the very different stellar parameters, model atmospheres, and NLTE effects of dwarf and giant stars. Indeed, in our consistent analysis of high resolution infrared spectra of both bulge and thick disk giants with similar stellar parameters (Meléndez et al. 2008), we have shown that the bulge is in fact chemically very similar to the thick disk in [C/Fe], [N/Fe] and [O/Fe]. Here, we extend this work to other α-elements (Mg, Si, Ti, Ca), and show that all the α-elements in bulge and local thick disk giants have essentially identical chemical abundance patterns.

2. Observations

The sample consists of 80 cool giant stars (Fig. 1) with effective temperatures $3800 \leq T_{\rm eff} \leq 5000$ K, surface gravities $0.5 \leq \log g \leq 3.5$, and metallicities $-1.5 <$[Fe/H]$< +0.5$. Similar number of thin disk (29), thick disk (22) and bulge (25) giants were selected, and a few (4) metal-rich halo giants were also included.

All of our bulge giants are located in Baade's window and are taken from Fulbright et al. (2006), who have cleaned the sample from nonbulge giants. For these bulge stars, we have already published an abundance analysis of C, N, O and Fe based on IR spectra (Meléndez et al. 2008). For the present study we make use of the equivalent widths measured in optical spectra using the HIRES spectrograph (at R = 45,000 or 67,000) on the Keck-I 10 m telescope by Fulbright et al. (2006, 2007).

To enable a proper comparison we have compiled a sample of thin disk, thick disk and halo stars for which we have obtained our own optical spectra. The assignment of population membership was based on UVW velocities (Bensby et al. 2004; Reddy et al. 2006). The sample selection was based on evaluating population membership in more than 1500 giant stars from the literature, in particular an updated version of the Cayrel de Strobel (2001) catalog (see Ramírez & Meléndez 2005a), the analysis of ∼180 clump giants by Mishenina et al. (2006), the study of ∼300 nearby giants by Luck & Heiter (2007), the survey of ∼380 giants by Hekker & Meléndez (2007), and the analysis of ∼320 giants by Takeda et al. (2008). Furthermore, the UVES library of stellar spectra (Bagnulo et al. 2003) was searched for suitable disk and halo giants.

Our analysis of thin disk, thick disk and halo stars is based mostly on high-resolution (R= 65,000) optical spectra taken in April 2007 with the MIKE spectrograph (Bernstein et al. 2003) on the Clay 6.5 m Magellan telescope, and complemented with observations using the 2dcoudé spectrograph (Tull et al. 1995, R = 60,000) on the 2.7 m Harlan J. Smith telescope at McDonald Observatory, the upgraded HIRES spectrograph (Vogt et al. 1994, R = 100,000) on the Keck I 10 m telescope, the UVES library[1] (Bagnulo et al. 2003, R = 80,000), and the ELODIE archive[2] (Moultaka et al. 2004, R = 42,000). The magnitudes, population membership and instrumentation used for the disk/halo sample are shown in Table 1.

The data were reduced with IRAF employing standard procedures: correction for bias, flat field, cosmic rays and background light, then optimal extraction of the spectra (using a bright star to trace the orders), wavelength calibration, barycentric and Doppler correction, and continuum normalization. In some cases, as described below, a variation to the reduction procedure was necessary. The tilt of the lines in the MIKE data is severe and varies across the CCD (e.g. Yong et al. 2006), therefore it must be carefully corrected to avoid degradation of the spectral resolution. The tilt was corrected using MTOOLS[3], specifically developed by J. Baldwin to account for the tilted slits in MIKE spectra. On the other hand, our HIRES spectra were extracted using a new version of MAKEE[4], an optimal extraction package developed by T. Barlow specifically for data reduction of the improved HIRES spectrograph. MAKEE also performs an automatic wavelength calibration cross-correlating the extracted ThAr spectra with a database of wavelength calibration solutions. Both the UVES and ELODIE archive data were already extracted and wavelength calibrated. The extracted spectra were shifted to the rest frame and continuum normalized using IRAF. The signal-to-noise ratio (S/N) per pixel of the reduced spectra ranges from $S/N \sim 45-100$ for the bulge giants (Fulbright et al. 2006), whereas for the disk and halo giants the S/N is typically ∼200 per pixel, ranging from ∼150 (2dCoude/McDonald) to ∼200 (MIKE/Magellan, ELODIE/OHP) to ∼250 (HIRES/Keck, UVES/VLT), as estimated from relatively line-free regions of the spectra.

3. Abundance Analysis

We have homogeneously performed all the equivalent width (EW) measurements for the disk and halo sample. In order to check that the EW measurements of the bulge giants by Fulbright et al. (2006, 2007) are consistent with our system for the disk and halo giants, we have observed one bulge star (IV-203) with the MIKE spectrograph and compared the EW measured by us with those obtained by Fulbright et al. (2006, 2007). The agreement is satisfactory, with a mean difference (This work - Fulbright et al. 2006, 2007) of −2.0 mÅ and a line-to-line scat-

---

[1] http://www.sc.eso.org/santiago/uvespop/

[2] http://atlas.obs-hp.fr/elodie/

[3] http://www.lco.cl/telescopes-information/magellan/instruments-1/mike/IRAF_tools/iraf-mtools-package/

[4] http://www2.keck.hawaii.edu/inst/hires/hires.html

Table 1. Program stars data

Star (1)	V [mag] (2)	P^* [%] (3)	Instrument (4)
Halo			
HD041667	8.533	00:01:99	MIKE/Magellan
HD078050	7.676	00:00:100	ELODIE/OHP
HD114095	8.353	00:29:71	MIKE/Magellan
HD210295	9.566	00:00:100	HIRES/Keck
Thick Disk			
HD023940	5.541	03:96:01	2dcoude/McDonald
HD032440	5.459	08:91:01	MIKE/Magellan
HD037763	5.178	15:84:01	MIKE/Magellan
HD040409	4.645	25:74:01	MIKE/Magellan
HD077236	7.499	00:58:42	MIKE/Magellan
HD077729	7.630	25:74:01	MIKE/Magellan
HD080811	8.35	00:97:03	MIKE/Magellan
HD083212	8.335	00:94:06	2dcoude/McDonald
HD099978	8.653	00:99:01	MIKE/Magellan
HD107328	4.967	43:57:01	2dcoude/McDonald
HD107773	6.355	20:78:02	MIKE/Magellan
HD119971	5.454	14:85:01	MIKE/Magellan
HD124897	-0.049	13:85:01	MIKE/Magellan
HD127243	5.590	00:96:04	ELODIE/OHP
HD130952	4.943	01:98:01	MIKE/Magellan
HD136014	6.195	24:75:01	MIKE/Magellan
HD145148	5.954	11:88:01	MIKE/Magellan
HD148451	6.564	00:64:36	UVES/VLT
HD180928	6.088	00:74:26	MIKE/Magellan
HD203344	5.570	00:97:02	ELODIE/OHP
HD219615	3.694	29:70:01	ELODIE/OHP
HD221345	5.220	14:85:01	ELODIE/OHP
Thin Disk			
HD000787	5.255	98:02:00	2dcoude/McDonald
HD003546	4.361	78:22:00	ELODIE/OHP
HD005268	6.163	86:14:00	HIRES/Keck
HD029139	0.868	98:02:00	ELODIE/OHP
HD029503	3.861	96:04:00	2dcoude/McDonald
HD030608	6.362	49:51:00	2dcoude/McDonald
HD045415	5.543	99:01:00	UVES/VLT
HD050778	4.065	87:13:00	2dcoude/McDonald
HD073017	5.673	86:14:00	ELODIE/OHP
HD099648	4.952	99:01:00	MIKE/Magellan
HD100920	4.301	99:01:00	MIKE/Magellan
HD115478	5.333	99:01:00	MIKE/Magellan
HD116976	4.753	99:01:00	MIKE/Magellan
HD117220	9.010	95:05:00	MIKE/Magellan
HD117818	5.205	99:01:00	MIKE/Magellan
HD128188	10.003	98:02:00	MIKE/Magellan
HD132345	5.838	97:03:00	MIKE/Magellan
HD142948	8.024	94:06:00	MIKE/Magellan
HD171496	8.501	98:02:00	2dcoude/McDonald
HD172223	6.485	91:09:00	MIKE/Magellan
HD174116	5.24	98:02:00	2dcoude/McDonald
HD175219	5.355	99:01:00	MIKE/Magellan
HD186378	7.21	97:03:00	2dcoude/McDonald
HD187195	6.022	99:01:00	MIKE/Magellan
HD211075	8.190	99:01:00	HIRES/Keck
HD212320	5.938	99:01:00	UVES/VLT
HD214376	5.036	99:01:00	HIRES/Keck
HD215030	5.92	98:02:00	ELODIE/OHP
HD221148	6.252	93:07:00	HIRES/Keck

Notes.— (*): The membership probabilities of the thin disk, thick disk and halo giants are given as thin:thick:halo.

Table 2. Sensitivities in the abundance ratios by employing the Kurucz models (Castelli et al. 1997). The atmospheric parameters and α-enhancement were changed by $\Delta T_{\rm eff} = \pm 75\,$K, $\Delta \log g = \pm 0.30\,$dex, $\Delta v_{\rm t} = \pm 0.20\,$km s^{-1}, and $\Delta[\alpha/{\rm Fe}] = \pm 0.10\,$dex. The total internal uncertainties are given in the last column

Abundance (1)	$\Delta T_{\rm eff}$ (2)	$\Delta \log g$ (3)	$\Delta v_{\rm t}$ (4)	$\Delta[\alpha/{\rm Fe}]$ (5)	$(\sum x^2)^{1/2}$ (6)
HD078050					
[FeI/H]	-0.09	0.01	0.07	0.00	0.11
[FeII/H]	0.02	-0.12	0.06	-0.02	0.14
[O/Fe]	-0.01	-0.13	0.00	-0.02	0.13
[Na/Fe]	-0.06	0.01	0.01	0.00	0.06
[Mg/Fe]	-0.06	0.05	0.04	0.00	0.09
[Al/Fe]	-0.06	0.00	0.00	0.00	0.06
[Si/Fe]	-0.03	-0.03	0.01	0.00	0.04
[Ca/Fe]	-0.08	0.02	0.06	0.00	0.10
[Ti/Fe]	-0.11	0.01	0.06	0.01	0.13
IV203					
[FeI/H]	0.01	-0.07	0.06	-0.01	0.09
[FeII/H]	0.18	-0.18	0.04	-0.02	0.26
[O/Fe]	-0.01	-0.11	0.01	-0.02	0.11
[Na/Fe]	-0.08	0.04	0.05	0.01	0.10
[Mg/Fe]	0.01	-0.04	0.03	-0.01	0.05
[Al/Fe]	-0.06	0.02	0.03	0.01	0.07
[Si/Fe]	0.11	-0.09	0.03	-0.01	0.14
[Ca/Fe]	-0.09	0.02	0.09	0.01	0.13
[Ti/Fe]	-0.14	0.00	0.03	0.00	0.14
HD083212					
[FeI/H]	-0.09	-0.01	0.04	0.00	0.09
[FeII/H]	0.05	-0.12	0.05	-0.02	0.14
[O/Fe]	0.00	-0.13	0.01	-0.02	0.13
[Na/Fe]	-0.07	0.01	0.01	0.00	0.07
[Mg/Fe]	-0.07	0.05	0.05	0.00	0.09
[Si/Fe]	-0.01	-0.04	0.00	-0.01	0.04
[Ca/Fe]	-0.09	0.02	0.05	0.01	0.10
[Ti/Fe]	-0.16	0.00	0.07	0.02	0.17
HD045415					
[FeI/H]	-0.04	-0.02	0.09	-0.01	0.10
[FeII/H]	0.08	-0.14	0.08	-0.03	0.18
[O/Fe]	0.00	-0.14	0.00	-0.03	0.14
[Na/Fe]	-0.06	0.08	0.05	0.00	0.11
[Mg/Fe]	-0.02	0.02	0.03	-0.01	0.04
[Al/Fe]	-0.05	0.02	0.04	0.01	0.07
[Si/Fe]	0.03	-0.05	0.03	-0.02	0.07
[Ca/Fe]	-0.08	0.04	0.10	0.00	0.13
[Ti/Fe]	-0.11	-0.01	0.01	0.00	0.11

ter of $\sigma_{\rm QD}$[5] = 5.5 mÅ (Fig. 2a). Additionally, A. McWilliam has kindly made available to us the HIRES/Keck spectrum of another bulge giant (I-322) for comparison purposes. Again, the agreement is good with a difference (This work - Fulbright et al. 2006, 2007) of +2.2 mÅ and $\sigma_{\rm QD}$ = 5.5 mÅ (Fig. 2b). Since most of the employed lines are relatively strong, the typical impact on

---

[5] we use here a robust standard deviation based on the quartile deviation QD (=Q3-Q1), $\sigma_{\rm QD}$ = QD/1.349; see for example Abu-Shawiesh et al. (2009)

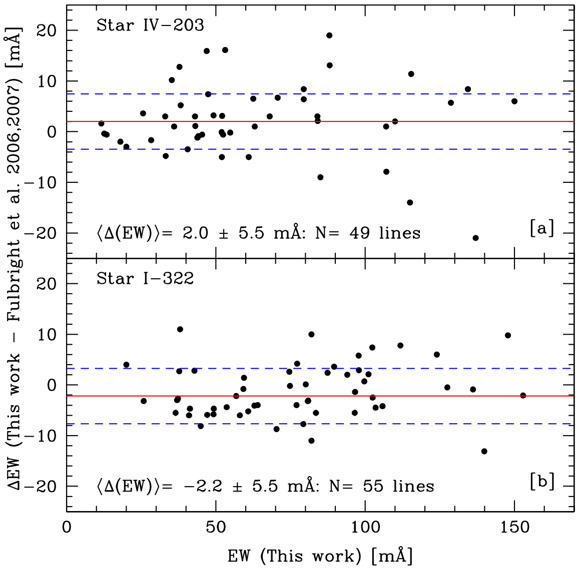

Fig. 2. Comparison of our equivalent width measurements with lines in common with Fulbright et al. (2006, 2007) for two bulge giant stars: (a) IV-203 and (b) I-322. The median (solid lines) and a robust proxy of standard deviation ($\sigma_{\rm QD}$; dashed lines) are also displayed.

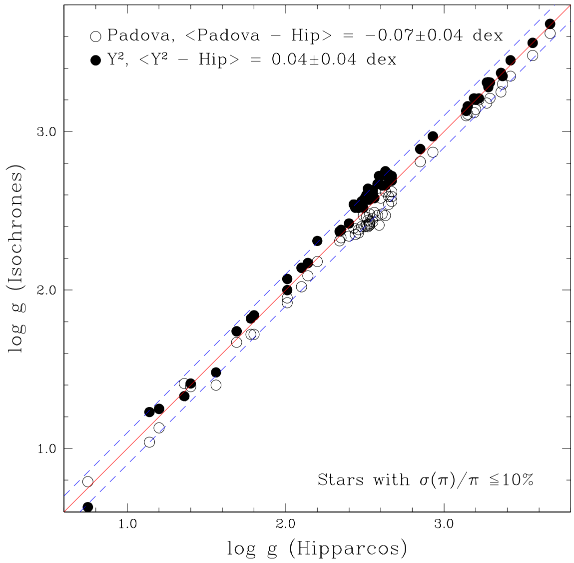

Fig. 3. Comparison between evolutionary gravities from Y^2 (filled circles) and Padova (open circles) isochrones, and trigonometric gravities for giant stars with good ($\sigma(\pi)/\pi \leq 10\%$) Hipparcos parallaxes. The solid and dashed lines depict perfect agreement and variations of ±0.1 dex, respectively.

abundances from these EW differences is negligible. Thus, the analysis of the faint bulge giants, the bright disk and the halo giants, is essentially in the same system.

Photometric temperatures were obtained using optical and infrared colors and the infrared flux method $T_{\rm eff}$-scale of Ramírez & Meléndez (2005b). We note that the new improved IRFM calibration of Casagrande et al. (2010) only applies to dwarf and subgiant stars and thus cannot be applied to our sample of giants. However, we do not expect any significant differences with respect to Ramírez & Meléndez (2005b) for the relevant stellar parameters, except perhaps for a small (~1%) zero-point offset in the $T_{\rm eff}$ scale, which is irrelevant here since we are performing a differential study.

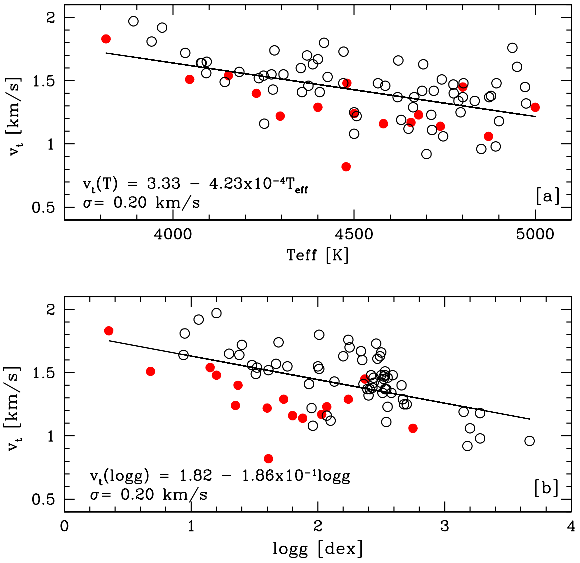

Fig. 4. Microturbulent velocity as a function of effective temperature (*upper panel*) and log *g* (*lower panel*). Giant stars with [Fe/H] < –0.70 and [Fe/H] ≥ –0.70 are, respectively, represented by *filled* and *open* circles. The solid line is a linear least squares fit to the data, whose results are labeled in the figure.

Reddening for the bulge stars was estimated from extinction maps (Stanek 1996), while for the comparison sample both extinction maps (Meléndez et al. 2006b) and Na I D ISM absorption lines were used. The E(B-V) values based on the D lines were obtained as follows. In the optical thin case the relation between column density N (units cm^{-2}) and equivalent width EW (units mÅ) is:

$$N = 1.13 \times 10^{17} EW/(f\,\lambda^2), \qquad (1)$$

(Spitzer 1968). The f values are 0.64 and 0.32, respectively, for the 5889.950 and 5895.924 Å lines (NIST database[6]). Note that the above relation between N(Na I) and equivalent width holds only for lines on the linear part of the curve of growth, i.e., for small values of E(B-V); for reddening larger than a few 0.01 mag the interstellar lines must be modeled in detail (e.g. Welty et al. 1994) to avoid underestimation of the column densities. In particular we use the profile fitting program FITS6P (Welty et al. 1994).

The N(Na I) density was transformed to N(H) using the relation found by Ferlet et al. (1985):

$$\log N(\mathrm{HI} + \mathrm{H}_2) = (\log N(\mathrm{NaI}) + 9.09)/1.04, \qquad (2)$$

where both N(Na I) and N(H) are in cm^{-2}. Finally, E(B-V) was computed from the total hydrogen density (Bohlin et al. 1978):

$$E(B-V) = N(\mathrm{HI} + \mathrm{H}_2)/5.8 \times 10^{21}, \qquad (3)$$

where N(H) is in cm^{-2} and E(B-V) in magnitudes. Although this relation seems not well established for E(B-V)<0.1, Ramirez et

---

[6] http://physics.nist.gov/PhysRefData/ASD/lines_form.html

al. (2006) have shown it to be very accurate for a E(B-V)=0.01 star.

Albeit not used in the present work, we should mention for completeness that in addition to reddening maps and Na D interstellar lines, E(B-V) can also be estimated from other interstellar features such as the diffuse interstellar band at 862 nm (Munari et al. 2008), as well as multicolor photometry (e.g. Sect. 4.2 of Meléndez et al. 2006b; Ramírez et al. 2006) and polarization (e.g. Fosalba et al. 2002).

The stellar surface gravities were derived from improved Hipparcos parallaxes (van Leeuwen 2007) for the sample of nearby giant stars and assuming a distance of 8 kpc for the bulge giants. In addition, Yonsei-Yale (Y^2; Demarque et al. 2004) and Padova isochrones (da Silva et al. 2006) were employed to determine evolutionary gravities, as well as the input masses that were adopted for the trigonometric gravities. In order to estimate the Y^2 gravities, we generated a fine grid of isochrones, assuming $[\alpha/\mathrm{Fe}] = 0$ and $+0.3$ for $[\mathrm{Fe/H}] > 0$ and $[\mathrm{Fe/H}] < -1$, respectively, and linearly interpolated in between. All solutions allowed by the error bars were searched for, adopting as final result the median values. The Padova gravities were obtained using the Bayesian tool PARAM[7]. As shown in Fig. 3, both (Y^2, Padova) evolutionary gravities are in excellent agreement with the trigonometric gravities of our nearby giants with reliable (uncertainties ≤10%) Hipparcos parallaxes. The evolutionary $\log g$ values required small zero-point corrections of -0.04 (Y^2) and $+0.07$ dex (Padova), to be on the same scale as the Hipparcos-based results for our sample giant stars (Fig. 3). Bolometric corrections from Alonso et al. (1999) were adopted.

We use iron lines to check our $T_{\rm eff}$ and log g, but we do not assume a priori that our adopted effective temperatures, surface gravities, 1D model atmospheres, gf-values, selection of lines, equivalent width measurements and LTE line formation, would result in *absolute* excitation (zero slope of Fe I abundances vs. excitation potential) and ionization ($A_{FeI} = A_{FeII}$) equilibria. We use the nearby disk/halo giants to determine the slopes ($d(A_{FeI})/d(\chi_{exc})$) and differences between Fe I and Fe II, followed by most stars. Our tests of the ionization and excitation balances of Fe I and Fe II lines revealed that most of the sample giants (58 stars) satisfy our *relative* spectroscopic equilibrium of iron lines within the uncertainties, therefore the overall agreement is encouraging. Nevertheless, the photometric stellar parameters of 22 stars (8 thin disk, 5 thick disk, 1 halo, and 8 bulge stars) required some adjustments to be on our *relative* spectroscopic equilibrium scale. The corrections based on the trend followed by the bright disk/halo giants, for which the photometric stellar parameters (and stellar spectra) were more reliable than for the bulge sample, is:

$$d(A_{FeI})/d(\chi_{exc}) = 0.008\,\mathrm{dex\,eV^{-1}}\ \text{(Kurucz overshooting)}, \quad (4)$$

$$d(A_{FeI})/d(\chi_{exc}) = 0.003\,\mathrm{dex\,eV^{-1}}\ \text{(MARCS)}, \quad (5)$$

stars within 2-σ ($\sigma = 0.011$ dex eV^{-1}) were considered to fulfill our *relative* excitation equilibrium. Ionization balance was achieved if

$$A(\mathrm{Fe\,II}) - A(\mathrm{Fe\,I}) = 0.08\,\mathrm{dex}\ \text{(Kurucz overshooting)}, \quad (6)$$

$$A(\mathrm{Fe\,II}) - A(\mathrm{Fe\,I}) = 0.00\,\mathrm{dex}\ \text{(MARCS)}, \quad (7)$$

and stars within ±0.07 dex were considered to fulfill our *relative* ionization equilibrium. After these corrections were performed the deviating thin disk, thick disk, halo and bulge stars, have stellar parameters in the same system, i.e. in the Ramírez & Meléndez (2005b) temperature scale and $\log g$ in the Hipparcos scale.

The microturbulence was obtained by flattening any trend in the [FeI/H] versus reduced equivalent width diagram. The microturbulence follow tight relations with temperature and $\log g$ (Fig. 4), with a scatter of only 0.20 km s^{-1}:

$$v_t(T_{\rm eff}) = 3.33 - 4.23 \times 10^{-4} T_{\rm eff} \qquad \text{(MARCS)(8)}$$

$$v_t(T_{\rm eff}) = 3.40 - 4.41 \times 10^{-4} T_{\rm eff} \qquad \text{(Kurucz overshooting)(9)}$$

$$v_t(\log g) = 1.82 - 0.186 \log g \qquad \text{(MARCS)(10)}$$

$$v_t(\log g) = 1.84 - 0.202 \log g \qquad \text{(Kurucz overshooting)(11)}$$

The lines used for analysis (presented as online material) have been carefully selected to minimize the impact of blends. Completely avoiding blends is almost an impossible task in cool, relatively metal-rich giants as in our sample, since their spectra are heavily blended with many atomic and molecular lines (e.g. Coelho et al. 2005), in particular due to CN. We have tried to avoid blending by performing spectral synthesis of CN (using the line list of Meléndez & Barbuy 1999) and discarding the atomic lines whose equivalent widths are contaminated by more than 10% by CN. The cool giant Arcturus (Hinkle et al. 2000) was also carefully inspected to discard lines that are severely contaminated with other features. In some cases even lines which are blended by more than 10% have to be included, especially for elements other than iron because only a few useful lines were available. For heavily blended lines we have performed the measurements by fitting only the unblended part of the profile, or deblending the feature using two or more components. A preliminary version of our line list (Hekker & Meléndez 2007) has been tested in ~380 field (Hekker & Meléndez 2007) and 39 open cluster (Santos et al. 2009) giants, and the final list has been already used in field bulge (Ryde et al. 2009b) and globular cluster (Meléndez & Cohen 2009) giants.

The stellar chemical abundances were obtained from an equivalent width analysis using the 2002 version of MOOG (Sneden 1973). The same transition probabilities were applied to both the bulge and comparison samples. In the present work, we employed both Kurucz models with convective overshooting (Castelli et al. 1997) and specially calculated MARCS (Gustafsson et al. 2008) 1D hydrostatic model atmospheres. For the MARCS models, both α-enhanced ($[\alpha/\mathrm{Fe}] = +0.2$ and $+0.4$) and scaled-solar abundances models were constructed; for the Kurucz models, adjustments of [Fe/H] were applied to simulate the effects of α-enhancement on the model atmospheres (Salaris et al. 1993):

$$\Delta[\mathrm{Fe/H}] = \log(0.64 \times 10^{[\alpha/\mathrm{Fe}]} + 0.36) \quad (12)$$

The effects of failing to account for the variations in $[\alpha/\mathrm{Fe}]$ are relatively small for a difference of $[\alpha/\mathrm{Fe}] = +0.1$ dex (Table 2), but could be important ($\sim$ 0.1 dex) for the typical enhancement of $[\alpha/\mathrm{Fe}] \sim +0.3$-$0.4$ seen in thick disk, halo and bulge stars.

We estimate that our stellar parameters have typical uncertainties of $\Delta T_{\rm eff} \approx \pm 75$ K, $\Delta \log g \approx \pm 0.3$ dex and $\Delta v_{\rm t} \approx 0.2$ km s^{-1}. The impact of these uncertainties on the abundance ratios, as well as the total abundance errors due to uncertainties in $T_{\rm eff}$, $\log g$, $v_{\rm t}$ and $[\alpha/\mathrm{Fe}]$ added in quadrature, are shown in Table 2, but note that some uncertainties are likely to be correlated to some degree (see, e.g., Fulbright et al. 2007). The uncertainties given in Table 2 are probably conservative in some cases,

---

[7] http://stev.oapd.inaf.it/cgi-bin/param

Table 3. Internal zero-point abundances adopted for our giant stars using MARCS and Kurucz models.

	Sun		Giants	
Specie	Literature[a]	This work[b]	MARCS[c]	Kurucz[d]
(1)	(2)	(3)	(4)	(5)
Fe	7.50,7.45,7.56,7.50	7.49±0.04	7.53	7.54
$O_{[O\,I]}$	8.83,8.73.8.71,8.69	8.74±0.04	8.83	8.84
Na	6.33,6.27,6.27,6.24	6.24±0.04	6.24	6.24
Mg	7.58,7.54,7.58,7.60	7.56±0.04	7.65	7.66
Al	6.47,6.28,6.47,6.45	6.39±0.04	6.56	6.56
Si	7.55,7.62,7.54,7.51	7.54±0.03	7.60	7.63
Ca	6.36,6.33,6.36,6.34	6.34±0.02	6.32	6.30
Ti	5.02,4.90,4.92,4.95	4.94±0.05	4.83	4.81

Notes.— (a): Solar photospheric abundances from Grevesse & Sauval (1998), Reddy et al. (2003), Bensby et al. (2003, 2004) and Asplund et al. (2009); (b): solar abundances based on our previous work (Meléndez et al. 2006a; Meléndez & Ramírez 2007; Meléndez et al. 2009) using different (e.g. McDonald, Keck, Magellan) solar spectra; (c,d): Our internal zero-points for giants represent the thin-disk abundances at [Fe/H] = 0.0. These zero-points are not absolute abundances and should only be used when both our same gf-values and analysis techniques are adopted

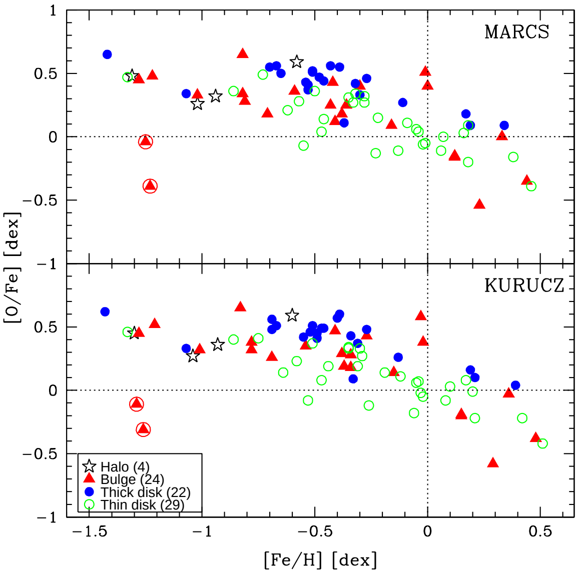

Fig. 5. [O/Fe] vs. [Fe/H] for the sample stars employing MARCS (*top*) and Kurucz (*bottom*) model atmospheres. Symbols are as explained in the figure. Note, however, that hereafter the bulge stars I-264 and IV-203 are omitted from all figures (refer to the text for detail).

as shown by the relatively low scatter (as a function of metallicity) of our abundance ratios; the uncertainties in the abundance ratios [X/Fe] are probably ≤ 0.10 dex.

The uncertainty of ±75K in $T_{\rm eff}$ is the based on the upper and lower envelopes (excluding outliers) of the differences between the slopes of iron abundance vs. excitation potential ($d(A_{FeI})/d(\chi_{exc})$) of the initial photometric temperatures and the adopted zero-points (relations 4 and 5). Note that these differences are due not only to errors in the temperature calibrations, photometric errors and the quality of the spectra, but also due to errors in E(B-V), which although for the nearby giants are low, for the bulge giants may be higher. Nevertheless, since we correct all outliers from our adopted zero-points (which in some cases may be due to incorrect reddenings), we are inmune to large errors in E(B-V). Our error of 0.3 dex in log g is based on the differences between FeII and FeI from the initial trigonometric log g and the adopted zero point in FeII-FeI (relations 6 and 7). Note that since we are basing our uncertainties on the upper and lower discrepancies of the initial input stellar parameters and the adopted zero-points, our uncertainties in $T_{\rm eff}$ and log g are conservative. For the bright disk/halo stars internal errors of 50K in $T_{\rm eff}$ and 0.2 dex in log g may be more adequate. Ryde et al. (2009b) suggests that the uncertainties adopted in the stellar parameters of our method (which was used to determine the atmospheric parameters in their sample) are sound for their bulge giants. In particular, uncertainties in $T_{\rm eff}$ higher than ~75K are excluded based on the relatively low star-to-star scatter of their [O/Fe] ratios.

No predictions of the effects of 3D hydrodynamical models instead of classical 1D models used here are available as yet for the exact stellar parameters of our targets (Asplund 2005). Collet et al. (2007) have performed such calculations for slightly less evolved red giants ($T_{\rm eff} \approx 4700$ and $\log g \approx 2$) and found that the the 3D abundance corrections for the species considered herein are expected to be modest: $|\Delta \log \epsilon| \lesssim 0.1$ dex at $[{\rm Fe/H}] \sim 0$. At lower metallicity the 3D effects become more severe so that at [Fe/H]= −1 our 1D-based abundances could be in error by $\lesssim 0.2$ dex. However, given the similarity in parameters between the bulge and disk giants, the *relative* abundance ratio differences – which we are primarily interested in here – will be significantly smaller and thus inconsequential for our conclusions.

Of particular importance to our work are the adopted zero-points of our abundance scale. Most works use the Sun to define the zero-point of the thin disk at [Fe/H] = 0.0, but due to the differences between dwarfs and giants, this approach may introduce systematic errors. Instead, in the present work we use seven thin disk giants with −0.1 < [Fe/H] <+0.1 dex (HD 29503, HD 45415, HD 99648, HD 100920, HD 115478, HD 186378, HD 214376) to define our zero points, which are shown in Table 3 for both the Kurucz and MARCS models. In Table 3 we also show for comparison different abundance analysis of the Sun. As can be seen, our zero-points for Fe, Na and Ca are roughly in agreement with the solar abundances, but for O, Mg, and Si the giants show a higher zero-point by ~+0.1 dex, and for Al differences as high as +0.15 are found. On the other hand, Ti is lower by ~0.1 dex. These zero-point offsets of −0.1 to +0.15 dex show that it is not straightforward to compare abundances obtained in giants with those found in dwarfs.

These zero points we have found for giants are internal for our particular set of gf-values and analysis techniques. For comparison with chemical evolution models, the absolute zero-points should be adopted from analysis of the Sun (Asplund et al. 2009), which represents well the local thin disk at [Fe/H] = 0.0, except for small peculiarities of a few 0.01 dex (Meléndez et al. 2009; Ramírez et al. 2009).

The final stellar parameters are given in Table 4 and Table 5 for the MARCS and the Kurucz models, respectively, while the abundance ratios are given in Table 6 and Table 7. The equivalent width measurements are given in Tables 8-15, which is available only in the electronic version of the article.

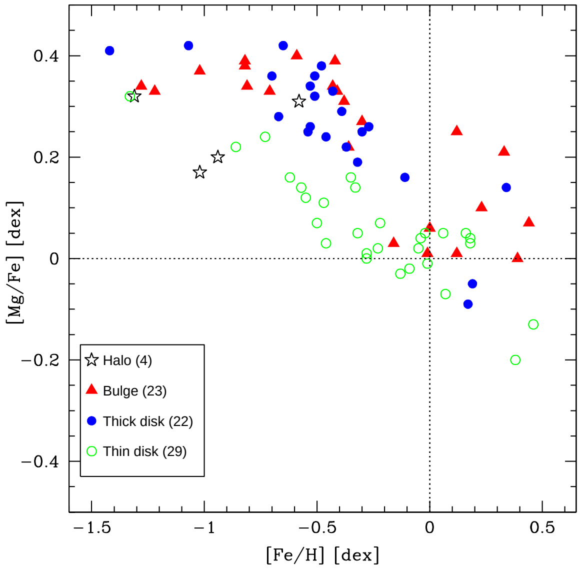

Fig. 6. [Mg/Fe] as a function of [Fe/H] for MARCS model atmospheres. Symbols as explained in the figure.

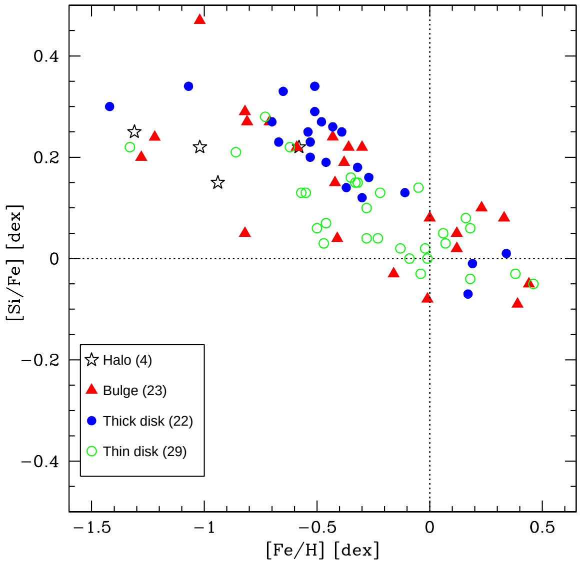

Fig. 7. [Si/Fe] vs. [Fe/H] for MARCS model atmospheres. Symbols as explained in the figure.

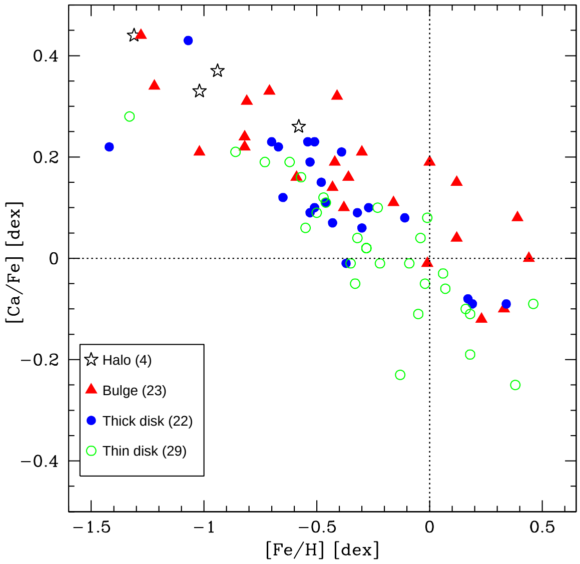

Fig. 8. [Ca/Fe] vs. [Fe/H] for MARCS model atmospheres. Symbols as explained in the figure.

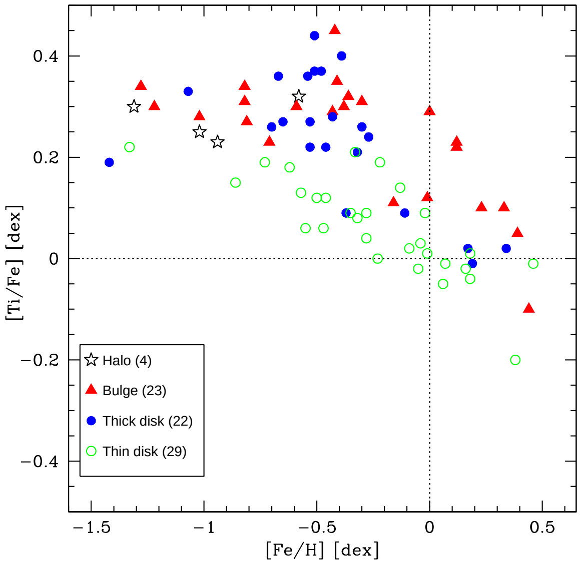

Fig. 9. Plot of [Ti/Fe] against [Fe/H] for the sample stars employing MARCS model atmospheres. Symbols are as explained in the figure.

4. Results

In Fig. 5 we show the [O/Fe] ratios obtained in this work for both MARCS and Kurucz overshooting model atmospheres. As can be seen, there is a good overall agreement between MARCS and Kurucz models. In particular, the difference in iron abundance (MARCS - Kurucz) is only −0.02 dex (σ = 0.03 dex). Thus, in the following figures, we present results based on the MARCS models only. Even though both set of models give similar chemical abundance ratios (see Tables 6,7), for comparison with chemical evolution models we suggest to adopt the MARCS results, since they were computed with the correct [α/Fe] ratio. Our disk/halo comparison sample shows that the oxygen abundances obtained here from the [O I] 630 and 636 nm lines and in Meléndez et al. (2008) from infrared OH lines are in excellent agreement. The mean difference is only −0.04 dex (OH - [O I]) with a scatter of 0.10 dex. Since this is identical to the estimated error in [O/Fe] from OH found in Meléndez et al. (2008), the uncertainties in our stellar parameters are likely somewhat overestimated, as already discussed above. Although the oxygen abundances obtained from [O I] and OH lines agree well, the results obtained from OH lines have less scatter, possibly because several OH lines were used instead of relying on only one or two forbidden lines. Therefore, for comparisons of oxygen abundances with detailed chemical evolution models of the thin disk, thick disk and bulge, we believe that the OH lines are preferable (Meléndez et al. 2008; Ryde et al. 2009a,b). The [O I]-based oxygen abundances confirms the similarity between

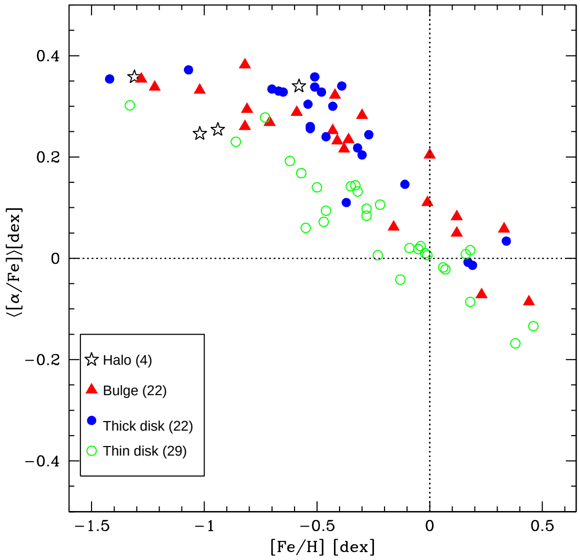

Fig. 10. Mean α-elements abundance ratio ([(O,Mg,Si,Ca,Ti)/Fe]) as a function of [Fe/H] for MARCS model atmospheres. Symbols as explained in the figure.

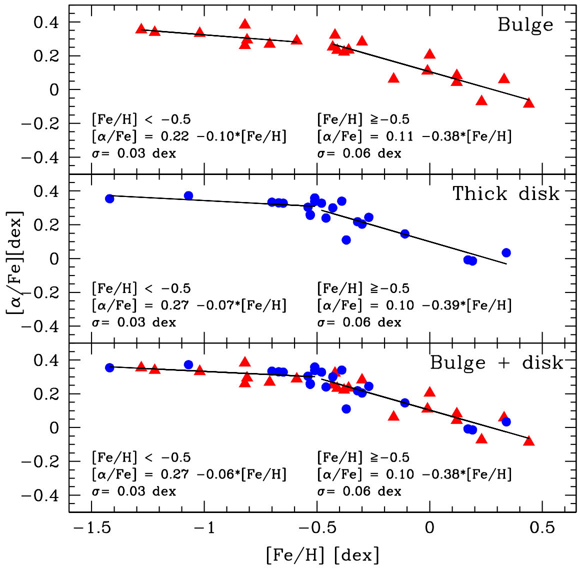

Fig. 11. Fit of [α/Fe] vs. [Fe/H] for metal-poor ([Fe/H] < -0.5) and metal-rich ([Fe/H] ≥ -0.5) bulge (*top*), thick disk (*center*) and both bulge and thick disk (*bottom*) stars. Both stellar populations can be fitted by similar relations, with a scatter as low as $\sigma = 0.03$ dex.

the bulge and the local thick disk, which we previously demonstrated based on OH lines. This is in contrast to some previous works on the topic (Zoccali et al. 2006; Fulbright et al. 2007; Lecureur et al. 2007), which argue that [O/Fe] in the bulge is higher than in the thick disk based on a comparison to disk dwarf stars.

As pointed out by Fulbright et al. (2007), two O-deficient stars (I-264 and IV-203) at [Fe/H] ≈ -1.25 have peculiar abundances similar to the O-Na anti-correlation seen in globular clusters (e.g. Gratton et al. 2004; Cohen & Meléndez 2005; Yong et al. 2005; Carretta et al. 2009). Fulbright et al. (2007) found that these two giants have high Na and Al abundances reminiscent of the abundance anomalies seen in globular clusters, which we confirm. Thus, the oxygen abundances of these two stars most likely do not reflect the typical bulge composition.

The results for the other α-elements (Mg, Si, Ca, Ti) studied here are shown in Figs. 6-9. As can be clearly seen, the chemical patterns of the bulge and thick disk are indistinguishable also for those elements, reinforcing our previous findings based on oxygen abundances. The average of our Mg abundances for the 7 stars with [Fe/H]≥ 0 is [Mg/Fe] $= 0.1\pm0.1$, in good agreement with the results from microlensed bulge dwarfs, which typically have [Mg/Fe]$\approx +0.1$ (Cohen et al. 2008, 2009; Johnson et al. 2008; Bensby et al. 2009a). The latest preliminary results based

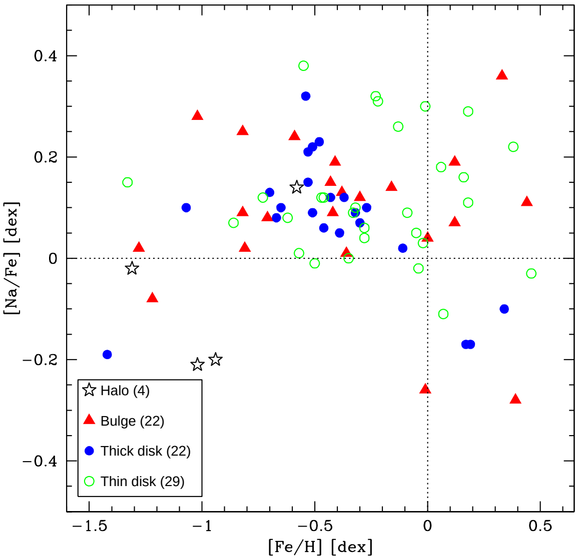

Fig. 12. [Na/Fe] vs. [Fe/H] for MARCS model atmospheres. Symbols as explained in the figure.

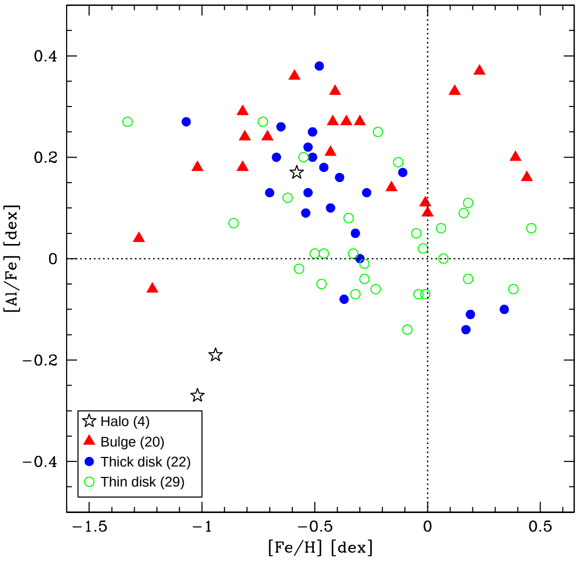

Fig. 13. [Al/Fe] vs. [Fe/H] for MARCS model atmospheres. Symbols as explained in the figure.

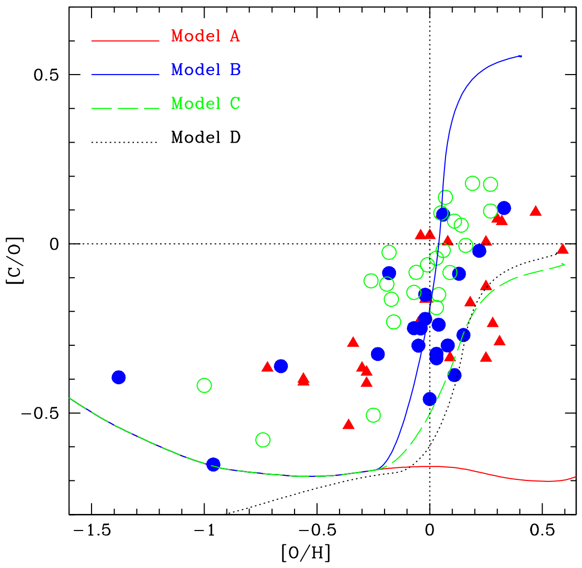

Fig. 14. [C/O] vs. [O/H] for the bulge (*triangles*), thick disk (*filled circles*) and thin disk (*open circles*) with data taken from Meléndez et al. (2008) and Ryde et al. (2009b). The original (undepleted) C abundances were estimated from C+N (refer to the text). Overplotted, we show model predictions as given in Cescutti et al. (2009; c.f. their Figure 5).

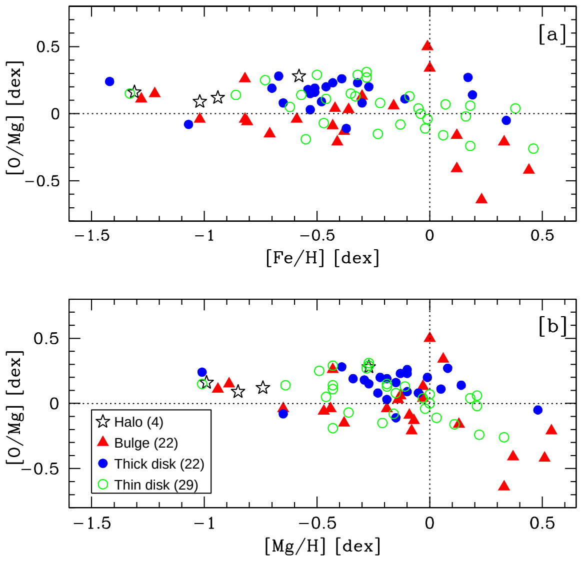

Fig. 15. [O/Mg] as a function of [Fe/H] (*top panel*) and [Mg/H] (*bottom panel*). Symbols as explained in the figure.

on microlensed bulge dwarf stars (Bensby et al. 2009b) also indicate similarities between the bulge and thick disk for Ti and Mg at all probed metallicities (−0.8 < [Fe/H] < +0.5).

Even more clear results are found when we combine the results for all α-elements, as shown in Fig. 10. It is clear that the chemical patterns of the bulge and thick disk are indistinguishable in their abundance patterns up to the metallicity range where the thick disk is unambiguously identified, i.e., up to [Fe/H] ≈ −0.3. Bensby et al. (2003, 2004) reported the existence of a knee connecting thick-disk stars from [Fe/H]≈ −0.3 and high [α/Fe] to [Fe/H]>0.0 and low [α/Fe], but Reddy et al. (2006) and Ramírez et al. (2007) did not find any evidence of such a knee. A re-examination of the latter results including new observations of kinematically selected thick-disk metal-rich objects is underway (Reddy et al., in preparation) and will address this discrepancy. The problem is that at high [Fe/H] there is a significant number of thick-disk candidates that follow the thin disk abundance pattern. That suggests that hot kinematics alone cannot be used to separate the thin from the thick disk, especially at high [Fe/H]. At super-solar metallicities the problem may be unsolvable because the abundance patterns of both disks merge. Interestingly, the chemical similarities between the Galactic bulge and the local thick disk giant stars we find in this work in fact extend to super-solar metallicities. Yet, as explained above, it remains to be demonstrated that the few selected thick disk stars are bona fide thick disk members rather than kinematically heated thin disk stars.

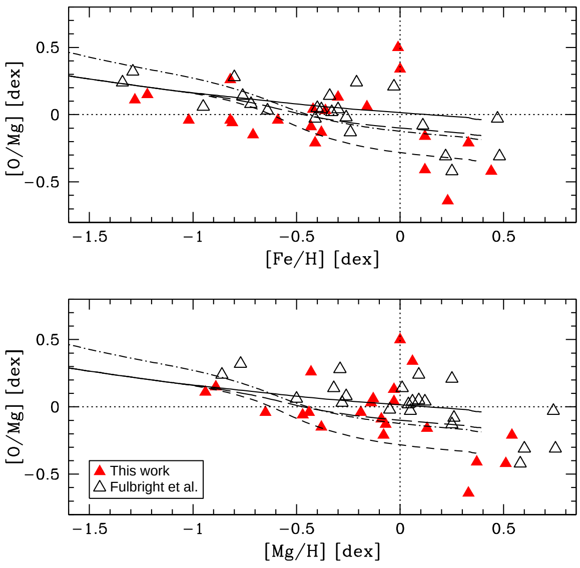

Fig. 16. [O/Mg] as a function of [Fe/H] for bulge giants according to Fulbright et al. (2007) (open triangles) and our work (filled triangles). Both studies show a shallow trend up to about solar metallicity and a step decrease in [O/Mg] for higher metallicities. Recent predictions by Cescutti et al. (2009) are shown as solid (WW95 model), short dashed (WW95+M92), long dashed (WW95+MM02) and dot-short dashed (MM02) lines. All models have been shifted by −0.2 dex in [O/Mg] (see Cescutti et al. 2009 for a description of the models and an explanation of the empirical offset).

From Table 1 we see that three giants, which are kinematically classified as thick disk (HD 77236, HD 107328) and thin disk (HD 30608) members, present ambiguous kinematical population. The star HD 77236 could be either a thick disk/halo star, while the stars HD 107328 and HD 30608 both have similar likelihood of belonging to the thin or thick disk populations. These stars have [Fe/H] = (−0.67, −0.43, −0.28) and [α/Fe] = (+0.33, +0.30, +0.08), respectively, which means that both HD 77236 and HD 107328 could be indeed thick disk stars, while the star HD 30608 has an abundance pattern consistent with a thin disk star at [Fe/H] ∼ −0.3.

Linear fits of both the bulge and the thick disk [α/Fe] vs. [Fe/H] relations up to [Fe/H] = −0.3, show that both populations follow identical patterns, with a star-to-star scatter of only σ =

0.03 dex. We thus set the most stringent constraints to date on the chemical similarity of bulge and local thick disk stars. The metallicity of the bulge extends to significantly higher [Fe/H] than that, which remains to be convincingly demonstrated for the thick disk, as previously discussed.

In order to quantify how similar are the bulge and the thick disk at all metallicities, we have divided the stars in a metal-poor and a metal-rich sample with the division set somewhat arbitrarily at [Fe/H] = −0.5, and we have performed linear fits of [α/Fe] vs. [Fe/H]. We find that the metal-poor part of both stellar populations can be fitted by essentially identical relations (Fig. 11): [α/Fe] = 0.22 - 0.10 × [Fe/H] for the bulge (σ = 0.03 dex) and [α/Fe] = 0.27 - 0.07 × [Fe/H] for the thick disk (σ = 0.03 dex). These relations are identical to within ±0.01 dex at [Fe/H] = −1.5 and to within ±0.02 dex at [Fe/H] = −0.5, hence both datasets can be fitted by a single relation followed by both stellar populations:

$$[\alpha/\mathrm{Fe}] = 0.268 - 0.065 \times [\mathrm{Fe/H}] \quad ([\mathrm{Fe/H}] < -0.5), \tag{13}$$

with a very low star-to-star scatter of only 0.03 dex (Fig. 11).

A similar exercise for the most metal-rich bulge and thick disk stars with [Fe/H] ≥ −0.5, results in a single relation followed by both stellar populations (Fig. 11):

$$[\alpha/\mathrm{Fe}] = 0.104 - 0.381 \times [\mathrm{Fe/H}] \quad ([\mathrm{Fe/H}] \geq -0.5), \tag{14}$$

with a low star-to-star scatter of only 0.06 dex (Fig. 11). This scatter is higher than for the more metal-poor stars (σ = 0.03 dex), but fully explained by the higher uncertainties in the analysis of the more crowded spectra of the metal-rich stars. Nevertheless, we do not discard that there may be some contamination in the metal-rich samples. We demonstrate thus that at all probed metallicities (−1.5 < [Fe/H] < +0.5), both the bulge and thick disk stellar populations have a striking chemical similarity.

The Al abundances of the most metal-rich bulge stars ([Fe/H] $\gtrsim$ 0) seem enhanced ([Al/Fe] ∼ +0.25), but Na seems solar (although with a large scatter) at these metallicities, as illustrated in Fig. 12-13. Thus, the enhancement in Al in metal-rich bulge giants is probably not related to the Al-Na correlation seen in globular clusters, but most likely due to the fact that the two Al I lines employed are blended and are more difficult to deblend in the relatively moderate S/N spectra of the metal-rich bulge giants. This is reinforced by recent studies of metal-rich bulge dwarfs through microlensing (Cohen et al. 2008; Johnson et al. 2008; Bensby et al. 2009a), which find [Al/Fe] ∼ +0.10 dex. Thus, our Al abundances for bulge stars with [Fe/H] $\gtrsim$ 0 are thus likely affected by systematic errors, which should be borne in mind in comparisons with chemical evolution models.

5. Discussion

Our previous homogeneous abundance analysis of OH lines in high resolution infrared Gemini+Phoenix spectra was the first to show that the Galactic bulge and the local thick disk have indistinguishable [O/Fe] trends up to at least metallicities [Fe/H] ≈ −0.3 where the thick disk is unambiguously identified (Meléndez et al. 2008). In the present work we have analyzed the forbidden oxygen lines and demonstrated that those indeed give consistent results with the OH lines. Importantly, we also extend the conclusions of Meléndez et al. (2008) to other α-elements (Mg, Si, Ca, Ti). The α-elements in the bulge and local thick disk stars are the same in the range −1.5 < [Fe/H] < −0.3, showing a very low star-to-star scatter in [α/Fe] of only 0.03 dex. Similarly, the [Na/Fe] and [Al/Fe] trends agree well for the bulge and the local thick disk, although this is not too surprising given that there is no obvious offset between the thick and thin disk for those two elements.

Previous works (Fulbright et al. 2007; Lecureur et al. 2007) have found high [Mg/Fe] ratios in bulge stars, as well as high [X/Fe] ratios in other elements with respect to the thick disk. It may seem surprising that using the same equivalent widths as Fulbright et al. (2007) we find significantly lower [Mg/Fe] in bulge giants at all metallicities. However, as mentioned in the section 3, the zero-points we use in our analysis are based on seven thin disk solar metallicity giants, which, as shown in Table 3, are not the same as the zero-points based on the Sun, which is ∼1400 K hotter and has a surface gravity ∼300 times higher than our giants. The differences shown in Table 3 between the Sun and our giants could be due to the different impact of 3D and non-LTE effects on giant and dwarfs, as well as problems with line blending in giants. Furthermore, since we compare bulge giants to thick disk giants, our conclusions on the similarity of the bulge and thick disk is independent of the adopted zero-point, unlike the comparisons of Zoccali et al. (2006), Fulbright et al. (2007) and Lecureur et al. (2007), that compared bulge giants to disk dwarfs. Although both Fulbright et al. (2007) and Lecureur et al. (2007) used the giants Arcturus ([Fe/H] ∼ −0.5) and μ Leo ([Fe/H] ∼+0.3) as reference stars, their zero-points are ultimately based on the Sun[8], which as shown in Table 3, may be inadequate for the study of giants. It is important to mention that Fulbright et al. (2007) also included 17 nearby disk giants (mostly from the thin disk) in order to check whether they follow the same abundance pattern as disk dwarfs, but most of their giants were observed at a lower resolving power, R ∼ 30,000, implying higher errors in the abundances obtained from the crowded spectra of metal-rich giant stars. Furthermore, their comparison sample of disk dwarfs included several studies which may have different systematic offsets between them. For example the study by Reddy et al. (2003) used Strömgren photometry to estimate effective temperatures using the $(b - y)$ calibration by Alonso et al. (1996). However, as recently shown by Meléndez et al. (2010, in preparation) using *uvby*-β photometry of solar twins, this calibration has a zero-point error of 130 K. In turn, this implies abundance variations (Δ[X/H]) from -0.12 dex (O based on OI triplet, which was the main abundance indicator used by Reddy et al. 2003) to +0.13 dex (Ti). Yet, due to a compensating change in iron, for most elements studied here (except for [O/Fe] that is affected by -0.22 dex; based on the OI triplet), the Δ[X/Fe] ranges from -0.08 dex ([Si/Fe]) to +0.03 dex ([Ti/Fe]). On the other hand, Bensby et al. (2003, 2004) adopted spectroscopic temperatures, therefore not only their Teff but also their [X/Fe] abundance ratios are likely more accurate for comparison of these reddened bulge regions.

Thus, the main reason why our conclusions regarding the abundance trends in the bulge in comparison with the thick and thin disk differ from the findings of previous studies (e.g. Zoccali et al. 2006; Fulbright et al. 2007; Lecureur et al. 2007) is that we perform a strictly differential analysis of red giants with very similar parameters for all populations rather than relying on either literature data or using dwarf stars for the disk samples.

---

[8] similar problems were already recognized by Gratton & Sneden (1990) in their abundance analysis of μ Leo, which was ultimately relative to the Sun since they used solar gf-values. They remark that their procedure might introduce inconsistencies due to the different atmospheric structures of μ Leo and the Sun. Furthermore, independently of the adopted gf-values, by definition the solar abundances are need to obtain [X/Fe].

We therefore bypass several potential systematic errors that can scupper any analysis (e.g. 3D, non-LTE, stellar parameters, gf-values, see discussion in Asplund 2005). It is also worth noting that Bensby et al. (2009b) have shown that microlensed dwarfs in the Galactic bulge present [α/Fe] abundance ratios similar to those of dwarfs in the Galactic thick disk, which is in agreement with our results for giant stars.

The identical enhancement of the α-elements in the bulge and the local thick disk – including the location of the knee that canonically is supposed to reflect the start of significant contribution of Fe production from SNe Ia – argues that the two stellar populations not only shared a similar star formation rate but also initial mass function, in contrast to the conclusions of some recent studies (e.g. Ballero et al. 2007; McWilliam et al. 2008; Cescutti et al. 2009). We emphasize that this similarity does not automatically imply a casual connection between the bulge and the local thick disk but it would be worthwhile exploring this possibility further, in particular since such a relationship has been proposed for other spiral galaxies (e.g. van der Kruit & Searle 1981). A worthwhile avenue to pursue would be the effects of Galactic radial migration (e.g. Sellwood & Binney 2002; Haywood 2008; Roskar et al. 2008; Schönrich & Binney 2009a,b). We note especially the hypothesis by Schönrich & Binney (2009b) that the thick disk is a natural consequence of radial mixing, i.e. the thick disk stars in the solar neighborhood originated in the inner part of the Galaxy. It would therefore be particularly interesting to carry out a detailed chemical analysis of a sample of in-situ inner disk stars to investigate any chemical similarities with the bulge and the local thick disk giants studied herein.

McWilliam et al. (2008) have argued that their observed steadily declining [O/Mg] vs. [Mg/H] trends for both the bulge and the solar vicinity are the result of metallicity-dependent O yields due to mass-loss in massive stars, possibly augmented by stellar rotation (e.g. Maeder 1992; Meynet & Maeder 2002). Since these stellar winds remove C that would otherwise be converted to O, the decreasing O production should be accompanied by enhanced C yields. Cescutti et al. (2009) have extended the chemical modelling of McWilliam et al. by investigating the resulting [C/O] trends. Although neither of their models match the observed [C/O] vs. [O/H] ratios for the bulge or disk in detail, they argue that the observations support the metallicity-dependent yields of massive stars.

In Fig. 14 we plot the [C/O] vs. [O/H] ratios of bulge and disk stars based on Melendez et al. (2008) and Ryde et al. (2009b), which are both in similar abundance scales. As in Cescutti et al. (2009), the primordial C abundances were estimated by adding C+N and subtracting a "primordial" N abundance assuming [N/Fe]=0. As can be seen, none of the Cescutti et al. models provide a good fit to the data. As mentioned by them, adopting an IMF not as skewed to massive stars as that adopted by Ballero et al. (2007) may help to alleviate the discrepancy, but on the other hand it may ruin their fit to the bulge metallicity distribution.

Regarding the [O/Mg] ratios, our own observational data paint a somewhat different picture than the one presented by McWilliam et al. (2008) and Cescutti et al. (2009). Fig. 15 shows our [O/Mg] results against both [Fe/H] and [Mg/H]. All three populations – bulge, thick and thin disk – are similar up to at least solar metallicity and follow an essentially flat trend with [O/Mg]$\approx$ 0.0 – 0.1. The similarities between the thick and thin disks extend even further provided the few stars with [Fe/H]$>$ 0 classified as belonging to the thick disk kinematically are truly bona-fide members. There is some indication that for the bulge [O/Mg] becomes negative for super-solar metallicities in line with the findings of Lecureur et al. (2007) and McWilliam et al. (2008). They claim however an essentially continuous downward trend over the entire metallicity span of their sample while we find a flat trend with a possible break around solar [Fe/H]. Nevertheless, a comparison between Fulbright et al. (2007) and our [O/Mg] ratios for bulge giants (Fig. 16), shows that their [O/Mg] ratios actually do not have a continuous downward trend, but instead their data show a shallow trend up to [Fe/H] $\sim +0.1$, and then a step decrease for higher metallicities. Thus, both Fulbright et al. (2006, 2007) and our own analysis shows that there may be a break around solar metallicity in the [O/Mg] ratios. However, none of the models presented in Cescutti et al. (2009) shows the sharp break around solar metallicity indicated by the bulge giants (Fig. 16). The existence of this break would have to be confirmed by a significantly larger bulge sample than we have access to here; adding the most metal-rich stars from the Lecureur et al. study would be worthwhile in this respect (as mentioned earlier, our bulge sample consists of the stars observed by Fulbright et al. 2006, 2007). If real, the downward trend could be a manifestation of metallicity-dependent O yields due to mass-loss in massive stars.

Acknowledgements. AAB acknowledges CAPES for financial support 4685-06-7 (PDE) and a FAPESP fellowship no. 04/00287-9. We would like to thank the anonymous referee for helpful constructive comments on the paper. Likewise, we are grateful to A. McWilliam for sharing the Keck spectrum of one bulge star used for comparison purposes, and G. Cescutti for sending the models shown in Figs.14,16. This work has been supported by the Australian Research Council (DP0588836), ANSTO (06/07-0-11), National Science Foundation (AST 06-46790), and the Portuguese FCT/MCTES (project PTDC/CTE-AST/65971/2006). J.M. is supported by a Ciencia 2007 contract funded by FCT/MCTES (Portugal) and POPH/FSE (EC).

Based partly on observations obtained at the Las Campanas Magellan telescopes (through Australian time with travel support provided by the Australian Access to Major Facilities Programme 06/07-O-11), Keck Observatory (operated jointly by the California Institute of Technology, the University of California and the National Aeronautics and Space Administration) and McDonald Observatory.

References

Abu-Shawiesh, M.O., Al-Athari, F.M. & Kittani, H.F. 2009. J. Applied Sci., 9, 2835
Alonso, A., Arribas, S., & Martínez-Roger, C. 1996, A&AS, 313, 873
Alonso, A., Arribas, S., & Martínez-Roger, C. 1999, A&AS, 140, 261
Asplund, M. 2005, ARA&A, 43, 481
Asplund, M., Grevesse, N, Sauval, A. J., Scott, P. 2009, ARA&A, 47, 481
Bagnulo, S., Jehin, E., Ledoux, C., Cabanac, R., Melo, C., Gilmozzi, R., & The ESO Paranal Science Operations Team 2003, The Messenger, 114, 10
Ballero, S. K., Matteucci, F., Origlia, L., & Rich, R. M. 2007, A&A, 467, 123
Bensby, T., Feltzing, S., & Lundström, I. 2003, A&A, 410, 527
Bensby, T., Feltzing, S., & Lundström, I. 2004, A&A, 415, 155
Bensby, T., Johnson, J. A., Cohen, J., Feltzing, S., Udalski, A., Gould, A., Huang, W., Thompson, I., Simmerer, J., Adén, D. 2009a, A&A, 499, 737
Bensby, T., Feltzing, S., Johnson, J. A., Gould, A., Adén, D., et al. 2009b, in press, arXiv0911.5076B
Bernstein, R., Shectman, S. A., Gunnels, S. M., Mochnacki, S., & Athey, A. E. 2003, Proc. SPIE, 4841, 1694
Bohlin, R.C., Savage, B.D., Drake, J.F. 1978, ApJ, 224, 132
Carretta, E., Bragaglia, A., Gratton, R., & Lucatello, S. 2009, A&A, 505, 139
Casagrande, L., Ramírez, I., Meléndez, J., Bessell, M. & Asplund, M. 2010, A&A, submitted
Castelli, F., Gratton, R. G., & Kurucz, R. L. 1997, A&A, 318, 841
Cayrel de Strobel, G., Soubiran, C., & Ralite, N. 2001, A&A, 373, 159
Cescutti, G., Matteucci, F., McWilliam, A., Chiappini, C. 2009, A&A, 505, 605
Coelho, P., Barbuy, B., Meléndez, J., Schiavon, R. P., Castilho, B. V. 2005, A&A, 443, 735
Cohen, J. G., & Meléndez, J. 2005, AJ, 129, 303
Cohen, J. G., Huang, W., Udalski, A., Gould, A., Johnson, J. A. 2008, ApJ, 682, 1029
Cohen, J. G., Thompson, I. B., Sumi, T., Bond, I., Gould, A., Johnson, J. A., Huang, W., Burley, G 2009, ApJ, 699, 66
Collet, R., Asplund, M., & Trampedach, R. 2007, A&A, 469, 687

Cunha, K. & Smith, V. V. 2006, ApJ, 651, 491
da Silva, L., Girardi, L., Pasquini, L., et al. 2006, A&A, 458, 609
Demarque, P., Woo, J.-H., Kim, Y.-C., & Yi, S. K. 2004, ApJS, 155, 667
Elmegreen, B. G., Bournaud, F., & Elmegreen, D. M. 2008, ApJ, 688, 67
Ferlet, R., Vidal-Madjar, A., & Gry, C. 1985, ApJ, 298, 838
Fosalba, P., Lazarian, A., Prunet, S., & Tauber, J. A. 2002, ApJ, 564, 762
Fulbright, J. P., McWilliam, A., & Rich, R. M. 2006, ApJ, 636, 821
Fulbright, J. P., McWilliam, A., & Rich, R. M. 2007, ApJ, 661, 1152
Genzel, R., et al. 2008, ApJ, 687, 59
Gratton, R.G., Sneden, C. 1990, A&A, 234, 366
Gratton, R., Sneden, C., & Carretta, E. 2004, ARA&A, 42, 385
Grevesse, N., & Sauval, A. J. 1998, Space Sci. Rev., 85, 161
Gustafsson, B., Edvardsson, B., Eriksson, K., Jorgensen, U. G., Nordlund, A., Plez, B 2008, A&A, 486, 951
Haywood, M. 2008, MNRAS, 388, 1175
Hekker, S., & Meléndez, J. 2007, A&A, 475, 1003
Hinkle, K., Wallace, L., Valenti, J., & Harmer, D. 2000, Visible and Near Infrared Atlas of the Arcturus Spectrum 3727-9300 A ed. Kenneth Hinkle, Lloyd Wallace, Jeff Valenti, and Dianne Harmer. (San Francisco: ASP) ISBN: 1-58381-037-4, 2000.,
Kormendy, J. & Kennicutt, Jr., R. C. 2004, ARA&A, 42, 603
Johnson, J. A., Gaudi, B. S., Sumi, T., Bond, I. A., Gould, A. 2008, ApJ, 685, 508
Lecureur, A., Hill, V., Zoccali, M., et al. 2007, A&A, 465, 799
Luck, R. E., & Heiter, U. 2007, AJ, 133, 2464
Maeder, A. 1992, A&A, 264, 105
McWilliam, A. & Rich, R. M. 1994, ApJS, 91, 749
McWilliam, A., Matteucci, F., Ballero, S., Rich, R. M., Fulbright, J. P., Cescutti, G. 2008, AJ, 136, 367
Meléndez, J., & Barbuy, B. 1999, ApJS, 124, 527
Meléndez, J., Dodds-Eden, K., & Robles, J. A. 2006a, ApJ, 641, L133
Meléndez, J., Shchukina, N. G., Vasiljeva, I. E., & Ramírez, I. 2006b, ApJ, 642, 1082
Meléndez, J., & Ramírez, I. 2007, ApJ, 669, L89
Meléndez, J., et al. 2008, A&A, 484, L21
Meléndez, J., Asplund, M., Gustafsson, B., & Yong, D. 2009, ApJ, 704, L66
Meléndez, J., & Cohen, J. G. 2009, ApJ, 699, 2017
Meynet, G., Maeder, A. 2002, A&A, 390, 561
Mishenina, T. V., Bienaymé, O., Gorbaneva, T. I., Charbonnel, C., Soubiran, C., Korotin, S. A., & Kovtyukh, V. V. 2006, A&A, 456, 1109
Moultaka, J., Ilovaisky, S. A., Prugniel, P., & Soubiran, C. 2004, PASP, 116, 693
Munari, U., et al. 2008, A&A, 488, 969
Ortolani, S., Renzini, A., Gilmozzi, R., Marconi, G., Barbuy, B., Bica, E., & Rich, R. M. 1995, Nature, 377, 701
Ramírez, I., Allende Prieto, C., & Lambert, D. L. 2007, A&A, 465, 271
Ramírez, I. & Meléndez, J. 2005a, ApJ, 626, 446
Ramírez, I. & Meléndez, J. 2005b, ApJ, 626, 465
Ramírez, I., Allende Prieto, C., Redfield, S., & Lambert, D. L. 2006, A&A, 459, 613
Ramírez, I., Meléndez, J., & Asplund, M. 2009, A&A, 508, L17
Reddy, B. E., Lambert, D. L., & Allende Prieto, C. 2006, MNRAS, 367, 1329
Roskar, R., Debattista, V. P., Quinn, T.R., Stinson, G. S., Wadsley, J. 2008, ApJ, 684
Ryde, N., Edvardsson, B., Gustafsson, B., Eriksson, K., Käufl, H. U., Siebenmorgen, R., & Smette, A. 2009a, A&A, 496, 701
Ryde, N., Edvardsson, B., Gustafsson, B., Meléndez, J., Alves-Brito, A. et al. 2009b, A&A, in press, arXiv:0910.0448
Salaris, M., Chieffi, A., & Straniero, O. 1993, ApJ, 414, 580
Santos, N. C., Lovis, C., Pace, G., Melendez, J., & Naef, D. 2009, A&A, 493, 309
Schonrich, R., Binney, J. 2009a, MNRAS, 396, 203
Schonrich, R., Binney, J. 2009b, MNRAStmp, 1255S
Sellwood, J.A, Binney, J.J. 2002, MNRAS, 336, 785
Sneden, C. A. 1973, PhD thesis, Univ. of Texas, Austin
Spitzer, L. 1968, Diffuse matter in space, New York: Interscience Publication, 1968
Stanek, K. Z. 1996, ApJ, 460, L37
Takeda, Y., Sato, B., & Murata, D. 2008, PASJ, 60, 781
Tull, R. G., MacQueen, P. J., Sneden, C., & Lambert, D. L. 1995, PASP, 107, 251
van der Kruit, P. C. & Searle, L. 1981, A&A, 95, 105
van Leeuwen, F. 2007, A&A, 474, 653
Vogt, S. S., et al. 1994, Proc. SPIE, 2198, 362
Welty, D. E., Hobbs, L. M., & Kulkarni, V. P. 1994, ApJ, 436, 152
Yong, D., Grundahl, F., Nissen, P. E., Jensen, H. R., & Lambert, D. L. 2005, A&A, 438, 875
Yong, D., Aoki, W., Lambert, D. L., & Paulson, D. B. 2006, ApJ, 639, 918
Zoccali, M., et al. 2003, A&A, 399, 931
Zoccali, M., Lecureur, A., Barbuy, B., et al. 2006, A&A, 457, L1

Table 4. Final atmospheric parameters using the MARCS models

Star (1)	$T_{\rm eff}$ [K] (2)	log g [dex] (3)	v_t [km/s] (4)	[FeI/H] ± σ (5)	N (6)	[FeII/H] ± σ (7)	N (8)
Halo							
HD041667	4581	1.80	1.16	-1.02 ± 0.07	41	-0.96 ± 0.08	6
HD078050	5000	2.24	1.29	-0.94 ± 0.07	36	-0.87 ± 0.08	7
HD114095	4794	2.68	1.25	-0.58 ± 0.07	42	-0.62 ± 0.06	7
HD210295	4738	1.88	1.14	-1.31 ± 0.07	35	-1.35 ± 0.09	5
Bulge							
I012	4237	1.61	1.52	-0.43 ± 0.08	26	-0.44 ± 0.06	3
I025	4370	2.25	1.70	0.44 ± 0.10	19	0.39 ± 0.12	4
I039	4386	2.20	1.63	0.33 ± 0.10	17	0.18 ± 0.21	2
I141	4356	1.93	1.41	-0.30 ± 0.09	27	-0.34 ± 0.10	3
I151	4400	1.73	1.29	-0.82 ± 0.09	25	-0.85 ± 0.08	2
I152	4663	2.67	1.29	0.00 ± 0.10	23	0.12 ± 0.02	2
I156	4296	1.60	1.22	-0.82 ± 0.10	28	-0.97 ± 0.06	3
I158	4500	2.70	1.25	-0.01 ± 0.09	26	-0.11 ± 0.13	3
I194	4183	1.67	1.57	-0.38 ± 0.08	20	-0.56 ± 0.16	2
I202	4252	2.07	1.16	0.12 ± 0.10	26	0.11 ± 0.20	3
I264	4046	0.68	1.51	-1.23 ± 0.08	25	-1.25 ± 0.09	4
I322	4250	1.52	1.54	-0.16 ± 0.08	24	-0.33 ± 0.11	4
II033	4230	1.37	1.40	-0.81 ± 0.07	28	-0.84 ± 0.02	3
II119	4478	1.61	0.82	-1.22 ± 0.13	16	-1.22 ± 0.06	3
II154	4650	2.1	1.12	-0.71 ± 0.07	24	-0.77 ± 0.12	4
II172	4500	1.96	1.08	-0.41 ± 0.11	27	-0.62 ± 0.09	4
III152	4143	1.51	1.49	-0.59 ± 0.09	28	-0.69 ± 0.08	3
III220	4507	1.95	1.22	-0.36 ± 0.09	29	-0.35 ± 0.06	2
IV003	4500	1.35	1.24	-1.28 ± 0.06	19	-1.38 ± 0.10	3
IV047	4622	2.50	1.66	-0.42 ± 0.10	25	-0.43 ± 0.10	3
IV072	4276	2.13	1.43	0.12 ± 0.09	21	0.12 ± 0.10	2
IV167	4374	2.44	1.46	0.39 ± 0.12	21	0.31 ± 0.09	3
IV203	3815	0.35	1.83	-1.25 ± 0.08	37	-1.11 ± 0.05	5
IV325	4353	2.35	1.60	0.23 ± 0.07	20	0.14 ± 0.08	4
IV329	4153	1.15	1.54	-1.02 ± 0.08	20	-1.01 ± 0.08	4
Thick Disk							
HD077236	4427	2.01	1.53	-0.67 ± 0.07	40	-0.74 ± 0.06	7
HD023940	4800	2.41	1.37	-0.30 ± 0.08	35	-0.33 ± 0.06	7
HD032440	3941	0.95	1.81	-0.37 ± 0.09	40	-0.27 ± 0.10	6
HD037763	4630	3.15	1.19	0.34 ± 0.08	41	0.36 ± 0.09	7
HD040409	4746	3.20	1.06	0.19 ± 0.07	42	0.18 ± 0.05	6
HD077729	4077	1.38	1.64	-0.51 ± 0.09	42	-0.49 ± 0.12	7
HD080811	4900	3.28	1.18	-0.51 ± 0.07	41	-0.51 ± 0.04	6
HD083212	4480	1.20	1.48	-1.42 ± 0.10	26	-1.22 ± 0.07	6
HD099978	4678	2.07	1.23	-1.07 ± 0.07	37	-1.03 ± 0.08	5
HD107328	4417	2.01	1.80	-0.43 ± 0.08	40	-0.42 ± 0.06	7
HD107773	4891	3.28	0.98	-0.39 ± 0.06	42	-0.37 ± 0.04	6
HD119971	4093	1.30	1.65	-0.65 ± 0.07	41	-0.55 ± 0.08	6
HD124897	4280	1.69	1.74	-0.53 ± 0.05	43	-0.58 ± 0.05	7
HD127243	4893	2.53	1.48	-0.70 ± 0.07	32	-0.55 ± 0.08	6
HD130952	4742	2.53	1.51	-0.32 ± 0.07	40	-0.26 ± 0.07	6
HD136014	4774	2.52	1.47	-0.46 ± 0.07	44	-0.39 ± 0.07	7
HD145148	4851	3.67	0.96	0.17 ± 0.06	41	0.18 ± 0.09	6
HD148451	4972	2.52	1.45	-0.54 ± 0.07	40	-0.52 ± 0.06	7
HD180928	4092	1.48	1.56	-0.48 ± 0.07	41	-0.47 ± 0.10	6
HD203344	4666	2.53	1.37	-0.11 ± 0.07	34	-0.07 ± 0.05	6
HD219615	4833	2.51	1.34	-0.53 ± 0.07	33	-0.5 ± 0.06	7
HD221345	4688	2.50	1.42	-0.27 ± 0.07	34	-0.27 ± 0.05	6
Thin Disk							
HD000787	3970	1.06	1.92	-0.22 ± 0.11	38	-0.17 ± 0.07	5

Table 4 – continued

Star (1)	$T_{\rm eff}$ [K] (2)	log g [dex] (3)	v_t [km/s] (4)	[FeI/H] ± σ (5)	N (6)	[FeII/H] ± σ (7)	N (8)
HD003546	4878	2.43	1.38	-0.62 ± 0.07	33	-0.51 ± 0.06	7
HD005268	4873	2.54	1.37	-0.50 ± 0.05	38	-0.38 ± 0.04	5
HD029139	3891	1.20	1.97	-0.13 ± 0.13	21	-0.15 ± 0.00	2
HD029503	4470	2.50	1.48	-0.05 ± 0.12	37	-0.02 ± 0.05	6
HD030608	4620	2.39	1.37	-0.28 ± 0.06	38	-0.28 ± 0.03	7
HD045415	4775	2.66	1.40	-0.04 ± 0.05	41	-0.02 ± 0.10	7
HD050778	4034	1.40	1.72	-0.33 ± 0.12	35	-0.25 ± 0.08	5
HD073017	4715	2.54	1.11	-0.47 ± 0.06	33	-0.50 ± 0.06	6
HD099648	4937	2.24	1.76	-0.01 ± 0.06	41	-0.10 ± 0.05	6
HD100920	4788	2.58	1.34	-0.09 ± 0.07	44	-0.04 ± 0.06	7
HD115478	4272	2.00	1.55	-0.02 ± 0.07	44	-0.06 ± 0.07	7
HD116976	4691	2.49	1.63	0.18 ± 0.07	40	0.15 ± 0.06	7
HD117220	4871	2.75	1.06	-0.86 ± 0.07	38	-0.87 ± 0.06	7
HD117818	4802	2.59	1.48	-0.28 ± 0.06	41	-0.18 ± 0.04	7
HD128188	4657	2.03	1.17	-1.33 ± 0.08	33	-1.21 ± 0.04	6
HD132345	4400	2.34	1.67	0.38 ± 0.07	41	0.38 ± 0.09	6
HD142948	4800	2.37	1.45	-0.73 ± 0.08	36	-0.53 ± 0.06	7
HD171496	4975	2.40	1.32	-0.57 ± 0.08	48	-0.43 ± 0.09	6
HD172223	4471	2.46	1.73	0.18 ± 0.08	42	0.26 ± 0.07	6
HD174116	4079	0.94	1.64	-0.55 ± 0.08	40	-0.64 ± 0.07	6
HD175219	4720	2.44	1.42	-0.32 ± 0.06	43	-0.22 ± 0.04	6
HD186378	4566	2.42	1.48	0.06 ± 0.07	41	0.01 ± 0.04	5
HD187195	4405	2.36	1.41	0.16 ± 0.07	41	0.02 ± 0.07	6
HD211075	4305	1.76	1.55	-0.35 ± 0.06	38	-0.30 ± 0.07	5
HD212320	4950	2.47	1.61	-0.23 ± 0.06	35	-0.26 ± 0.08	7
HD214376	4586	2.55	1.46	0.07 ± 0.06	38	0.07 ± 0.09	5
HD215030	4713	2.55	1.23	-0.46 ± 0.06	35	-0.46 ± 0.07	6
HD221148	4700	3.18	0.92	0.46 ± 0.07	35	0.38 ± 0.10	4

Table 5. Final atmospheric parameters using the Kurucz models

Star (1)	$T_{\rm eff}$ [K] (2)	log g [dex] (3)	v_t [km/s] (4)	[FeI/H] ± σ (5)	N (6)	[FeII/H] ± σ (7)	N (8)
				Halo			
HD041667	4581	1.80	1.15	-1.04 ± 0.07	41	-0.95 ± 0.09	6
HD078050	5000	2.24	1.22	-0.93 ± 0.07	36	-0.79 ± 0.09	7
HD114095	4794	2.68	1.23	-0.60 ± 0.07	42	-0.62 ± 0.06	7
HD210295	4738	1.88	1.11	-1.30 ± 0.07	35	-1.35 ± 0.09	5
				Bulge			
I012	4237	1.61	1.52	-0.38 ± 0.08	26	-0.24 ± 0.07	3
I025	4370	2.25	1.70	0.48 ± 0.09	19	0.53 ± 0.11	4
I039	4386	2.20	1.63	0.36 ± 0.10	17	0.31 ± 0.19	2
I141	4356	1.93	1.41	-0.27 ± 0.09	27	-0.19 ± 0.09	3
I151	4400	1.73	1.27	-0.83 ± 0.09	25	-0.82 ± 0.07	2
I152	4663	2.67	1.27	-0.02 ± 0.09	23	0.13 ± 0.00	2
I156	4296	1.60	1.22	-0.78 ± 0.10	28	-0.81 ± 0.06	3
I158	4500	2.70	1.20	-0.03 ± 0.09	26	-0.10 ± 0.11	3
I194	4183	1.67	1.58	-0.34 ± 0.08	20	-0.42 ± 0.15	2
I202	4252	2.07	1.15	0.15 ± 0.10	26	0.25 ± 0.19	3
I264	4046	0.68	1.54	-1.26 ± 0.08	25	-1.27 ± 0.09	4
I322	4250	1.52	1.55	-0.15 ± 0.08	24	-0.27 ± 0.10	4
II033	4230	1.37	1.40	-0.78 ± 0.08	28	-0.70 ± 0.03	3
II119	4478	1.61	0.81	-1.21 ± 0.13	16	-1.14 ± 0.06	3
II154	4650	2.10	1.12	-0.69 ± 0.07	24	-0.61 ± 0.12	4
II172	4500	1.96	1.07	-0.37 ± 0.11	27	-0.45 ± 0.09	4
III152	4143	1.51	1.49	-0.54 ± 0.09	28	-0.51 ± 0.07	3
III220	4507	1.95	1.22	-0.34 ± 0.09	29	-0.26 ± 0.07	2
IV003	4500	1.35	1.24	-1.28 ± 0.06	19	-1.37 ± 0.09	3
IV047	4622	2.50	1.64	-0.41 ± 0.10	25	-0.36 ± 0.10	3
IV072	4276	2.13	1.44	0.15 ± 0.09	21	0.27 ± 0.07	2
IV167	4374	2.44	1.45	0.40 ± 0.12	21	0.42 ± 0.08	3
IV203	3815	0.35	1.88	-1.29 ± 0.08	37	-1.16 ± 0.05	5
IV325	4353	2.35	1.60	0.29 ± 0.07	20	0.33 ± 0.08	4
IV329	4153	1.15	1.55	-1.01 ± 0.08	20	-0.92 ± 0.08	4
				Thick Disk			
HD077236	4427	2.01	1.48	-0.67 ± 0.07	40	-0.70 ± 0.06	7
HD023940	4800	2.41	1.36	-0.31 ± 0.08	35	-0.27 ± 0.06	7
HD032440	3941	0.95	1.80	-0.33 ± 0.09	40	-0.14 ± 0.10	6
HD037763	4630	3.15	1.08	0.39 ± 0.07	41	0.49 ± 0.09	7
HD040409	4746	3.20	1.04	0.21 ± 0.07	42	0.30 ± 0.05	6
HD077729	4077	1.38	1.61	-0.49 ± 0.08	42	-0.38 ± 0.12	7
HD080811	4900	3.28	1.17	-0.51 ± 0.07	41	-0.46 ± 0.04	6
HD083212	4480	1.20	1.47	-1.43 ± 0.10	26	-1.24 ± 0.07	6
HD099978	4678	2.07	1.19	-1.07 ± 0.08	37	-1.02 ± 0.09	5
HD107328	4417	2.01	1.78	-0.40 ± 0.08	40	-0.29 ± 0.07	7
HD107773	4891	3.28	0.96	-0.39 ± 0.06	42	-0.30 ± 0.05	6
HD119971	4093	1.30	1.61	-0.69 ± 0.07	41	-0.60 ± 0.08	6
HD124897	4280	1.69	1.74	-0.49 ± 0.05	43	-0.41 ± 0.05	7
HD127243	4893	2.53	1.44	-0.69 ± 0.07	32	-0.52 ± 0.08	6
HD130952	4742	2.53	1.50	-0.34 ± 0.07	40	-0.25 ± 0.07	6
HD136014	4774	2.52	1.45	-0.46 ± 0.07	44	-0.32 ± 0.07	7
HD145148	4851	3.67	0.85	0.19 ± 0.06	41	0.27 ± 0.08	6
HD148451	4972	2.52	1.42	-0.55 ± 0.06	40	-0.52 ± 0.06	7
HD180928	4092	1.48	1.53	-0.47 ± 0.07	41	-0.38 ± 0.11	6
HD203344	4666	2.53	1.35	-0.13 ± 0.07	34	-0.09 ± 0.05	6
HD219615	4833	2.51	1.31	-0.52 ± 0.07	33	-0.41 ± 0.06	7
HD221345	4688	2.50	1.39	-0.27 ± 0.07	34	-0.22 ± 0.05	6
				Thin Disk			
HD000787	3970	1.06	1.91	-0.19 ± 0.11	38	-0.03 ± 0.07	5

Table 5 – continued

Star (1)	$T_{\rm eff}$ [K] (2)	log g [dex] (3)	v_t [km/s] (4)	[FeI/H] ± σ (5)	N (6)	[FeII/H] ± σ (7)	N (8)
HD003546	4878	2.43	1.39	-0.64 ± 0.07	33	-0.58 ± 0.06	7
HD005268	4873	2.54	1.36	-0.51 ± 0.05	38	-0.36 ± 0.04	5
HD029139	3891	1.20	1.94	-0.06 ± 0.13	21	0.07 ± 0.03	2
HD029503	4470	2.50	1.50	-0.05 ± 0.12	37	0.06 ± 0.05	6
HD030608	4620	2.39	1.36	-0.29 ± 0.06	38	-0.22 ± 0.03	7
HD045415	4775	2.66	1.42	-0.04 ± 0.05	41	0.07 ± 0.10	7
HD050778	4034	1.40	1.68	-0.31 ± 0.11	35	-0.16 ± 0.07	5
HD073017	4715	2.54	1.12	-0.47 ± 0.06	33	-0.44 ± 0.07	6
HD099648	4937	2.24	1.77	-0.03 ± 0.07	41	-0.06 ± 0.05	6
HD100920	4788	2.58	1.36	-0.12 ± 0.08	44	-0.04 ± 0.06	7
HD115478	4272	2.00	1.55	-0.02 ± 0.06	44	0.01 ± 0.06	7
HD116976	4691	2.49	1.63	0.17 ± 0.07	40	0.19 ± 0.06	7
HD117220	4871	2.75	1.06	-0.86 ± 0.07	38	-0.80 ± 0.06	7
HD117818	4802	2.59	1.47	-0.30 ± 0.06	41	-0.16 ± 0.04	7
HD128188	4657	2.03	1.14	-1.33 ± 0.08	33	-1.21 ± 0.04	6
HD132345	4400	2.34	1.62	0.42 ± 0.07	41	0.52 ± 0.09	6
HD142948	4800	2.37	1.45	-0.75 ± 0.08	36	-0.62 ± 0.05	7
HD171496	4975	2.40	1.30	-0.58 ± 0.09	48	-0.46 ± 0.10	6
HD172223	4471	2.46	1.72	0.21 ± 0.08	42	0.39 ± 0.07	6
HD174116	4079	0.94	1.64	-0.53 ± 0.08	40	-0.55 ± 0.06	6
HD175219	4720	2.44	1.42	-0.35 ± 0.06	43	-0.24 ± 0.04	6
HD186378	4566	2.42	1.51	0.08 ± 0.07	41	0.16 ± 0.04	5
HD187195	4405	2.36	1.37	0.20 ± 0.08	41	0.13 ± 0.06	6
HD211075	4305	1.76	1.55	-0.35 ± 0.06	38	-0.23 ± 0.07	5
HD212320	4950	2.47	1.64	-0.26 ± 0.06	35	-0.26 ± 0.07	7
HD214376	4586	2.55	1.47	0.10 ± 0.06	38	0.22 ± 0.09	5
HD215030	4713	2.55	1.21	-0.44 ± 0.07	35	-0.34 ± 0.07	6
HD221148	4700	3.18	0.85	0.51 ± 0.07	35	0.51 ± 0.10	4

Table 6. Abundance ratios using the MARCS models

Star (1)	[O/Fe] (2)	$\sigma_{[O/Fe]}$ (3)	[Na/Fe] (4)	$\sigma_{[Na/Fe]}$ (5)	[Mg/Fe] (6)	$\sigma_{[Mg/Fe]}$ (7)	[Al/Fe] (8)	$\sigma_{[Al/Fe]}$ (9)	[Si/Fe] (10)	$\sigma_{[Si/Fe]}$ (11)	[Ca/Fe] (12)	$\sigma_{[Ca/Fe]}$ (13)	[Ti/Fe] (14)	$\sigma_{[Ti/Fe]}$ (15)
Halo														
HD041667	0.26	0.01	-0.21	0.09	0.17	0.04	-0.27	0.12	0.22	0.12	0.33	0.07	0.25	0.08
HD078050	0.32	0.07	-0.20	0.07	0.20	0.06	-0.19	...	0.15	0.07	0.37	0.05	0.23	0.07
HD114095	0.59	...	0.14	0.06	0.31	0.06	0.17	0.05	0.22	0.10	0.26	0.08	0.32	0.07
HD210295	0.48	0.01	-0.02	0.09	0.32	0.07	...	...	0.25	0.13	0.44	0.07	0.30	0.08
Bulge														
I012	0.25	0.01	0.15	0.19	0.34	0.11	0.21	0.03	0.24	0.04	0.14	0.06	0.29	0.09
I025	-0.35	0.10	0.11	0.22	0.07	0.10	0.16	0.07	-0.05	0.04	0.00	0.04	-0.10	0.09
I039	0.00	0.15	0.36	0.03	0.21	0.05	...	...	0.08	0.11	-0.1	0.07	0.10	0.11
I141	0.40	0.10	0.12	0.11	0.27	0.09	0.27	0.16	0.22	0.04	0.21	0.07	0.31	0.08
I151	0.65	0.03	0.09	0.11	0.39	0.07	0.29	0.12	0.29	0.09	0.24	0.16	0.34	0.09
I152	0.40	0.05	0.04	0.25	0.06	0.11	0.09	0.15	0.08	0.11	0.19	0.10	0.29	0.14
I156	0.34	0.05	0.25	0.02	0.38	0.09	0.18	0.12	0.05	0.26	0.22	0.10	0.31	0.07
I158	0.51	0.01	-0.26	0.14	0.01	0.07	0.11	0.01	-0.08	0.27	-0.01	0.06	0.12	0.09
I194	0.18	0.05	0.13	0.10	0.31	0.24	...	...	0.22	0.07	0.10	0.10	0.30	0.07
I202	-0.15	...	0.07	...	0.01	0.07	0.33	0.01	0.02	0.08	0.15	0.08	0.18	0.07
I264	-0.39	0.04	0.68	0.11	0.4	0.15	0.86	0.10	0.35	0.06	0.45	0.11	0.36	0.11
I322	0.09	0.02	0.14	0.09	0.03	0.09	0.14	0.03	-0.03	0.03	0.11	0.05	0.11	0.08
II033	0.28	0.02	0.02	0.19	0.34	0.09	0.24	0.06	0.27	0.09	0.31	0.06	0.27	0.07
II119	0.48	0.13	-0.08	0.07	0.33	0.16	-0.06	...	0.24	0.06	0.34	0.15	0.30	0.09
II154	0.18	0.05	0.08	0.04	0.33	0.10	0.24	0.10	0.27	0.09	0.33	0.10	0.23	0.08
II172	0.12	0.03	0.19	0.11	0.33	0.10	0.33	0.06	0.04	0.04	0.32	0.12	0.35	0.07
III152	0.36	0.12	0.24	0.09	0.40	0.10	0.36	0.09	0.22	0.06	0.16	0.04	0.30	0.08
III220	0.25	0.15	0.01	0.01	0.22	0.06	0.27	0.15	0.22	0.11	0.16	0.14	0.32	0.08
IV003	0.45	0.03	0.02	0.16	0.34	0.09	0.04	0.04	0.20	0.11	0.44	0.09	0.34	0.08
IV047	0.43	...	0.09	...	0.39	0.08	0.27	0.11	0.15	0.07	0.19	0.06	0.45	0.10
IV072	-0.16	0.02	0.19	0.14	0.25	0.04	...	...	0.05	0.08	0.04	0.05	0.23	0.09
IV167	...	...	-0.28	...	0.00	0.31	0.20	0.02	-0.09	0.06	0.08	0.06	0.05	0.10
IV203	-0.04	0.05	0.26	0.10	0.47	0.05	0.34	0.14	0.43	0.08	0.21	0.10	0.26	0.12
IV325	-0.54	...	...	...	0.10	0.11	0.37	0.03	0.10	0.03	-0.12	0.12	0.10	0.12
IV329	0.33	0.03	0.28	0.23	0.37	0.08	0.18	0.04	0.47	0.12	0.21	0.10	0.28	0.10
Thick Disk														
HD077236	0.56	0.01	0.08	0.05	0.28	0.10	0.20	0.02	0.23	0.07	0.22	0.07	0.36	0.09
HD023940	0.33	...	0.07	0.08	0.25	0.10	0.00	0.03	0.12	0.09	0.06	0.05	0.26	0.15
HD032440	0.11	0.01	0.12	0.15	0.22	0.08	-0.08	...	0.14	0.11	-0.01	0.11	0.09	0.09
HD037763	0.09	...	-0.10	0.23	0.14	0.17	-0.10	0.15	0.01	0.08	-0.09	0.08	0.02	0.08
HD040409	0.09	0.13	-0.17	0.35	-0.05	0.06	-0.11	0.10	-0.01	0.10	-0.09	0.10	-0.01	0.07
HD077729	0.52	0.17	0.22	0.10	0.36	0.09	0.20	0.02	0.34	0.15	0.10	0.04	0.37	0.10
HD080811	0.51	...	0.09	0.13	0.32	0.03	0.25	0.05	0.29	0.07	0.23	0.07	0.44	0.11
HD083212	0.65	...	-0.19	0.02	0.41	0.13	...	...	0.30	0.03	0.22	0.08	0.19	0.08
HD099978	0.34	0.01	0.10	0.09	0.42	0.08	0.27	0.02	0.34	0.06	0.43	0.08	0.33	0.04
HD107328	0.56	0.01	0.12	0.09	0.33	0.06	0.10	0.10	0.26	0.04	0.07	0.09	0.28	0.05
HD107773	0.55	0.04	0.05	0.12	0.29	0.08	0.16	0.06	0.25	0.13	0.21	0.04	0.40	0.12
HD119971	0.50	0.03	0.10	0.04	0.42	0.06	0.26	0.28	0.33	0.10	0.12	0.05	0.27	0.11
HD124897	0.37	...	0.21	0.12	0.34	0.04	0.22	0.07	0.23	0.06	0.09	0.04	0.27	0.03
HD127243	0.55	0.08	0.13	0.05	0.36	0.04	0.13	0.03	0.27	0.09	0.23	0.08	0.26	0.08
HD130952	0.42	0.02	0.09	0.02	0.19	0.06	0.05	...	0.18	0.08	0.09	0.07	0.21	0.09
HD136014	0.44	0.03	0.06	0.05	0.24	0.06	0.18	0.18	0.19	0.07	0.11	0.04	0.22	0.09
HD145148	0.18	...	-0.17	0.26	-0.09	0.15	-0.14	0.05	-0.07	0.10	-0.08	0.06	0.02	0.09
HD148451	0.43	0.05	0.32	0.03	0.25	0.08	0.09	0.06	0.25	0.12	0.23	0.08	0.36	0.08
HD180928	0.47	0.01	0.23	0.09	0.38	0.06	0.38	0.25	0.27	0.12	0.15	0.06	0.37	0.10
HD203344	0.27	0.05	0.02	0.15	0.16	0.01	0.17	0.11	0.13	0.08	0.08	0.13	0.09	0.09
HD219615	0.41	0.06	0.15	0.07	0.26	0.05	0.13	0.02	0.20	0.07	0.19	0.07	0.22	0.06
HD221345	0.46	0.13	0.10	0.13	0.26	0.08	0.13	0.06	0.16	0.06	0.10	0.04	0.24	0.09
Thin Disk														
HD000787	0.15	...	0.31	0.09	0.07	0.11	0.25	0.13	0.13	0.12	-0.01	0.15	0.19	0.18
HD003546	0.21	...	0.08	0.04	0.16	0.03	0.12	0.08	0.22	0.03	0.19	0.10	0.18	0.08
HD005268	0.36	...	-0.01	0.01	0.07	0.10	0.01	0.06	0.06	0.04	0.09	0.08	0.12	0.10

Table 6 – continued

Star (1)	[O/Fe] (2)	$\sigma_{[\mathrm{O/Fe}]}$ (3)	[Na/Fe] (4)	$\sigma_{[\mathrm{Na/Fe}]}$ (5)	[Mg/Fe] (6)	$\sigma_{[\mathrm{Mg/Fe}]}$ (7)	[Al/Fe] (8)	$\sigma_{[\mathrm{Al/Fe}]}$ (9)	[Si/Fe] (10)	$\sigma_{[\mathrm{Si/Fe}]}$ (11)	[Ca/Fe] (12)	$\sigma_{[\mathrm{Ca/Fe}]}$ (13)	[Ti/Fe] (14)	$\sigma_{[\mathrm{Ti/Fe}]}$ (15)
HD029139	-0.11	0.15	0.26	0.26	-0.03	0.00	0.19	0.02	0.02	...	-0.23	0.16	0.14	0.21
HD029503	0.06	...	0.05	0.15	0.02	0.07	0.05	0.04	0.14	0.06	-0.11	0.14	-0.02	0.07
HD030608	0.27	...	0.04	0.13	0.00	0.06	-0.04	0.04	0.04	0.05	0.02	0.06	0.09	0.12
HD045415	0.04	0.07	-0.02	0.19	0.04	0.12	-0.07	0.05	-0.03	0.08	0.04	0.08	0.03	0.09
HD050778	0.27	...	-0.09	0.12	0.14	0.11	0.01	0.04	0.15	0.09	-0.05	0.10	0.21	0.14
HD073017	0.04	0.17	0.12	0.11	0.11	0.06	-0.05	0.00	0.03	0.03	0.12	0.09	0.06	0.06
HD099648	-0.05	0.02	0.30	0.10	-0.01	0.08	-0.07	0.01	0.00	0.09	0.08	0.08	0.01	0.11
HD100920	0.11	0.13	0.09	0.15	-0.02	0.1	-0.14	0.13	0.00	0.05	-0.01	0.06	0.02	0.09
HD115478	-0.06	...	0.03	0.20	0.05	0.09	0.02	0.01	0.02	0.09	-0.05	0.06	0.09	0.08
HD116976	0.09	0.25	0.29	0.22	0.03	0.07	0.11	0.13	0.06	0.11	-0.11	0.13	0.01	0.17
HD117220	0.36	0.03	0.07	0.02	0.22	0.06	0.07	0.08	0.21	0.10	0.21	0.07	0.15	0.02
HD117818	0.32	0.03	0.06	0.07	0.01	0.05	-0.01	0.08	0.10	0.08	0.02	0.05	0.04	0.06
HD128188	0.47	0.07	0.15	0.04	0.32	0.07	0.27	0.07	0.22	0.07	0.28	0.07	0.22	0.09
HD132345	-0.16	...	0.22	0.31	-0.20	0.08	-0.06	0.10	-0.03	0.09	-0.25	0.21	-0.20	0.21
HD142948	0.49	0.03	0.12	0.01	0.24	0.10	0.27	0.15	0.28	0.05	0.19	0.07	0.19	0.11
HD171496	0.28	0.06	0.01	0.04	0.14	0.07	-0.02	0.04	0.13	0.07	0.16	0.07	0.13	0.08
HD172223	-0.20	...	0.11	0.31	0.04	0.14	-0.04	0.08	-0.04	0.08	-0.19	0.14	-0.04	0.12
HD174116	-0.07	0.03	0.38	0.04	0.12	0.10	0.20	0.04	0.13	0.05	0.06	0.07	0.06	0.07
HD175219	0.34	0.17	0.10	0.04	0.05	0.08	-0.07	0.10	0.15	0.06	0.04	0.07	0.08	0.12
HD186378	-0.11	0.12	0.18	0.21	0.05	0.05	0.06	0.01	0.05	0.05	-0.03	0.11	-0.05	0.07
HD187195	0.03	0.20	0.16	0.31	0.05	0.14	0.09	0.06	0.08	0.15	-0.10	0.11	-0.02	0.09
HD211075	0.31	0.09	0.00	0.07	0.16	0.06	0.08	0.08	0.16	0.11	-0.01	0.06	0.09	0.07
HD212320	-0.13	...	0.32	0.10	0.02	0.05	-0.06	0.08	0.04	0.04	0.10	0.13	0.00	0.13
HD214376	0.00	0.14	-0.11	0.18	-0.07	0.16	0.00	0.06	0.03	0.03	-0.06	0.13	-0.01	0.05
HD215030	0.14	0.21	0.12	0.13	0.03	0.03	0.01	0.02	0.07	0.07	0.11	0.04	0.12	0.10
HD221148	-0.39	...	-0.03	0.33	-0.13	0.09	0.06	0.11	-0.05	0.08	-0.09	0.11	-0.01	0.08

Table 7. Abundance ratios using the Kurucz models

Star (1)	[O/Fe] (2)	$\sigma_{[O/Fe]}$ (3)	[Na/Fe] (4)	$\sigma_{[Na/Fe]}$ (5)	[Mg/Fe] (6)	$\sigma_{[Mg/Fe]}$ (7)	[Al/Fe] (8)	$\sigma_{[Al/Fe]}$ (9)	[Si/Fe] (10)	$\sigma_{[Si/Fe]}$ (11)	[Ca/Fe] (12)	$\sigma_{[Ca/Fe]}$ (13)	[Ti/Fe] (14)	$\sigma_{[Ti/Fe]}$ (15)
Halo														
HD041667	0.27	0.01	-0.18	0.09	0.19	0.05	-0.24	0.12	0.22	0.12	0.37	0.07	0.24	0.08
HD078050	0.36	0.07	-0.19	0.07	0.22	0.04	-0.19	...	0.14	0.07	0.39	0.05	0.25	0.07
HD114095	0.59	...	0.15	0.06	0.31	0.06	0.19	0.05	0.22	0.10	0.29	0.08	0.34	0.07
HD210295	0.45	0.01	0.00	0.09	0.33	0.07	...	...	0.24	0.14	0.48	0.07	0.33	0.08
Bulge														
I012	0.29	0.01	0.09	0.18	0.33	0.12	0.14	0.03	0.27	0.04	0.08	0.07	0.21	0.09
I025	-0.38	0.09	0.04	0.24	0.07	0.11	0.14	0.07	-0.04	0.04	-0.02	0.06	-0.13	0.09
I039	-0.03	0.15	0.33	0.02	0.22	0.06	...	...	0.10	0.13	-0.11	0.08	0.07	0.10
I141	0.43	0.10	0.07	0.12	0.26	0.09	0.22	0.15	0.23	0.05	0.16	0.07	0.25	0.08
I151	0.65	0.03	0.09	0.10	0.39	0.07	0.30	0.12	0.29	0.09	0.25	0.16	0.33	0.08
I152	0.38	0.05	0.03	0.27	0.07	0.11	0.10	0.15	0.08	0.11	0.22	0.11	0.31	0.14
I156	0.38	0.05	0.20	0.02	0.36	0.10	0.13	0.11	0.06	0.27	0.17	0.09	0.25	0.09
I158	0.58	0.02	-0.28	0.16	0.01	0.06	0.13	0.01	-0.09	0.27	0.03	0.06	0.14	0.09
I194	0.18	0.05	0.07	0.10	0.30	0.24	...	...	0.20	0.07	0.04	0.11	0.25	0.07
I202	-0.19	...	0.00	0.01	0.01	0.08	0.32	0.01	0.04	0.09	0.13	0.08	0.19	0.06
I264	-0.31	0.04	0.69	0.11	0.42	0.15	0.89	0.09	0.34	0.06	0.47	0.10	0.36	0.12
I322	0.14	0.02	0.12	0.09	0.01	0.09	0.13	0.03	-0.03	0.03	0.10	0.05	0.09	0.00
II033	0.32	0.02	-0.03	0.19	0.32	0.09	0.20	0.06	0.28	0.10	0.25	0.06	0.22	0.08
II119	0.52	0.12	-0.09	0.07	0.31	0.16	-0.07	...	0.24	0.06	0.33	0.14	0.29	0.11
II154	0.26	0.06	0.07	0.06	0.32	0.10	0.21	0.10	0.30	0.09	0.30	0.10	0.20	0.07
II172	0.19	0.03	0.16	0.09	0.31	0.11	0.26	0.05	0.05	0.05	0.26	0.13	0.28	0.07
III152	0.35	0.12	0.17	0.08	0.38	0.11	0.29	0.09	0.23	0.06	0.10	0.04	0.24	0.09
III220	0.28	0.15	-0.02	...	0.19	0.07	0.22	0.14	0.22	0.12	0.23	0.15	0.28	0.11
IV003	0.45	0.03	0.04	0.16	0.35	0.08	0.05	0.04	0.19	0.11	0.46	0.08	0.36	0.08
IV047	0.47	...	0.09	...	0.38	0.09	0.24	0.10	0.15	0.07	0.16	0.05	0.43	0.09
IV072	-0.20	0.02	0.14	0.17	0.26	0.04	...	...	0.07	0.08	0.04	0.06	0.21	0.09
IV167	...	...	-0.35	...	0.01	0.32	0.22	0.02	-0.07	0.07	0.11	0.06	0.05	0.10
IV203	-0.11	0.03	0.33	0.08	0.50	0.06	0.40	0.14	0.43	0.08	0.29	0.10	0.29	0.12
IV325	-0.58	...	...	...	0.10	0.11	0.34	0.03	0.11	0.03	-0.14	0.13	0.05	0.12
IV329	0.32	0.03	0.26	0.23	0.37	0.08	0.16	0.04	0.49	0.12	0.19	0.11	0.24	0.11
Thick Disk														
HD077236	0.51	0.01	0.07	0.05	0.27	0.10	0.19	0.02	0.22	0.07	0.22	0.07	0.35	0.09
HD023940	0.37	...	0.08	0.07	0.25	0.10	0.00	0.03	0.13	0.09	0.07	0.05	0.26	0.15
HD032440	0.09	0.01	0.07	0.15	0.20	0.08	-0.13	...	0.14	0.10	-0.04	0.11	0.05	0.09
HD037763	0.04	...	-0.17	0.26	0.13	0.17	-0.11	0.17	0.00	0.08	-0.09	0.09	-0.01	0.08
HD040409	0.10	0.13	-0.20	0.36	-0.06	0.05	-0.12	0.11	0.01	0.09	-0.09	0.10	-0.03	0.07
HD077729	0.45	0.18	0.17	0.11	0.36	0.09	0.17	0.02	0.36	0.15	0.10	0.05	0.31	0.08
HD080811	0.51	...	0.08	0.14	0.31	0.03	0.24	0.05	0.29	0.07	0.24	0.06	0.45	0.11
HD083212	0.62	...	-0.16	0.02	0.42	0.12	...	...	0.30	0.04	0.27	0.08	0.19	0.07
HD099978	0.33	0.01	0.11	0.09	0.42	0.09	0.28	0.02	0.33	0.06	0.46	0.08	0.34	0.03
HD107328	0.57	0.01	0.09	0.08	0.32	0.06	0.06	0.10	0.27	0.05	0.03	0.09	0.23	0.05
HD107773	0.60	0.04	0.06	0.12	0.29	0.08	0.16	0.06	0.26	0.13	0.23	0.04	0.40	0.11
HD119971	0.48	0.03	0.14	0.06	0.44	0.07	0.28	0.27	0.33	0.10	0.14	0.06	0.27	0.11
HD124897	0.41	...	0.16	0.12	0.33	0.04	0.17	0.07	0.26	0.05	0.04	0.05	0.21	0.03
HD127243	0.56	0.08	0.14	0.05	0.36	0.04	0.13	0.03	0.26	0.09	0.25	0.07	0.28	0.07
HD130952	0.43	0.02	0.10	0.03	0.19	0.06	0.06	...	0.18	0.09	0.11	0.06	0.23	0.09
HD136014	0.49	0.03	0.07	0.04	0.24	0.06	0.18	0.18	0.20	0.07	0.12	0.04	0.22	0.09
HD145148	0.16	...	-0.21	0.28	-0.11	0.15	-0.14	0.05	-0.08	0.09	-0.07	0.07	0.01	0.09
HD148451	0.42	0.05	0.33	0.04	0.25	0.08	0.10	0.06	0.23	0.11	0.26	0.07	0.39	0.08
HD180928	0.49	...	0.20	0.09	0.38	0.06	0.35	0.25	0.28	0.12	0.13	0.06	0.33	0.09
HD203344	0.26	0.05	0.03	0.16	0.16	0.01	0.18	0.11	0.11	0.08	0.11	0.13	0.11	0.09
HD219615	0.46	0.06	0.15	0.05	0.25	0.05	0.11	0.02	0.21	0.08	0.19	0.06	0.22	0.07
HD221345	0.48	0.16	0.10	0.13	0.26	0.08	0.11	0.06	0.15	0.06	0.10	0.04	0.23	0.09
Thin Disk														
HD000787	0.14	...	0.25	0.08	0.06	0.11	0.20	0.13	0.15	0.12	-0.05	0.15	0.13	0.17
HD003546	0.14	...	0.10	0.04	0.18	0.03	0.15	0.08	0.21	0.03	0.24	0.10	0.22	0.08

Table 7 – continued

Star (1)	[O/Fe] (2)	$\sigma_{[O/Fe]}$ (3)	[Na/Fe] (4)	$\sigma_{[Na/Fe]}$ (5)	[Mg/Fe] (6)	$\sigma_{[Mg/Fe]}$ (7)	[Al/Fe] (8)	$\sigma_{[Al/Fe]}$ (9)	[Si/Fe] (10)	$\sigma_{[Si/Fe]}$ (11)	[Ca/Fe] (12)	$\sigma_{[Ca/Fe]}$ (13)	[Ti/Fe] (14)	$\sigma_{[Ti/Fe]}$ (15)
HD005268	0.37	...	0.01	0.01	0.08	0.10	0.03	0.06	0.06	0.04	0.13	0.08	0.15	0.10
HD029139	-0.18	0.14	0.21	0.29	-0.02	0.00	0.17	0.02	0.04	...	-0.25	0.14	0.11	0.21
HD029503	0.06	...	0.05	0.14	0.02	0.07	0.04	0.04	0.15	0.07	-0.10	0.14	-0.02	0.07
HD030608	0.27	...	0.04	0.13	0.01	0.06	-0.04	0.05	0.05	0.05	0.03	0.06	0.09	0.12
HD045415	0.07	0.07	-0.03	0.18	0.04	0.12	-0.08	0.05	-0.02	0.08	0.04	0.08	0.02	0.09
HD050778	0.19	...	0.08	0.14	0.14	0.11	0.00	0.04	0.16	0.10	-0.06	0.10	0.17	0.12
HD073017	0.08	0.17	0.13	0.10	0.11	0.06	-0.06	...	0.04	0.03	0.13	0.09	0.06	0.06
HD099648	-0.02	0.02	0.31	0.10	0.00	0.08	-0.06	0.01	0.01	0.09	0.10	0.08	0.00	0.10
HD100920	0.11	0.13	0.10	0.15	0.00	0.10	-0.12	0.13	0.01	0.05	0.03	0.06	0.03	0.08
HD115478	-0.05	...	0.02	0.21	0.14	0.04	0.02	0.01	0.02	0.09	-0.05	0.06	0.09	0.08
HD116976	0.08	0.17	0.28	0.23	0.03	0.07	0.11	0.14	0.06	0.11	-0.09	0.13	0.01	0.17
HD117220	0.40	0.03	0.08	0.02	0.23	0.06	0.08	0.08	0.23	0.10	0.23	0.07	0.16	0.03
HD117818	0.33	0.03	0.08	0.07	0.02	0.05	0.00	0.08	0.10	0.08	0.06	0.05	0.06	0.06
HD128188	0.46	0.07	0.17	0.04	0.34	0.07	0.29	0.07	0.21	0.06	0.33	0.07	0.26	0.09
HD132345	-0.22	...	0.17	0.35	-0.21	0.08	-0.06	0.10	-0.01	0.09	-0.25	0.21	-0.24	0.21
HD142948	0.41	0.03	0.15	0.01	0.26	0.09	0.30	0.15	0.25	0.04	0.24	0.07	0.23	0.11
HD171496	0.23	0.06	0.03	0.04	0.15	0.08	0.00	0.04	0.11	0.07	0.21	0.07	0.17	0.08
HD172223	-0.22	...	0.08	0.32	0.03	0.14	-0.06	0.07	-0.03	0.08	-0.21	0.14	-0.07	0.11
HD174116	-0.08	0.03	0.36	0.04	0.11	0.11	0.17	0.04	0.13	0.05	0.04	0.07	0.03	0.07
HD175219	0.33	0.17	0.12	0.05	0.06	0.08	-0.05	0.10	0.15	0.06	0.08	0.07	0.10	0.11
HD186378	-0.08	0.12	0.17	0.20	0.05	0.05	0.03	0.01	0.08	0.06	-0.05	0.11	-0.08	0.07
HD187195	-0.01	0.21	0.13	0.34	0.03	0.15	0.09	0.05	0.09	0.14	-0.10	0.11	-0.05	0.1
HD211075	0.34	0.08	-0.01	0.08	0.16	0.05	0.09	0.08	0.17	0.11	-0.01	0.06	0.06	0.07
HD212320	-0.12	...	0.35	0.10	0.04	0.05	-0.04	0.09	0.05	0.04	0.13	0.13	0.03	0.13
HD214376	0.03	0.14	-0.14	0.18	-0.08	0.15	-0.03	0.07	0.05	0.03	-0.09	0.13	-0.05	0.06
HD215030	0.19	0.21	0.11	0.12	0.02	0.04	-0.02	0.02	0.08	0.07	0.09	0.03	0.09	0.09
HD221148	-0.42	...	-0.09	0.34	-0.16	0.09	0.03	0.11	-0.07	0.07	-0.11	0.11	-0.02	0.08

Online Material

Table 8. Line list and measured equivalent widths given in mÅ

λ [Å] (1)	χ [eV] (2)	$\log gf$ (3)	HD041667 (4)	HD078050 (5)	HD114095 (6)	HD210295 (7)	I012 (8)	I025 (9)	I039 (10)	I141 (11)	I151 (12)	I152 (13)	I156 (14)	I158 (15)
FeI														
5560.21	4.43	-1.120	41.3	29.1	48.6	23.2	73.0	109.0	96.0	69.0	47.0	79.0	56.0	79.0
5633.95	4.99	-0.180	...	41.6	59.3	29.3	80.0	136.0	...	81.0	56.0	...	62.0	94.0
5638.26	4.22	-0.800	64.3	61.5	76.9	47.8	105.0	...	...	100.0	...	110.0	84.0	103.0
5651.47	4.47	-1.850	9.5	...	18.6	5.3	36.0	76.0	65.0	40.0	21.0	48.0	23.0	44.0
5662.52	4.18	-0.573	81.6	73.4	98.3	62.7	...	...	...	119.0	91.0	128.0	96.0	121.0
5679.02	4.65	-0.810	40.3	36.0	54.0	26.7	...	115.0	99.0	81.0	51.0	...	50.0	76.0
5731.76	4.26	-1.110	45.7	39.4	57.8	30.2	86.0	129.0	...	81.0	65.0	81.0	67.0	86.0
5775.08	4.22	-1.230	46.9	40.5	62.6	30.8	88.0	116.0	122.0	82.0	69.0	82.0	61.0	...
5778.45	2.59	-3.430	33.6	18.0	43.4	15.3	82.0	112.0	...	80.0	...	69.0	54.0	79.0
5811.91	4.14	-2.440	...	5.3	12.8	2.6	...	70.0	56.0	38.0	16.0	28.0	21.0	37.0
5853.15	1.49	-5.260	19.5	...	26.0	10.7	65.0	...	88.0	...	...	54.0	47.0	62.0
5902.47	4.59	-1.880	8.3	5.9	16.2	...	33.0	66.0	63.0	32.0	...	...	...	29.0
5916.25	2.45	-2.994	74.2	52.5	80.9	48.4	...	...	...	...	...	...	...	...
5956.69	0.86	-4.608	88.6	60.0	93.0	62.4	...	...	...	...	...	...	...	...
6027.05	4.08	-1.089	56.6	50.0	69.0	39.2	99.0	...	...	94.0	73.0	...	70.0	93.0
6056.00	4.73	-0.480	51.2	49.2	67.4	35.9	...	...	120.0	...	...	...	...	...
6065.48	2.61	-1.530	...	114.0	...	...	...	...	...	...	...	...	...	86.0
6078.49	4.79	-0.400	52.4	48.2	69.5	36.8	93.0	...	...	...	63.0	89.0	73.0	...
6093.64	4.61	-1.430	22.9	15.3	29.0	10.8	50.0	84.0	77.0	49.0	27.0	54.0	32.0	52.0
6096.67	3.98	-1.900	30.2	22.0	44.6	18.9	78.0	107.0	97.0	71.0	45.0	67.0	50.0	62.0
6098.24	4.56	-1.810	12.4	7.1	15.2	...	37.0	66.0	65.0	32.0	17.0	40.0	18.0	43.0
6120.25	0.92	-5.970	17.9	7.0	21.4	8.6	76.0	110.0	...	65.0	41.0	53.0	43.0	65.0
6151.62	2.18	-3.299	66.3	46.8	74.1	43.8	121.0	...	...	114.0	89.0	110.0	94.0	...
6173.34	2.22	-2.880	91.0	68.5	92.5	65.8	82.0	...	...	...	...	...	...	...
6187.99	3.94	-1.690	44.2	30.9	55.2	24.6	...	...	118.0	80.0	62.0	...	55.0	...
6240.65	2.22	-3.320	67.0	46.1	76.0	42.8	...	...	...	...	...	...	...	...
6246.32	3.60	-0.877	...	92.5	...	...	...	...	...	...	...	...	...	...
6252.56	2.40	-1.687	...	114.7	...	...	...	...	...	...	...	...	...	...
6301.50	3.65	-0.718	100.5	94.2	...	...	...	...	...	...	...	...	...	...
6302.49	3.69	-1.310	74.8	...	83.4	...	115.0	...	...	125.0	84.0	...	...	124.0
6322.69	2.59	-2.426	86.2	72.0	92.8	13.8	...	...	...	...	...	...	...	...
6392.54	2.28	-4.070	24.6	14.6	35.1	67.2	...	...	...	...	...	...	...	...
6393.60	2.43	-1.580	...	120.9	...	...	...	...	...	...	...	...	...	...
6481.87	2.28	-2.984	81.3	65.0	94.3	60.0	...	...	...	...	...	...	...	...
6518.37	2.83	-2.570	66.1	53.4	71.1	44.3	...	...	...	116.0	85.0	...	86.0	...
6574.23	0.99	-5.004	62.4	...	75.3	35.7	...	...	...	...	...	...	...	...
6593.87	2.43	-2.422	100.9	...	104.0	79.4	...	...	...	...	...	...	...	...
6677.99	2.69	-1.418	...	118.5	...	...	...	...	...	...	...	...	...	...
6703.57	2.76	-3.080	44.2	28.0	53.9	27.1	...	...	...	...	...	...	...	...
6725.36	4.10	-2.260	16.3	9.2	20.4	6.8	42.0	75.0	74.0	44.0	24.0	53.0	31.0	45.0
6726.67	4.61	-1.140	28.6	22.3	42.5	16.1	70.0	100.0	102.0	68.0	42.0	74.0	46.0	70.0
6842.69	4.64	-1.200	30.8	...	36.5	12.9	61.0	94.0	90.0	67.0	43.0	69.0	45.0	69.0
6857.25	4.08	-2.190	18.4	...	24.6	10.0	48.0	79.0	84.0	49.0	29.0	57.0	32.0	58.0
6858.15	4.61	-0.930	...	...	46.9	19.9	...	...	...	...	...	...	...	...
7114.55	2.69	-4.070	12.0	...	15.9	...	54.0	80.0	...	41.0	19.0	47.0	27.0	45.0
7421.56	4.64	-1.680	12.5	...	16.5	...	37.0	...	61.0	33.0	...	43.0	18.0	42.0
7531.15	4.37	-0.590	70.0	...	81.5	...	...	...	...	...	...	...	...	...
7547.90	5.10	-1.080	15.1	...	...	...	29.0	83.0	...	37.0	17.0	45.0	18.0	36.0
7723.21	2.28	-3.617	59.9	...	63.7	...	120.0	...	...	...	88.0	107.0	79.0	97.0
FeII														
5264.81	3.23	-3.130	39.8	54.5	36.7	...	...	...	...	...	...	...	...	...
5425.26	3.20	-3.220	...	44.7	35.1	...	...	67.0	...	...	...	...	...	...
5435.26	3.20	-3.220	...	...	...	...	...	...	...	...	...	...	...	...
6247.56	3.89	-2.300	47.6	54.5	38.8	37.0	45.0	57.0	51.0	44.0	36.0	...	31.0	36.0
6369.46	2.89	-4.110	18.6	22.8	17.6	10.8	...	...	...	...	...	...	...	...
6432.68	2.89	-3.570	38.3	46.1	37.7	31.9	46.0	64.0	60.0	49.0	38.0	56.0	34.0	41.0
6456.38	3.90	-2.050	56.9	70.7	55.3	50.6	60.0	78.0	...	54.0	...	70.0	42.0	49.0
6516.08	2.89	-3.310	53.1	62.0	46.7	42.3	...	...	...	...	...	...	...	...
[O I]														
6300.30	0.00	-9.720	27.0	20.0	32.0	24.8	63.0	35.0	50.3	53.0	58.0	56.0	42.0	58.0
6363.78	0.02	-10.190	10.4	9.0	12.7	9.7	28.0	18.0	31.0	30.0	25.0	22.0	20.0	26.0
NaI														
5682.64	2.10	-0.706	...	...	104.7	33.8	...	208.0	...	128.0	89.0	127.0	107.0	124.0
5688.20	2.10	-0.406	69.3	62.7	120.1	54.9	130.0	236.0	...	170.0	118.0	171.0	130.0	155.0
6154.23	2.10	-1.547	15.3	7.5	38.8	10.8	156.0	158.0	146.0	89.0	...	98.0	55.0	78.0
6160.75	2.10	-1.246	19.5	17.0	59.7	13.9	97.0	...	171.0	98.0	...	...	...	...
MgI														
4702.99	4.35	-0.471	...	170.0	...	...	...	...	...	...	...	...	...	...
4730.03	4.35	-2.389	...	45.0	...	...	...	...	...	...	...	...	...	...
5528.40	4.35	-0.522	...	168.0	...	156.7	162.0	...	...	...	...	...	...	...
5711.09	4.34	-1.729	89.9	82.8	117.8	79.9	...	...	...	155.0	117.0	...	130.0	150.0
6318.72	5.11	-1.945	30.0	28.5	51.3	17.8	75.0	116.0	120.0	73.0	...	81.0	57.0	70.0
6319.24	5.11	-2.165	19.8	...	40.6	13.0	65.0	94.0	100.0	66.0	47.0	56.0	40.0	61.0
6765.45	5.75	-2.000	7.5	...	21.6	...	...	...	...	36.0	18.0	...	...	...
6894.92	5.75	-1.620	14.4	...	...	...	...	...	...	...	...	...	...	...
7387.69	5.75	-1.070	33.6	...	71.6	...	94.0	147.0	...	89.0	63.0	102.0	65.0	88.0

Table 8 – continued

λ [Å] (1)	χ [eV] (2)	log*gf* (3)	HD041667 (4)	HD078050 (5)	HD114095 (6)	HD210295 (7)	I012 (8)	I025 (9)	I039 (10)	I141 (11)	I151 (12)	I152 (13)	I156 (14)	I158 (15)
AlI														
6696.02	3.14	-1.481	13.5	...	54.1	...	94.0	146.0	...	6.61	66.0	96.0	63.0	97.0
6698.67	3.14	-1.782	10.4	7.0	33.2	...	71.0	132.0	...	6.40	38.0	64.0	36.0	77.0
SiI														
5488.98	5.61	-1.690	15.9	12.0	22.2	10.8	...	50.0	...	...	...	...	...	...
5701.10	4.93	-1.950	27.2	29.4	41.4	21.4	60.0	78.0	74.0	57.0	44.0	68.0	20.0	56.0
5772.15	5.08	-1.740	...	34.2	...	...	...	...	...	...	...	...	...	...
6142.48	5.62	-1.410	16.9	17.0	31.8	11.2	40.0	59.0	56.0	41.0	26.0	43.0	26.0	34.0
7235.33	5.62	-1.390	24.1	...	40.1	...	42.0	...	...	...	27.0	...	...	43.0
7235.82	5.62	-1.600	...	...	30.4	...	30.0	46.0	...	...	...	...	...	29.4
7250.63	5.62	-1.050	...	...	41.6	...	...	80.0	...	62.0	...	65.0	40.0	27.0
7423.50	5.62	-0.420	69.7	...	86.8	...	...	130.0	133.0	101.0	85.0	113.0	...	93.0
7800.00	6.18	-0.710	31.3	...	39.0	...	...	...	74.0	...	...	...	...	...
CaI														
5512.98	2.93	-0.464	80.5	69.5	91.0	61.1	125.0	174.0	...	134.0	103.0	128.0	100.0	...
5590.11	2.52	-0.571	90.5	86.9	102.7	79.7	...	...	...	148.0	105.0	...	114.0	...
5867.56	2.93	-1.570	26.2	18.5	35.2	15.7	72.0	112.0	102.0	68.0	38.0	...	41.0	72.0
6156.02	2.52	-2.420	15.4	...	19.3	5.7	46.0	...	76.0	...	...	51.0	25.0	51.0
6166.44	2.52	-1.142	69.5	61.0	88.2	55.0	...	...	156.0	...	...	...	...	...
6169.04	2.52	-0.797	92.3	81.0	112.1	77.9	...	...	...	...	...	...	...	...
6455.60	2.52	-1.340	61.5	53.0	82.0	49.7	119.0	166.0	...	120.0	...	119.0	...	108.0
6471.66	2.52	-0.686	99.9	...	111.9	80.6	...	...	...	151.0	120.0	...	126.0	143.0
6499.65	2.52	-0.818	89.9	83.5	103.9	72.5	...	...	...	...	...	...	...	...
TiI														
5020.03	0.84	-0.195	109.4	88.5	...	...	...	...	...	...	...	...	...	...
5024.84	0.82	-0.362	99.6	83.0	...	...	...	...	...	...	...	...	...	...
5210.39	0.05	-0.700	138.6	107.9	...	...	...	...	...	...	...	...	...	...
5453.64	1.44	-1.610	...	...	26.5	6.9	82.0	101.0	...	...	...	...	...	...
5460.47	0.05	-2.804	38.0	16.9	...	20.7	...	95.0	...	...	...	...	...	...
5648.57	2.50	-0.250	...	7.2	31.2	8.7	...	...	99.0	72.0	36.0	60.0	49.0	57.0
5739.46	2.25	-0.600	...	6.5	27.0	7.0	77.0	96.0	90.0	73.0	38.0	63.0	46.0	65.0
5913.71	0.02	-4.100	...	...	6.8	...	63.0	72.0	...	58.0	25.0	...	...	...
5918.54	1.07	-1.470	...	18.0	54.5	16.3	114.0	134.0	...	115.0	78.0	94.0	81.0	...
5944.65	0.00	-3.910	...	...	...	...	80.0	92.0	90.0	60.0	30.0	45.0	38.0	53.0
6092.80	1.89	-1.378	...	...	19.5	...	71.0	88.0	87.0	66.0	30.0	45.0	36.0	52.0
6258.10	1.44	-0.355	74.7	55.0	...	54.4	...	...	...	...	...	...	...	...
6261.10	1.43	-0.479	78.0	51.8	...	50.2	...	...	...	...	...	...	...	...
6273.39	0.02	-4.170	...	...	...	...	...	...	86.0	...	...	...	...	...
6706.29	1.50	-2.780	...	...	...	...	14.0	27.0	...	...	...	...	...	...
6716.71	2.49	-1.010	...	...	6.5	...	38.0	59.0	68.0	35.0	13.0	29.0	17.0	33.0
6746.31	1.89	-2.000	...	...	...	...	...	...	56.0	...	...	...	...	...
7138.08	1.43	-2.760	...	...	...	...	23.0	43.0	38.0	...	...	...	...	...
7352.16	2.49	-0.980	...	...	9.4	...	38.0	66.0	69.0	34.0	14.0	40.0	...	33.0
7391.52	1.50	-2.610	...	...	...	...	28.0	50.0	...	...	...	29.0	...	21.0

Table 9. Line list and measured equivalent widths given in mÅ

λ [Å] (1)	χ [eV] (2)	log*gf* (3)	I194 (4)	I202 (5)	I264 (6)	I322 (7)	II033 (8)	II119 (9)	II154 (10)	II172 (11)	III152 (12)	III220 (13)	IV003 (14)	IV047 (15)	IV072 (16)	IV167 (17)	IV325 (18)	IV329 (19)	IV203 (20)
FeI																			
5560.21	4.43	-1.120	...	76.0	48.0	89.0	60.0	33.0	51.0	58.0	66.0	68.0	32.0	63.0	86.0	90.0	...	52.0	43.1
5633.95	4.99	-0.180	94.0	97.0	52.0	95.0	67.0	38.0	56.0	70.0	78.0	76.0	40.0	88.0	103.0	121.0	110.0	...	52.4
5638.26	4.22	-0.800	...	112.0	78.0	118.0	86.0	55.0	74.0	86.0	92.0	97.0	59.0	97.0	...	...	...	...	84.1
5651.47	4.47	-1.850	39.0	52.0	17.0	53.0	20.0	...	...	33.0	31.0	37.0	...	32.0	51.0	62.0	52.0	...	13.4
5662.52	4.18	-0.573	122.0	...	95.0	...	102.0	74.0	89.0	100.0	117.0	108.0	...	113.0	...	...	...	...	107.0
5679.02	4.65	-0.810	77.0	79.0	45.0	93.0	62.0	...	56.0	...	76.0	73.0	40.0	79.0	86.0	...	97.0	...	52.1
5731.76	4.26	-1.110	...	88.0	61.0	102.0	72.0	37.0	57.0	72.0	78.0	74.0	40.0	82.0	...	109.0	117.0	64.0	63.0
5775.08	4.22	-1.230	88.0	89.0	55.0	99.0	73.0	...	59.0	75.0	77.0	80.0	43.0	78.0	106.0	113.0	110.0	68.0	...
5778.45	2.59	-3.430	84.0	88.0	57.0	99.0	67.0	32.0	42.0	70.0	67.0	62.0	35.0	...	101.0	97.0	101.0	62.0	...
5811.91	4.14	-2.440	35.0	42.0	9.0	35.0	16.0	...	14.0	22.0	25.0	34.0	...	...	45.0	51.0	51.0	...	12.6
5853.15	1.49	-5.260	75.0	...	...	...	...	...	...	...	64.0	43.0	...	...	79.0	...	...	...	62.2
5902.47	4.59	-1.880	26.0	48.0	...	42.0	17.0	...	17.0	24.0	...	30.0	...	...	49.0	54.0	56.0	12.0	11.6
5916.25	2.45	-2.994	...	...	...	...	...	...	...	...	...	...	...	...	...	...	...	...	111.3
5956.69	0.86	-4.608	...	...	...	...	...	...	...	...	...	...	...	...	...	...	...	...	157.9
6027.05	4.08	-1.089	...	99.0	70.0	104.0	82.0	42.0	72.0	76.0	88.0	87.0	54.0	83.0	...	112.0	...	75.0	79.4
6056.00	4.73	-0.480	84.0	...	...	...	...	...	...	...	...	...	...	...	103.0	...	...	...	64.4
6065.48	2.61	-1.530	...	...	...	...	...	...	...	...	...	...	...	...	...	...	...	...	...
6078.49	4.79	-0.400	90.0	104.0	57.0	105.0	67.0	...	67.0	88.0	85.0	79.0	45.0	95.0	111.0	...	...	67.0	62.5
6093.64	4.61	-1.430	51.0	60.0	25.0	68.0	40.0	...	32.0	43.0	44.0	48.0	13.0	49.0	62.0	83.0	77.0	29.0	...
6096.67	3.98	-1.900	67.0	74.0	42.0	81.0	57.0	22.0	40.0	56.0	62.0	63.0	21.0	57.0	80.0	99.0	97.0	52.0	43.8
6098.24	4.56	-1.810	39.0	58.0	17.0	54.0	22.0	11.0	...	32.0	34.0	31.0	...	30.0	60.0	56.0	62.0	...	...
6120.25	0.92	-5.970	...	82.0	56.0	86.0	57.0	...	26.0	55.0	70.0	52.0	17.0	46.0	...	97.0	93.0	...	84.0
6151.62	2.18	-3.299	...	125.0	105.0	...	102.0	60.0	83.0	89.0	114.0	105.0	...	102.0	...	...	...	99.0	128.7
6173.34	2.22	-2.880	...	...	...	...	...	...	...	...	...	...	...	...	...	...	...	...	150.6
6187.99	3.94	-1.690	79.0	88.0	53.0	98.0	70.0	32.0	52.0	76.0	71.0	...	33.0	70.0	101.0	111.0	108.0	64.0	54.8
6240.65	2.22	-3.320	...	...	...	...	...	...	...	...	...	...	...	...	...	...	...	...	118.9
6246.32	3.60	-0.877	...	...	...	...	...	...	...	...	...	...	...	...	...	...	...	...	...
6252.56	2.40	-1.687	...	...	...	...	...	...	...	...	...	...	...	...	...	...	...	...	...
6301.50	3.65	-0.718	...	...	...	...	...	...	...	...	...	...	...	...	...	...	...	...	138.0
6302.49	3.69	-1.310	...	...	96.0	...	98.0	67.0	...	102.0	117.0	106.0	...	114.0	130.0	...	...	95.0	107.6
6322.69	2.59	-2.426	...	...	...	...	...	...	...	...	...	...	...	...	...	...	...	...	...
6392.54	2.28	-4.070	...	...	...	...	...	...	...	...	...	...	...	...	...	...	...	...	71.0
6393.60	2.43	-1.580	...	...	...	...	...	...	...	...	...	...	...	...	...	...	...	...	...
6481.87	2.28	-2.984	...	...	...	...	...	...	...	...	...	...	...	...	...	...	...	...	136.3
6518.37	2.83	-2.570	116.0	122.0	...	...	94.0	...	77.0	89.0	...	99.0	62.0	108.0	...	...	...	...	104.0
6574.23	0.99	-5.004	...	...	...	...	...	...	...	...	...	...	...	...	...	...	...	...	139.6
6593.87	2.43	-2.422	...	...	...	...	...	...	...	...	...	...	...	...	...	...	...	...	...
6677.99	2.69	-1.418	...	...	...	...	...	...	...	...	...	...	...	...	...	...	...	...	...
6703.57	2.76	-3.080	...	...	...	...	...	...	...	...	...	...	...	...	...	...	...	...	90.3
6725.36	4.10	-2.260	39.0	52.0	20.0	55.0	31.0	...	22.0	32.0	35.0	34.0	11.0	30.0	58.0	73.0	69.0	25.0	18.0
6726.67	4.61	-1.140	61.0	72.0	44.0	84.0	52.0	30.0	44.0	63.0	59.0	57.0	27.0	67.0	77.0	88.0	88.0	44.0	36.0
6842.69	4.64	-1.200	...	72.0	37.0	73.0	50.0	20.0	38.0	54.0	50.0	59.0	20.0	48.0	74.0	87.0	82.0	39.0	40.0
6857.25	4.08	-2.190	47.0	67.0	20.0	64.0	37.0	12.0	29.0	43.0	39.0	42.0	13.0	39.0	65.0	75.0	71.0	28.0	25.6
6858.15	4.61	-0.930	...	...	...	...	...	...	...	...	...	...	...	...	...	...	...	...	42.3
7114.55	2.69	-4.070	...	59.0	34.0	66.0	34.0	13.0	...	37.0	40.0	42.0	...	...	...	76.0	66.0	25.0	38.2
7421.56	4.64	-1.680	33.0	49.0	13.0	47.0	25.0	...	16.0	34.0	35.0	32.0	...	26.0	52.0	58.0	60.0	19.0	20.0
7531.15	4.37	-0.590	...	...	...	...	...	...	...	...	...	...	...	...	...	...	...	...	92.5
7547.90	5.10	-1.080	...	46.0	...	45.0	18.0	...	20.0	29.0	23.0	30.0	...	28.0	...	66.0	60.0	15.0	...
7723.21	2.28	-3.617	...	...	...	...	...	...	...	...	105.0	96.0	52.0	90.0	...	...	...	100.0	115.4
FeII																			
5264.81	3.23	-3.130	...	...	...	...	...	...	...	...	...	...	...	...	...	...	...	...	32.8
5425.26	3.20	-3.220	...	...	32.0	54.0	39.0	...	42.0	42.0	...	...	...	...	...	...	50.0	36.0	...
5435.26	3.20	-3.220	...	...	...	...	...	...	...	...	...	...	...	...	...	...	...	...	...
6247.56	3.89	-2.300	31.0	40.0	31.0	46.0	40.0	33.0	42.0	39.0	32.0	...	35.0	46.0	47.0	49.0	49.0	32.0	28.3
6369.46	2.89	-4.110	...	...	...	...	...	...	...	...	...	...	...	...	...	...	...	...	...
6432.68	2.89	-3.570	37.0	52.0	35.0	53.0	...	31.0	50.0	44.0	36.0	48.0	40.0	50.0	50.0	51.0	53.0	38.0	33.2
6456.38	3.90	-2.050	...	51.0	48.0	58.0	50.0	44.0	55.0	54.0	41.0	64.0	45.0	58.0	...	65.0	65.0	48.0	40.5
6516.08	2.89	-3.310	...	...	...	...	...	...	...	...	...	...	...	...	...	...	...	...	45.1
[O I]																			
6300.30	0.00	-9.720	57.0	...	19.0	59.0	54.0	43.0	27.0	40.0	63.0	41.0	38.0	42.0	40.0	...	17.0	53.0	51.9
6363.78	0.02	-10.190	22.0	16.0	6.0	25.0	25.0	13.0	12.0	18.0	21.0	25.0	17.0	...	17.0	...	...	21.0	20.0
NaI																			
5682.64	2.10	-0.706	139.0	173.0	113.0	153.0	91.0	46.0	88.0	114.0	137.0	...	45.0	...	176.0	...	...	101.0	115.0
5688.20	2.10	-0.406	166.0	209.0	142.0	177.0	128.0	69.0	111.0	142.0	159.0	133.0	77.0	151.0	225.0	202.0	...	122.0	137.0
6154.23	2.10	-1.547	98.0	...	68.0	108.0	...	...	33.0	74.0	91.0	60.0	...	...	130.0	...	...	46.0	51.9
6160.75	2.10	-1.246	112.0	...	98.0	...	...	...	...	...	98.0	...	...	...	150.0	...	...	98.0	86.0
MgI																			
4702.99	4.35	-0.471	...	...	...	...	...	...	...	...	...	...	...	...	...	...	...	...	...
4730.03	4.35	-2.389	...	...	...	...	...	...	...	...	...	...	...	...	...	...	...	...	...
5528.40	4.35	-0.522	...	...	...	...	...	...	...	...	...	...	...	...	...	...	...	...	...
5711.09	4.34	-1.729	163.0	...	128.0	155.0	129.0	96.0	122.0	141.0	156.0	134.0	94.0	161.0	...	...	...	123.0	134.4
6318.72	5.11	-1.945	84.0	80.0	41.0	72.0	58.0	22.0	52.0	66.0	73.0	66.0	24.0	73.0	105.0	104.0	96.0	47.0	47.4
6319.24	5.11	-2.165	42.0	68.0	27.0	60.0	40.0	18.0	39.0	56.0	57.0	...	17.0	66.0	86.0	92.0	88.0	40.0	37.8
6765.45	5.75	-2.000	42.0	...	...	29.0	21.0	...	...	35.0	...	...	...	...	...	28.0	...	...	11.0
6894.92	5.75	-1.620	57.0	...	...	...	...	...	...	...	...	...	...	...	82.0	...	...	...	20.0
7387.69	5.75	-1.070	...	100.0	46.0	92.0	66.0	38.0	59.0	86.0	80.0	84.0	38.0	94.0	...	148.0	131.0	62.0	53.1

Table 9 – continued

λ [Å] (1)	χ [eV] (2)	loggf (3)	I194 (4)	I202 (5)	I264 (6)	I322 (7)	II033 (8)	II119 (9)	II154 (10)	II172 (11)	III152 (12)	III220 (13)	IV003 (14)	IV047 (15)	IV072 (16)	IV167 (17)	IV325 (18)	IV329 (19)	IV203 (20)
AlI																			
6696.02	3.14	-1.481	...	126.0	94.0	110.0	71.0	18.0	56.0	83.0	100.0	89.0	20.0	86.0	...	142.0	146.0	57.0	79.4
6698.67	3.14	-1.782	...	109.0	66.0	87.0	46.0	...	32.0	61.0	72.0	58.0	10.0	55.0	...	120.0	128.0	35.0	44.1
SiI																			
5488.98	5.61	-1.690	27.0	...	...	27.0	23.0	...	27.0	24.0	...	...	...	29.0	40.0	38.0	43.0	17.0	...
5701.10	4.93	-1.950	48.0	56.0	30.0	58.0	44.0	...	47.0	51.0	49.0	...	29.0	48.0	57.0	64.0	74.0	42.0	33.0
5772.15	5.08	-1.740	...	...	...	...	...	...	...	...	...	...	...	...	...	...	...	...	...
6142.48	5.62	-1.410	35.0	48.0	20.0	40.0	30.0	15.0	...	32.0	30.0	40.0	13.0	41.0	46.0	50.0	57.0	37.5	...
7235.33	5.62	-1.390	...	39.0	24.0	...	...	...	...	34.0	29.0	...	...	36.0	...	56.0	...	...	...
7235.82	5.62	-1.600	...	32.0	...	...	18.0	...	23.0	26.0	20.0	...	...	25.0	...	36.0	46.0	...	...
7250.63	5.62	-1.050	87.0	...	34.0	59.0	42.0	31.0	50.0	52.0	...	...	26.0	...	...	70.0	...	44.0	29.0
7423.50	5.62	-0.420	39.0	99.0	70.0	95.0	86.0	62.0	94.0	87.0	83.0	103.0	68.0	97.0	104.0	114.0	118.0	86.9	68.0
7800.00	6.18	-0.710	...	...	...	...	...	...	...	...	...	...	...	...	...	...	...	...	...
CaI																			
5512.98	2.93	-0.464	133.0	145.0	107.0	138.0	112.0	64.0	95.0	118.0	...	123.0	70.0	118.0	...	...	146.0	102.0	107.1
5590.11	2.52	-0.571	146.0	167.0	123.0	...	127.0	88.0	100.0	120.0	146.0	135.0	94.0	134.0	...	...	...	116.0	...
5867.56	2.93	-1.570	83.0	90.0	39.0	84.0	52.0	...	39.0	62.0	65.0	69.0	18.0	...	95.0	109.0	92.0	42.0	45.4
6156.02	2.52	-2.420	55.0	...	...	...	...	10.0	...	...	52.0	35.0	...	...	76.0	...	...	...	44.3
6166.44	2.52	-1.142	133.0	...	...	...	...	...	...	...	...	...	73.0	...	...	...	...	...	130.7
6169.04	2.52	-0.797	163.0	...	...	...	...	...	...	...	...	...	90.0	...	...	...	...	...	139.6
6455.60	2.52	-1.340	161.0	141.0	100.0	137.0	103.0	48.0	75.0	101.0	111.0	98.0	59.0	105.0	...	151.0	147.0	97.0	110.0
6471.66	2.52	-0.686	...	173.0	140.0	...	135.0	88.0	112.0	124.0	150.0	131.0	98.0	139.0	...	...	...	131.0	150.0
6499.65	2.52	-0.818	148.0	...	...	...	...	...	...	...	...	...	...	...	...	...	...	...	137.3
TiI																			
5020.03	0.84	-0.195	...	...	...	...	...	...	...	...	...	...	...	...	...	...	...	...	...
5024.84	0.82	-0.362	...	...	...	...	...	...	...	...	...	...	...	...	...	...	...	...	...
5210.39	0.05	-0.700	...	...	...	...	...	...	...	...	...	...	...	...	...	...	...	...	...
5453.64	1.44	-1.610	...	94.0	65.0	92.0	59.0	...	21.0	60.0	...	...	16.0	58.0	...	105.0	116.0	58.0	88.1
5460.47	0.05	-2.804	...	...	...	...	...	...	...	...	...	...	...	...	...	...	...	...	...
5648.57	2.50	-0.250	...	86.0	51.0	79.0	52.0	19.0	26.0	56.0	74.0	62.0	15.0	56.0	95.0	96.0	93.0	50.0	52.0
5739.46	2.25	-0.600	...	90.0	46.0	80.0	48.0	...	22.0	50.0	72.0	59.0	14.0	56.0	90.0	89.0	93.0	43.0	...
5913.71	0.02	-4.100	...	80.0	35.0	72.0	29.0	...	8.0	29.0	65.0	...	...	...	...	74.0	72.0	26.0	88.0
5918.54	1.07	-1.470	...	128.0	98.0	128.0	94.0	40.0	52.0	86.0	113.0	90.0	38.0	99.0	...	130.0	139.0	94.0	...
5944.65	0.00	-3.910	87.0	96.0	52.0	85.0	47.0	...	13.0	40.0	81.0	...	...	44.0	98.0	94.0	92.0	39.0	89.6
6092.80	1.89	-1.378	75.0	81.0	39.0	75.0	44.0	...	14.0	43.0	69.0	...	10.0	42.0	90.0	88.0	83.0	39.0	49.2
6258.10	1.44	-0.355	...	...	...	...	...	...	...	...	...	...	...	...	...	...	...	...	...
6261.10	1.43	-0.479	...	...	...	...	...	...	...	...	...	...	...	...	...	...	...	...	...
6273.39	0.02	-4.170	65.0	...	...	...	...	...	...	...	...	...	...	...	77.0	...	...	...	68.2
6706.29	1.50	-2.780	...	32.0	...	16.0	...	...	...	...	18.0	...	...	...	...	31.0	...	...	20.3
6716.71	2.49	-1.010	42.0	61.0	11.0	40.0	17.0	...	7.0	21.0	36.0	...	...	18.0	66.0	64.0	54.0	18.0	...
6746.31	1.89	-2.000	37.0	...	...	...	...	...	...	...	...	...	...	...	59.0	...	...	...	28.1
7138.08	1.43	-2.760	36.0	45.0	...	29.0	13.0	...	...	...	26.0	...	...	...	49.0	40.0	30.0	8.0	17.8
7352.16	2.49	-0.980	42.0	58.0	14.0	40.0	23.0	...	...	21.0	40.0	...	...	...	71.0	...	60.0	18.0	...
7391.52	1.50	-2.610	...	52.0	16.0	34.0	...	...	...	14.0	27.0	...	...	...	...	...	50.0	15.0	...

Table 10. Line list and measured equivalent widths given in mÅ

λ [Å] (1)	χ [eV] (2)	loggf (3)	HD077236 (4)	HD023940 (5)	HD032440 (6)	HD037763 (7)	HD040409 (8)	HD077729 (9)	HD080811 (10)	HD083212 (11)	HD099978 (12)
FeI											
5560.21	4.43	-1.120	56.4	63.5	81.2	81.9	75.5	66.9	49.7	25.5	35.4
5633.95	4.99	-0.180	67.0	81.2	102.5	92.3	95.6	81.1	63.1	33.5	43.7
5638.26	4.22	-0.800	87.2	94.7	127.9	122.4	110.2	103.4	73.5	52.7	64.2
5651.47	4.47	-1.850	26.7	29.4	50.6	52.2	44.7	37.0	17.6	...	10.3
5662.52	4.18	-0.573	105.1	107.7	136.0	136.0	126.1	120.1	100.6	77.1	79.4
5679.02	4.65	-0.810	63.2	77.5	86.1	87.9	84.0	67.4	54.9	...	41.0
5731.76	4.26	-1.110	71.1	75.3	101.3	101.7	89.4	84.5	57.9	...	43.9
5775.08	4.22	-1.230	73.9	58.3	98.2	100.2	91.1	87.3	60.7	...	46.2
5778.45	2.59	-3.430	58.1	...	108.1	78.5	71.5	83.6	34.9	...	27.9
5811.91	4.14	-2.440	15.9	20.9	38.2	42.5	34.0	26.5	11.6	5.7	7.2
5853.15	1.49	-5.260	47.6	36.7	99.6	66.5	51.0	81.0	17.4	14.3	14.6
5902.47	4.59	-1.880	15.4	26.6	41.6	42.7	38.8	28.4	15.5	...	...
5916.25	2.45	-2.994	...	99.2	140.5	118.2	104.8	119.8	74.1	66.8	61.6
5956.69	0.86	-4.608	130.3	109.3	191.2	133.7	114.8	166.0	85.9	85.0	78.1
6027.05	4.08	-1.089	88.4	90.0	...	...	94.9	95.5	69.2	49.6	51.7
6056.00	4.73	-0.480	75.0	82.9	90.2	105.7	96.5	78.6	64.8	38.5	53.9
6065.48	2.61	-1.530	...	...	...	...	...	...	...	...	...
6078.49	4.79	-0.400	77.4	...	99.3	114.2	104.9	78.8	71.4	...	55.2
6093.64	4.61	-1.430	39.0	43.8	53.2	63.1	59.5	38.8	...	...	17.2
6096.67	3.98	-1.900	51.7	57.4	81.5	85.0	75.6	66.9	40.0	21.8	25.9
6098.24	4.56	-1.810	21.0	28.9	...	52.6	46.8	38.0	17.1	6.6	...
6120.25	0.92	-5.970	49.7	35.0	108.4	65.0	49.6	83.1	16.2	17.1	...
6151.62	2.18	-3.299	96.8	91.2	147.5	108.1	97.5	124.8	67.2	63.9	62.9
6173.34	2.22	-2.880	117.9	114.7	164.7	131.4	121.2	144.1	82.3	88.3	79.8
6187.99	3.94	-1.690	63.2	...	96.2	94.2	85.3	85.5	50.5	...	35.8
6240.65	2.22	-3.320	99.4	84.9	146.4	109.1	99.3	124.5	69.0	61.2	61.0
6246.32	3.60	-0.877	...	...	...	...	...	...	...	...	...
6252.56	2.40	-1.687	...	...	...	...	...	...	...	...	...
6301.50	3.65	-0.718	...	...	...	...	...	...	...	...	...
6302.49	3.69	-1.310	...	...	128.7	120.7	114.2	...	85.6	...	71.9
6322.69	2.59	-2.426	120.5	123.6	167.8	143.3	126.4	139.6	95.8	96.4	78.2
6392.54	2.28	-4.070	60.3	50.2	101.8	75.6	65.1	80.8	30.2	18.6	20.5
6393.60	2.43	-1.580	...	...	...	...	...	...	...	...	...
6481.87	2.28	-2.984	113.6	109.8	158.6	124.2	125.3	137.6	77.9	...	81.5
6518.37	2.83	-2.570	95.6	...	131.1	117.8	100.8	112.7	73.2	56.4	59.9
6574.23	0.99	-5.004	108.5	82.5	172.8	109.7	102.5	142.8	63.3	57.6	50.8
6593.87	2.43	-2.422	133.3	132.5	189.4	161.7	131.1	162.7	99.1	106.2	90.4
6677.99	2.69	-1.418	...	...	113.0	...	...	...	...	...	...
6703.57	2.76	-3.080	73.4	73.4	68.8	90.3	82.3	102.7	49.2	39.1	40.7
6725.36	4.10	-2.260	29.8	31.5	...	54.7	46.0	34.2	19.1	9.0	12.1
6726.67	4.61	-1.140	54.0	60.8	...	80.5	75.0	62.3	43.9	21.5	29.0
6842.69	4.64	-1.200	47.0	48.1	71.9	75.4	67.9	55.9	36.5	12.6	...
6857.25	4.08	-2.190	36.6	42.9	58.0	59.2	51.7	45.9	25.0	...	...
6858.15	4.61	-0.930	55.4	70.3	81.7	85.6	78.4	69.2	47.4	22.9	35.0
7114.55	2.69	-4.070	33.1	30.7	62.4	51.7	41.6	56.6	14.5	...	9.4
7421.56	4.64	-1.680	20.8	29.0	41.1	51.7	42.4	28.9	15.2	...	8.0
7531.15	4.37	-0.590	101.7	...	124.5	143.1	125.9	112.1	88.9	...	66.5
7547.90	5.10	-1.080	21.9	...	43.4	...	...	34.5	...	...	...
7723.21	2.28	-3.617	...	...	141.6	99.2	98.9	113.0	57.2	...	42.3
FeII											
5264.81	3.23	-3.130	40.8	60.2	54.5	50.0	48.7	37.2	34.1	47.9	...
5425.26	3.20	-3.220	...	51.9	46.4	49.6	49.8	...	...	38.6	...
5435.26	3.20	-3.220	33.3	...	...	...	...	36.2	...	...	...
6247.56	3.89	-2.300	39.1	61.8	45.2	44.2	48.4	32.7	35.5	49.6	38.7
6369.46	2.89	-4.110	18.1	29.6	32.1	23.3	25.1	22.6	13.8	23.8	15.3
6432.68	2.89	-3.570	41.6	55.1	49.0	48.2	45.1	42.7	31.9	47.8	35.7
6456.38	3.90	-2.050	49.1	73.7	49.4	59.4	59.7	42.1	48.8	62.5	55.8
6516.08	2.89	-3.310	49.2	...	...	57.1	...	52.7	38.8	...	45.9
[O I]											
6300.30	0.00	-9.720	50.0	...	81.0	31.9	23.1	67.5	19.0	...	21.3
6363.78	0.02	-10.190	21.9	16.9	40.7	...	12.5	47.6	...	22.5	8.1
NaI											
5682.64	2.10	-0.706	...	118.8	148.2	165.1	118.7	...	...	33.1	...
5688.20	2.10	-0.406	126.4	128.3	179.8	186.3	157.9	161.7	124.1	51.4	90.8
6154.23	2.10	-1.547	52.0	55.2	118.5	108.4	98.4	94.5	43.2	6.6	17.2
6160.75	2.10	-1.246	71.7	73.9	135.0	137.1	114.2	117.4	65.1	11.6	29.4
MgI											
4702.99	4.35	-0.471	...	...	...	...	...	...	...	158.0	...
4730.03	4.35	-2.389	...	...	...	...	...	...	...	42.2	...
5528.40	4.35	-0.522	...	...	...	...	...	...	...	181.8	...
5711.09	4.34	-1.729	134.4	129.1	155.8	157.8	150.5	151.5	124.3	89.9	100.2
6318.72	5.11	-1.945	57.7	78.9	80.6	109.2	81.3	79.3	57.6	21.5	35.1
6319.24	5.11	-2.165	40.1	52.1	67.8	87.9	61.0	55.8	41.3	...	23.2
6765.45	5.75	-2.000	14.2	29.0	31.9	...	...	33.0	21.2	...	12.2
6894.92	5.75	-1.620	34.4	...	55.3	...	...	46.5	...	...	...
7387.69	5.75	-1.070	79.4	...	79.5	129.8	99.6	84.9	82.8		45.6

Table 10 – continued

λ [Å] (1)	χ [eV] (2)	log*gf* (3)	HD077236 (4)	HD023940 (5)	HD032440 (6)	HD037763 (7)	HD040409 (8)	HD077729 (9)	HD080811 (10)	HD083212 (11)	HD099978 (12)
AlI											
6696.02	3.14	-1.481	67.2	60.4	98.9	109.1	88.9	95.3	59.6	...	32.9
6698.67	3.14	-1.782	45.9	39.3	77.3	75.1	61.1	77.2	37.7	...	20.9
SiI											
5488.98	5.61	-1.690	24.2	27.6	28.0	46.6	42.2	32.9	26.3	9.3	14.1
5701.10	4.93	-1.950	45.0	51.6	60.2	64.7	60.9	50.6	42.1	23.8	31.7
5772.15	5.08	-1.740	...	64.1	...	...	...	...	...	...	...
6142.48	5.62	-1.410	27.1	41.2	35.6	49.0	43.8	28.9	36.3	15.1	21.5
7235.33	5.62	-1.390	33.4	...	...	...	57.7	36.4	42.5	...	29.4
7235.82	5.62	-1.600	...	...	...	...	39.4	34.4	23.8	...	16.4
7250.63	5.62	-1.050	47.0	...	43.1	74.8	63.3	...	57.3	...	...
7423.50	5.62	-0.420	81.9	107.7	81.1	106.2	104.2	77.4	91.7	...	77.5
7800.00	6.18	-0.710	37.7	55.3	29.3	58.5	52.6	38.1	43.6	...	29.3
CaI											
5512.98	2.93	-0.464	101.9	100.0	155.9	137.4	118.5	130.8	91.0	63.2	80.9
5590.11	2.52	-0.571	127.6	113.7	...	...	126.1	156.2	103.1	80.6	91.5
5867.56	2.93	-1.570	51.8	44.9	87.9	78.6	62.9	80.3	36.9	11.6	22.2
6156.02	2.52	-2.420	27.8	25.4	70.4	56.2	41.4	56.0	20.5	...	10.9
6166.44	2.52	-1.142	105.8	94.5	145.6	131.0	113.9	133.8	88.1	50.9	74.8
6169.04	2.52	-0.797	125.7	117.1	182.2	176.9	145.2	158.3	112.0	76.4	93.9
6455.60	2.52	-1.340	93.7	80.9	137.8	125.0	108.0	123.1	77.5	39.2	68.6
6471.66	2.52	-0.686	137.9	113.8	177.0	154.1	135.0	161.6	108.2	86.2	97.9
6499.65	2.52	-0.818	123.4	113.4	169.7	152.1	138.1	154.2	104.4	80.6	90.4
TiI											
5020.03	0.84	-0.195	...	...	...	...	...	...	...	106.4	...
5024.84	0.82	-0.362	...	...	...	...	...	...	...	102.5	...
5210.39	0.05	-0.700	...	...	...	...	...	...	...	...	...
5453.64	1.44	-1.610	55.0	30.3	108.5	70.9	52.4	104.1	23.4	...	13.7
5460.47	0.05	-2.804	...	...	...	...	...	...	...	30.2	...
5648.57	2.50	-0.250	49.1	33.2	88.2	73.0	53.4	82.8	29.7	...	15.5
5739.46	2.25	-0.600	44.6	30.4	91.5	66.0	50.0	83.5	25.8	...	14.0
5913.71	0.02	-4.100	28.8	...	106.4	39.4	21.7	84.2	...	...	3.6
5918.54	1.07	-1.470	90.8	...	155.1	101.1	82.2	141.8	56.7	24.0	...
5944.65	0.00	-3.910	34.2	21.6	118.7	50.6	28.2	103.2	12.6	...	...
6092.80	1.89	-1.378	38.0	21.5	83.9	61.7	39.3	76.0	18.2	...	...
6258.10	1.44	-0.355	...	...	...	...	...	...	...	67.3	...
6261.10	1.43	-0.479	...	...	...	...	...	...	...	65.1	...
6273.39	0.02	-4.170	...	...	99.3	33.9	16.5	82.8	...	...	...
6706.29	1.50	-2.780	4.9	...	29.3	...	4.8	23.9	...	...	...
6716.71	2.49	-1.010	21.9	15.4	57.4	33.6	22.9	48.3	13.2	...	...
6746.31	1.89	-2.000	10.7	...	48.7	17.8	14.9	43.5	...	...	...
7138.08	1.43	-2.760	7.1	...	53.8	19.7	8.3	45.2	...	...	...
7352.16	2.49	-0.980	20.0	19.6	55.4	38.4	21.9	43.9	14.3	...	...
7391.52	1.50	-2.610	13.1	...	53.4	18.2	9.9	40.9	...	...	...

Table 11. Line list and measured equivalent widths given in mÅ

λ [Å] (1)	χ [eV] (2)	loggf (3)	HD107328 (4)	HD107773 (5)	HD119971 (6)	HD124897 (7)	HD127243 (8)	HD130952 (9)	HD136014 (10)	HD145148 (11)	HD148451 (12)
FeI											
5560.21	4.43	-1.120	71.2	52.3	66.1	72.5	47.2	65.1	60.0	79.1	50.0
5633.95	4.99	-0.180	89.9	63.4	73.0	84.0	59.3	81.3	74.2	94.8	59.0
5638.26	4.22	-0.800	111.5	76.8	97.9	105.0	78.0	92.2	89.0	107.2	78.1
5651.47	4.47	-1.850	36.6	22.0	33.2	34.0	15.4	30.8	24.3	37.8	18.9
5662.52	4.18	-0.573	126.7	94.1	121.3	123.0	91.1	118.9	106.3	127.4	94.7
5679.02	4.65	-0.810	78.7	59.1	68.4	76.0	51.8	68.5	66.9	80.0	55.1
5731.76	4.26	-1.110	85.5	62.6	82.7	91.0	54.2	81.8	72.1	83.7	60.0
5775.08	4.22	-1.230	90.0	61.5	80.6	86.0	52.8	82.7	69.9	82.6	...
5778.45	2.59	-3.430	79.2	40.1	...	80.0	32.4	61.7	52.2	62.0	...
5811.91	4.14	-2.440	27.3	14.2	23.2	24.0	...	23.2	16.3	28.8	...
5853.15	1.49	-5.260	61.3	24.0	66.3	68.0	18.6	42.6	32.2	45.2	21.0
5902.47	4.59	-1.880	30.3	17.3	25.3	27.0	...	22.1	17.5	...	12.7
5916.25	2.45	-2.994	127.7	76.1	123.8	121.0	75.2	103.9	96.1	97.1	78.5
5956.69	0.86	-4.608	160.0	81.0	159.9	159.0	92.5	124.7	107.1	102.3	92.2
6027.05	4.08	-1.089	100.0	70.3	94.7	98.0	69.8	90.8	87.3	...	71.7
6056.00	4.73	-0.480	94.0	68.2	80.1	87.0	64.5	86.1	80.2	98.2	69.3
6065.48	2.61	-1.530	...	...	...	...	...	...	...	...	...
6078.49	4.79	-0.400	96.8	71.8	81.9	90.0	...	90.9	79.7	100.2	71.0
6093.64	4.61	-1.430	50.8	33.4	42.5	48.0	26.4	46.7	42.1	55.2	30.6
6096.67	3.98	-1.900	69.2	47.3	63.0	66.0	37.5	63.3	57.7	63.5	42.7
6098.24	4.56	-1.810	33.4	22.2	31.7	32.6	16.5	...	25.9	37.3	18.8
6120.25	0.92	-5.970	65.8	19.1	77.1	67.9	13.6	35.9	25.6	35.7	18.3
6151.62	2.18	-3.299	116.6	69.8	120.5	120.8	69.2	95.9	88.2	88.3	73.5
6173.34	2.22	-2.880	149.9	85.8	140.4	145.8	90.6	114.0	105.3	106.3	93.8
6187.99	3.94	-1.690	81.4	53.1	74.4	79.3	45.6	77.3	63.3	78.2	53.3
6240.65	2.22	-3.320	115.0	70.2	120.4	122.0	67.4	101.6	85.6	89.0	74.0
6246.32	3.60	-0.877	...	...	...	...	...	...	...	...	...
6252.56	2.40	-1.687	...	...	...	...	...	...	...	...	...
6301.50	3.65	-0.718	...	122.6	149.8	...	...	...	130.8	174.2	...
6302.49	3.69	-1.310	...	86.7	...	120.0	86.8	105.4	100.9	122.2	91.3
6322.69	2.59	-2.426	145.2	92.4	136.3	142.6	94.3	120.1	110.3	117.6	96.6
6392.54	2.28	-4.070	74.8	32.3	73.3	74.6	26.8	54.7	46.3	57.4	30.6
6393.60	2.43	-1.580	...	...	...	...	...	...	...	...	...
6481.87	2.28	-2.984	146.5	84.5	138.5	140.9	94.5	116.0	107.3	110.1	90.6
6518.37	2.83	-2.570	125.8	72.1	115.5	122.0	68.8	95.4	94.3	96.6	72.4
6574.23	0.99	-5.004	133.2	...	143.0	135.3	58.5	97.1	88.2	85.5	65.7
6593.87	2.43	-2.422	166.3	103.6	163.5	166.9	105.6	133.1	124.8	129.8	110.5
6677.99	2.69	-1.418	...	...	...	...	...	...	...	...	...
6703.57	2.76	-3.080	98.8	58.9	92.6	97.2	48.6	80.9	69.2	74.1	49.3
6725.36	4.10	-2.260	40.0	21.8	37.2	37.9	14.3	32.9	23.5	37.9	16.9
6726.67	4.61	-1.140	70.6	46.8	58.1	64.8	38.7	59.9	52.0	67.5	40.8
6842.69	4.64	-1.200	60.2	40.0	...	60.0	...	52.5	56.0	68.9	37.0
6857.25	4.08	-2.190	46.0	25.0	39.0	42.9	...	40.8	36.5	49.5	24.6
6858.15	4.61	-0.930	77.6	60.1	64.7	71.1	...	67.5	69.3	79.6	50.0
7114.55	2.69	-4.070	45.0	16.1	38.3	41.2	...	25.0	18.8	35.7	15.6
7421.56	4.64	-1.680	33.3	18.2	26.2	33.0	...	...	27.0	45.2	15.5
7531.15	4.37	-0.590	116.9	87.5	110.6	115.0	...	107.3	100.3	122.3	88.3
7547.90	5.10	-1.080	...	30.1	35.4	32.6	...	...	27.4	40.7	17.7
7723.21	2.28	-3.617	...	...	114.0	117.4	...	79.6	85.0	...	63.6
FeII											
5264.81	3.23	-3.130	58.0	35.8	50.0	44.0	61.3	...	55.1	44.8	56.5
5425.26	3.20	-3.220	49.4	37.5	39.3	43.0	48.8	51.7	57.7	...	46.7
5435.26	3.20	-3.220	...	...	...	...	...	...	...	...	...
6247.56	3.89	-2.300	53.7	39.9	40.6	44.0	57.5	57.3	60.9	43.0	59.6
6369.46	2.89	-4.110	28.3	16.1	23.8	23.8	26.4	29.0	30.6	23.7	27.3
6432.68	2.89	-4.110	50.4	33.3	45.9	46.1	51.2	55.1	52.0	37.7	52.9
6456.38	3.90	-3.570	64.0	50.3	49.2	56.0	71.9	74.7	66.3	49.1	70.0
6516.08	2.89	-3.310	71.4	...	...	59.0	...	71.6	71.7	49.8	68.2
[O I]											
6300.30	0.00	-9.720	64.0	24.4	78.8	66.0	32.8	40.0	38.0	20.0	30.7
6363.78	0.02	-10.190	28.8	10.4	42.6	29.8	16.0	17.1	16.6	...	13.8
NaI											
5682.64	2.10	-0.706	...	117.1	...	154.0	91.8	...	...	...	104.7
5688.20	2.10	-0.406	155.8	126.3	153.4	157.6	108.6	144.7	128.1	158.2	127.2
6154.23	2.10	-1.547	72.7	45.9	69.7	77.5	29.9	58.4	44.7	83.0	47.9
6160.75	2.10	-1.246	102.9	70.1	95.1	99.2	45.5	81.7	69.4	103.7	70.7
MgI											
4702.99	4.35	-0.471	...	...	...	...	...	...	...	...	...
4730.03	4.35	-2.389	...	...	...	...	...	...	...	...	...
5528.40	4.35	-0.522	...	...	...	...	...	...	...	...	...
5711.09	4.34	-1.729	161.8	128.2	151.0	156.8	117.6	136.1	133.5	154.1	119.6
6318.72	5.11	-1.945	84.0	57.6	74.8	75.0	52.1	68.0	56.2	65.8	51.8
6319.24	5.11	-2.165	62.0	51.2	56.8	65.0	35.1	48.8	48.5	68.0	34.4
6765.45	5.75	-2.000	32.0	20.1	25.2	28.0	...	29.0	20.9	...	12.4
6894.92	5.75	-1.620	...	57.1	48.5	45.0	...	...	36.8	48.7	36.5
7387.69	5.75	-1.070	...	90.2	85.5	86.1	...	81.9	81.5	...	67.3

Table 11 – continued

λ [Å] (1)	χ [eV] (2)	loggf (3)	HD107328 (4)	HD107773 (5)	HD119971 (6)	HD124897 (7)	HD127243 (8)	HD130952 (9)	HD136014 (10)	HD145148 (11)	HD148451 (12)
AlI											
6696.02	3.14	-1.481	86.0	61.0	103.3	92.2	41.1	64.9	71.2	80.2	46.4
6698.67	3.14	-1.782	54.0	38.5	56.4	63.5	23.8	45.8	36.5	56.4	25.8
SiI											
5488.98	5.61	-1.690	32.3	28.6	29.8	25.8	23.8	35.7	30.9	37.2	21.9
5701.10	4.93	-1.950	60.2	41.7	45.8	56.5	39.7	52.0	46.6	54.0	45.6
5772.15	5.08	-1.740	...	...	...	...	54.0	...	...	...	...
6142.48	5.62	-1.410	41.9	36.7	34.6	37.5	32.6	47.1	41.1	40.0	35.9
7235.33	5.62	-1.390	...	44.7	...	42.4	...	43.9	...	...	51.1
7235.82	5.62	-1.600	...	39.2	...	29.4	...	30.9	...	...	38.5
7250.63	5.62	-1.050	...	50.1	46.0	53.9	...	...	...	...	67.9
7423.50	5.62	-0.420	109.3	90.6	83.7	86.9	...	111.0	104.2	97.1	100.6
7800.00	6.18	-0.710	50.0	54.7	36.4	37.5	...	56.3	48.7	50.5	42.2
CaI											
5512.98	2.93	-0.464	122.6	101.4	125.0	125.5	86.8	101.6	101.0	130.9	90.0
5590.11	2.52	-0.571	136.5	109.9	143.5	142.9	106.0	121.6	114.9	129.2	102.9
5867.56	2.93	-1.570	58.0	40.2	61.7	62.0	27.6	45.1	38.9	61.1	32.3
6156.02	2.52	-2.420	35.6	20.4	44.6	43.3	10.8	29.0	18.3	34.1	13.0
6166.44	2.52	-1.142	126.3	89.9	128.9	122.8	76.6	101.6	91.7	110.2	83.2
6169.04	2.52	-0.797	152.6	111.5	149.6	146.6	99.8	126.5	112.1	141.8	106.2
6455.60	2.52	-1.340	109.0	76.0	111.6	113.1	61.7	94.9	78.9	97.2	73.2
6471.66	2.52	-0.686	151.0	111.1	152.8	151.7	104.1	130.0	118.4	132.6	108.6
6499.65	2.52	-0.818	143.3	104.5	144.4	142.2	100.4	120.5	109.6	130.8	104.8
TiI											
5020.03	0.84	-0.195	...	...	...	...	114.3	...	...	...	...
5024.84	0.82	-0.362	...	...	...	...	...	...	...	...	...
5210.39	0.05	-0.700	...	...	...	...	141.9	...	...	...	...
5453.64	1.44	-1.610	70.9	27.6	82.7	76.1	13.9	35.3	26.2	42.8	19.1
5460.47	0.05	-2.804	...	...	...	...	38.2	...	...	...	...
5648.57	2.50	-0.250	61.3	31.7	72.4	68.9	20.2	41.1	31.5	47.9	23.4
5739.46	2.25	-0.600	58.5	29.3	66.7	65.1	12.8	34.9	29.2	42.1	20.7
5913.71	0.02	-4.100	35.5	10.7	65.3	45.0	...	...	9.7	14.6	...
5918.54	1.07	-1.470	115.0	63.4	131.4	123.3	...	69.5	67.2	72.1	56.0
5944.65	0.00	-3.910	50.6	12.0	78.2	65.0	...	21.6	...	25.4	...
6092.80	1.89	-1.378	49.6	24.9	63.5	57.0	...	28.8	...	31.6	14.5
6258.10	1.44	-0.355	...	...	...	...	79.3	...	...	...	...
6261.10	1.43	-0.479	...	...	...	...	79.3	...	...	...	...
6273.39	0.02	-4.170	31.0	...	58.8	42.8	...	...	...	10.1	...
6706.29	1.50	-2.780	9.7	4.7	17.2	12.8	...	...	...	3.6	...
6716.71	2.49	-1.010	22.4	9.0	28.4	26.6	...	14.8	9.7	15.5	...
6746.31	1.89	-2.000	17.6	...	29.4	20.2	...	...	...	11.5	...
7138.08	1.43	-2.760	14.7	3.3	23.8	15.9	...	4.8	...	9.2	...
7352.16	2.49	-0.980	26.5	14.2	34.1	30.4	...	13.3	7.8	18.7	...
7391.52	1.50	-2.610	...	5.5	45.5	18.3	...	...	...	...	...

Table 12. Line list and measured equivalent widths given in mÅ

λ [Å] (1)	χ [eV] (2)	$\log gf$ (3)	HD180928 (4)	HD203344 (5)	HD219615 (6)	HD221345 (7)	HD000787 (8)	HD003546 (9)	HD005268 (10)	HD029139 (11)	HD029503 (12)
FeI											
5560.21	4.43	-1.120	69.7	74.5	58.5	71.6	90.0	50.4	57.3	91.0	80.4
5633.95	4.99	-0.180	79.8	92.0	66.8	85.4	109.5	64.0	68.6	...	92.6
5638.26	4.22	-0.800	102.2	106.0	83.5	100.4	137.0	80.1	84.1	...	111.5
5651.47	4.47	-1.850	38.4	37.4	19.7	32.9	53.4	16.8	21.4	...	49.1
5662.52	4.18	-0.573	117.5	114.7	98.3	110.0	140.7	91.4	100.7	...	135.8
5679.02	4.65	-0.810	72.8	77.7	58.7	73.2	95.5	54.1	60.9	106.0	85.9
5731.76	4.26	-1.110	87.7	87.6	66.5	77.0	109.7	61.4	66.3	117.0	99.2
5775.08	4.22	-1.230	80.5	84.7	61.8	78.0	...	58.9	67.3	109.0	...
5778.45	2.59	-3.430	82.1	70.9	40.5	60.4	115.0	33.6	41.4	121.0	77.8
5811.91	4.14	-2.440	27.3	28.0	15.3	28.0	43.4	12.1	15.4	50.4	35.4
5853.15	1.49	-5.260	75.0	52.0	22.5	44.8	108.0	21.8	24.2	118.1	64.9
5902.47	4.59	-1.880	...	34.0	...	...	46.3	17.1	13.9	...	36.5
5916.25	2.45	-2.994	114.8	105.3	...	106.7	150.0	...	80.8	...	121.7
5956.69	0.86	-4.608	156.6	133.8	104.0	120.8	207.0	100.0	97.2	...	135.8
6027.05	4.08	-1.089	95.4	96.6	76.2	93.9	116.0	70.9	77.3	134.6	109.5
6056.00	4.73	-0.480	82.4	90.4	71.4	85.7	103.0	67.0	72.5	96.3	102.5
6065.48	2.61	-1.530	...	...	...	...	...	...	...	...	...
6078.49	4.79	-0.400	80.8	97.0	75.2	88.7	115.0	69.3	76.2	107.2	...
6093.64	4.61	-1.430	43.4	52.3	33.0	47.8	64.2	28.0	33.7	...	60.7
6096.67	3.98	-1.900	61.5	66.4	44.7	63.7	85.0	38.1	47.8	81.5	76.9
6098.24	4.56	-1.810	37.3	39.0	19.4	31.5	60.0	16.3	22.5	63.5	45.0
6120.25	0.92	-5.970	73.8	49.5	23.0	45.7	121.0	14.4	22.8	110.0	72.8
6151.62	2.18	-3.299	122.9	103.0	78.3	98.4	167.7	74.7	78.1	158.0	119.0
6173.34	2.22	-2.880	140.9	126.0	98.3	120.5	181.5	93.8	99.3	...	139.0
6187.99	3.94	-1.690	80.3	82.3	56.5	73.7	...	48.2	57.4	...	...
6240.65	2.22	-3.320	119.5	103.4	74.7	95.3	150.0	69.3	78.9	...	105.7
6246.32	3.60	-0.877	...	...	...	...	...	...	...	...	...
6252.56	2.40	-1.687	...	...	...	...	166.7	...	...	...	...
6301.50	3.65	-0.718	...	143.0	115.0	...	...	...	...	...	...
6302.49	3.69	-1.310	...	112.9	...	106.8	...	88.3	95.6	162.0	...
6322.69	2.59	-2.426	132.4	128.8	102.0	121.8	...	93.1	104.1	186.2	151.0
6392.54	2.28	-4.070	76.6	68.1	39.3	57.3	111.0	28.8	36.6	114.0	78.5
6393.60	2.43	-1.580	...	...	...	...	...	...	...	...	...
6481.87	2.28	-2.984	138.6	...	94.5	123.1	174.0	83.4	90.9	...	144.5
6518.37	2.83	-2.570	112.6	...	88.7	104.6	148.0	79.1	79.3	158.0	105.6
6574.23	0.99	-5.004	134.9	105.8	74.1	97.4	169.0	...	70.3	176.5	140.0
6593.87	2.43	-2.422	159.4	147.0	113.8	140.8	215.0	107.4	116.3	209.8	178.0
6677.99	2.69	-1.418	...	...	...	...	...	...	...	...	...
6703.57	2.76	-3.080	94.2	92.6	62.0	81.3	126.0	52.9	59.1	134.0	88.0
6725.36	4.10	-2.260	33.9	39.7	23.3	33.6	65.0	17.4	23.1	...	49.0
6726.67	4.61	-1.140	61.4	68.6	51.4	60.3	79.0	40.9	49.4	...	72.7
6842.69	4.64	-1.200	61.2	...	...	...	84.0	...	41.4	...	69.5
6857.25	4.08	-2.190	46.4	...	...	...	63.0	...	26.0	...	66.0
6858.15	4.61	-0.930	71.4	...	...	...	95.0	...	54.2	...	84.6
7114.55	2.69	-4.070	51.1	...	...	...	82.5	...	...	...	48.5
7421.56	4.64	-1.680	28.3	...	...	...	45.0	...	...	...	47.4
7531.15	4.37	-0.590	104.8	...	...	...	154.0	...	...	...	128.6
7547.90	5.10	-1.080	30.0	...	...	...	...	...	...	...	...
7723.21	2.28	-3.617	119.2	...	...	...	...	...	...	...	...
FeII											
5264.81	3.23	-3.130	35.3	58.0	54.8	56.4	58.5	53.5	...	...	53.5
5425.26	3.20	-3.220	...	53.4	47.1	49.0	50.0	51.3	...	44.7	49.2
5435.26	3.20	-3.220	36.0	...	...	...	...	...	...	...	...
6247.56	3.89	-2.300	38.3	57.5	57.2	54.3	...	60.7	61.4	...	49.9
6369.46	2.89	-4.110	...	32.5	25.6	29.4	...	27.9	30.8	...	29.1
6432.68	2.89	-3.570	36.6	51.5	50.6	53.4	53.6	54.6	58.7	...	52.9
6456.38	3.90	-2.050	40.2	64.0	64.2	64.2	58.2	76.2	73.9	50.4	64.0
6516.08	2.89	-3.310	51.7	...	65.3	...	69.0	66.3	71.4	...	...
[O I]											
6300.30	0.00	-9.720	72.8	37.0	31.7	58.0	...	23.0	...	66.0	...
6363.78	0.02	-10.190	36.1	17.0	14.5	18.3	48.0	...	12.8	42.0	14.0
NaI											
5682.64	2.10	-0.706	...	...	...	136.8	...	91.4	91.4	...	...
5688.20	2.10	-0.406	164.9	144.0	119.2	138.2	209.0	107.8	114.6	209.0	177.0
6154.23	2.10	-1.547	96.2	76.0	46.8	67.6	134.4	31.8	33.9	145.5	95.8
6160.75	2.10	-1.246	116.6	99.0	63.9	85.7	156.3	47.1	52.3	182.0	121.0
MgI											
4702.99	4.35	-0.471	...	...	...	...	...	...	...	...	...
4730.03	4.35	-2.389	...	...	...	...	...	...	...	...	...
5528.40	4.35	-0.522	...	...	...	...	...	...	205.9	...	...
5711.09	4.34	-1.729	154.9	145.8	118.1	141.9	157.5	107.0	114.6	162.5	157.3
6318.72	5.11	-1.945	84.9	78.0	53.0	82.2	93.8	41.3	46.4	...	81.0
6319.24	5.11	-2.165	62.0	65.1	46.0	57.7	63.2	31.8	29.3	...	61.8
6765.45	5.75	-2.000	29.8	...	...	...	...	12.6	15.3	...	26.0
6894.92	5.75	-1.620	50.6	...	...	...	50.9	...	...	...	52.5
7387.69	5.75	-1.070	79.2	...	...	...	...	...	...	...	...

Table 12 – continued

λ [Å] (1)	χ [eV] (2)	loggf (3)	HD180928 (4)	HD203344 (5)	HD219615 (6)	HD221345 (7)	HD000787 (8)	HD003546 (9)	HD005268 (10)	HD029139 (11)	HD029503 (12)
AlI											
6696.02	3.14	-1.481	118.3	94.0	52.0	78.0	139.0	46.9	47.4	143.0	95.6
6698.67	3.14	-1.782	76.6	64.3	33.3	52.9	105.0	25.1	26.6	120.0	79.0
SiI											
5488.98	5.61	-1.690	24.9	37.0	25.8	35.2	38.1	23.8	21.5	...	36.8
5701.10	4.93	-1.950	56.6	64.7	54.0	55.2	55.6	48.0	45.3	...	58.7
5772.15	5.08	-1.740	...	...	...	...	...	...	...	...	...
6142.48	5.62	-1.410	29.1	43.5	34.5	44.1	37.0	34.0	30.6	33.7	45.7
7235.33	5.62	-1.390	...	...	...	...	...	...	...	...	...
7235.82	5.62	-1.600	...	...	...	...	...	...	...	...	...
7250.63	5.62	-1.050	56.5	...	...	...	...	...	...	...	...
7423.50	5.62	-0.420	79.4	...	...	...	91.7	...	...	...	114.9
7800.00	6.18	-0.710	27.4	...	...	...	41.7	...	...	...	55.1
CaI											
5512.98	2.93	-0.464	133.1	118.5	93.5	113.3	163.0	86.5	90.5	167.9	128.5
5590.11	2.52	-0.571	149.7	131.0	109.0	124.3	168.0	99.1	101.9	190.0	142.0
5867.56	2.93	-1.570	78.3	59.4	33.3	53.0	92.0	28.6	28.4	...	72.8
6156.02	2.52	-2.420	55.1	35.2	15.0	30.9	86.2	13.2	11.8	91.5	43.2
6166.44	2.52	-1.142	135.2	109.0	86.0	105.2	154.0	76.7	80.7	...	121.0
6169.04	2.52	-0.797	161.2	131.8	106.0	128.1	200.0	97.8	102.2	...	145.0
6455.60	2.52	-1.340	124.4	100.5	74.8	97.0	156.2	64.2	71.9	143.4	128.5
6471.66	2.52	-0.686	159.9	156.0	113.8	131.2	190.0	105.1	110.1	182.8	139.0
6499.65	2.52	-0.818	151.7	142.0	105.0	121.0	190.8	108.0	101.5	186.5	143.0
TiI											
5020.03	0.84	-0.195	...	...	...	...	...	...	...	...	...
5024.84	0.82	-0.362	...	...	...	...	...	...	...	...	...
5210.39	0.05	-0.700	...	...	...	...	...	...	...	...	...
5453.64	1.44	-1.610	101.8	54.0	25.4	46.7	130.0	14.3	18.1	...	65.0
5460.47	0.05	-2.804	...	...	...	...	...	...	43.6	...	...
5648.57	2.50	-0.250	85.3	52.9	26.3	48.0	100.0	19.5	20.6	...	62.6
5739.46	2.25	-0.600	81.0	47.5	20.6	41.9	95.0	22.2	17.2	119.0	56.8
5913.71	0.02	-4.100	87.6	20.5	...	20.6	122.5	...	...	...	31.0
5918.54	1.07	-1.470	135.3	79.2	51.2	79.7	159.0	37.4	...	...	112.5
5944.65	0.00	-3.910	101.3	24.0	...	20.2	134.0	...	...	...	43.7
6092.80	1.89	-1.378	77.9	36.0	14.0	33.2	98.4	8.3	12.6	101.0	48.0
6258.10	1.44	-0.355	...	...	...	...	...	...	84.3	...	...
6261.10	1.43	-0.479	...	...	...	...	...	...	86.0	...	...
6273.39	0.02	-4.170	75.8	14.0	...	13.8	115.0	...	...	...	26.0
6706.29	1.50	-2.780	25.0	...	...	...	45.0	...	...	62.8	7.8
6716.71	2.49	-1.010	48.9	14.9	7.0	...	73.0	...	4.2	102.0	25.6
6746.31	1.89	-2.000	41.8	...	...	...	68.0	...	...	...	19.8
7138.08	1.43	-2.760	37.2	...	...	...	85.0	...	...	...	10.5
7352.16	2.49	-0.980	41.9	...	...	...	73.0	...	...	...	32.1
7391.52	1.50	-2.610	46.8	...	...	...	...	...	...	...	...

Table 13. Line list and measured equivalent widths given in mÅ

λ [Å] (1)	χ [eV] (2)	loggf (3)	HD030608 (4)	HD045415 (5)	HD050778 (6)	HD073017 (7)	HD099648 (8)	HD100920 (9)	HD115478 (10)	HD116976 (11)	HD117220 (12)
FeI											
5560.21	4.43	-1.120	69.5	77.7	74.7	58.7	82.9	75.2	86.4	98.4	36.9
5633.95	4.99	-0.180	80.3	90.9	91.9	70.6	99.6	87.9	103.8	110.8	45.8
5638.26	4.22	-0.800	99.6	108.9	113.0	85.8	118.9	102.3	121.5	122.2	61.3
5651.47	4.47	-1.850	33.7	43.2	46.2	25.3	42.7	39.4	56.2	56.5	11.4
5662.52	4.18	-0.573	115.0	124.2	128.5	96.0	138.0	121.3	138.8	144.6	76.5
5679.02	4.65	-0.810	69.7	81.1	...	62.6	88.0	75.7	87.0	96.4	42.4
5731.76	4.26	-1.110	83.0	88.9	96.0	66.0	102.4	86.3	105.1	108.8	45.0
5775.08	4.22	-1.230	...	86.0	...	64.4	101.7	85.0	102.1	106.7	44.3
5778.45	2.59	-3.430	66.4	...	95.5	46.1	74.2	64.7	97.9	91.7	...
5811.91	4.14	-2.440	25.2	...	35.8	16.9	32.1	29.2	42.5	44.3	7.1
5853.15	1.49	-5.260	48.8	49.8	90.0	34.8	46.6	43.3	81.6	69.3	13.0
5902.47	4.59	-1.880	25.5	31.2	38.1	22.2	36.5	32.8	41.1	51.4	...
5916.25	2.45	-2.994	105.5	108.4	130.0	...	116.5	108.3	136.4	...	57.2
5956.69	0.86	-4.608	125.0	123.4	186.0	98.9	132.1	116.2	161.8	...	67.8
6027.05	4.08	-1.089	88.0	100.3	98.0	76.1	114.6	99.3	111.3	122.0	54.0
6056.00	4.73	-0.480	85.7	96.3	90.0	75.9	106.1	93.8	103.5	119.2	54.7
6065.48	2.61	-1.530	...	...	...	...	...	...	...	...	...
6078.49	4.79	-0.400	92.1	101.5	...	76.7	106.7	96.8	106.7	118.8	55.5
6093.64	4.61	-1.430	47.7	57.9	55.0	36.4	...	54.9	68.9	74.0	22.3
6096.67	3.98	-1.900	62.6	72.1	77.4	47.7	77.2	71.0	81.9	82.1	26.6
6098.24	4.56	-1.810	37.0	45.8	46.7	23.7	...	40.2	54.5	56.2	...
6120.25	0.92	-5.970	50.4	52.9	97.7	28.8	47.7	40.3	83.5	67.4	10.8
6151.62	2.18	-3.299	98.8	104.7	136.0	85.2	112.0	99.1	133.6	...	59.1
6173.34	2.22	-2.880	119.7	128.4	155.7	98.7	138.1	118.2	154.6	150.7	71.9
6187.99	3.94	-1.690	...	84.4	...	60.8	94.2	78.4	97.2	102.3	34.1
6240.65	2.22	-3.320	103.0	106.2	143.4	78.9	108.7	101.0	130.6	126.3	49.0
6246.32	3.60	-0.877	...	...	...	...	...	...	...	...	...
6252.56	2.40	-1.687	...	...	...	...	...	...	...	...	...
6301.50	3.65	-0.718	...	...	...	...	161.6	145.0	173.6	177.4	99.7
6302.49	3.69	-1.310	...	121.0	...	92.5	128.1	121.0	137.7	148.5	...
6322.69	2.59	-2.426	129.0	131.2	141.5	103.9	138.4	121.2	155.8	151.4	76.0
6392.54	2.28	-4.070	59.5	67.1	86.0	47.7	62.0	63.1	93.0	87.5	18.2
6393.60	2.43	-1.580	...	...	...	...	...	...	...	...	...
6481.87	2.28	-2.984	115.0	125.9	155.5	99.4	131.9	119.3	157.5	152.0	69.8
6518.37	2.83	-2.570	97.2	106.6	128.0	...	111.0	101.6	134.4	129.6	59.3
6574.23	0.99	-5.004	100.5	109.0	163.0	78.2	105.9	94.9	143.5	126.0	43.7
6593.87	2.43	-2.422	137.9	147.3	175.0	117.3	160.6	140.8	184.3	181.8	85.1
6677.99	2.69	-1.418	...	...	...	...	...	...	...	...	...
6703.57	2.76	-3.080	79.2	86.9	112.0	63.8	99.8	84.4	116.1	...	36.7
6725.36	4.10	-2.260	37.0	43.2	49.3	25.2	46.9	40.9	54.9	58.7	10.6
6726.67	4.61	-1.140	62.5	71.7	64.0	50.2	80.2	70.2	81.7	91.4	31.2
6842.69	4.64	-1.200	56.6	67.4	60.5	...	80.4	68.3	81.2	91.2	31.0
6857.25	4.08	-2.190	46.5	51.2	52.6	...	55.4	53.3	61.8	72.2	...
6858.15	4.61	-0.930	70.7	80.1	91.5	...	91.7	82.2	89.3	106.2	40.2
7114.55	2.69	-4.070	36.1	41.4	63.0	...	32.5	31.5	62.9	55.2	11.0
7421.56	4.64	-1.680	31.4	38.7	33.5	...	43.1	43.1	50.1	55.4	...
7531.15	4.37	-0.590	113.5	122.6	...	...	137.9	117.5	132.3	154.3	66.9
7547.90	5.10	-1.080	...	44.5	...	...	...	36.6	50.5	59.5	9.9
7723.21	2.28	-3.617	...	100.0	...	...	109.7	93.8	128.5	123.3	50.1
FeII											
5264.81	3.23	-3.130	53.8	69.5	48.9	50.7	79.4	62.5	56.7	66.8	36.5
5425.26	3.20	-3.220	48.2	55.9	42.8	42.8	...	57.2	50.5	68.7	32.4
5435.26	3.20	-3.220	...	...	...	...	...	...	...	...	...
6247.56	3.89	-2.300	53.5	62.1	...	46.4	90.0	70.6	50.7	76.9	38.7
6369.46	2.89	-4.110	28.0	35.6	...	24.4	55.9	38.0	29.4	44.2	16.8
6432.68	2.89	-3.570	48.8	62.7	46.0	45.4	80.9	62.8	48.7	64.8	30.9
6456.38	3.90	-2.050	63.5	75.4	46.5	61.3	104.4	80.4	55.5	86.9	45.8
6516.08	2.89	-3.310	62.0	78.9	54.2	...	98.8	72.9	63.0	84.3	47.7
[O I]											
6300.30	0.00	-9.720	...	28.0	...	18.5	40.0	29.0	47.0	38.7	18.0
6363.78	0.02	-10.190	15.8	13.0	37.4	11.0	15.0	16.0	...	24.4	7.0
NaI											
5682.64	2.10	-0.706	...	117.2	...	114.8	...	150.6	...		
5688.20	2.10	-0.406	136.0	148.8	173.0	123.3	166.0	146.3	174.6	192.9	94.5
6154.23	2.10	-1.547	66.7	78.6	102.0	51.5	91.7	69.7	115.7	125.0	20.4
6160.75	2.10	-1.246	89.5	100.2	130.0	71.3	111.6	89.6	127.1	142.8	36.3
MgI											
4702.99	4.35	-0.471	...	...	...	...	...	...	...		
4730.03	4.35	-2.389	...	...	...	...	...	...	...		
5528.40	4.35	-0.522	...	...	...	...	...	...	...	...	...
5711.09	4.34	-1.729	130.0	139.6	153.6	114.0	137.7	139.2	157.9	161.7	94.7
6318.72	5.11	-1.945	64.0	81.6	73.4	56.2	79.9	69.5	78.8	91.4	30.2
6319.24	5.11	-2.165	44.0	50.9	52.1	36.6	51.6	46.7	65.0	75.8	26.4
6765.45	5.75	-2.000	18.1	27.5	32.2	...	31.1	18.6	41.1	42.0	7.1
6894.92	5.75	-1.620	33.6	69.4	46.0	...	46.2	47.1	64.0	72.4	...
7387.69	5.75	-1.070	...	90.3	...	...	92.9	87.3	101.8	125.1	47.1

Table 13 – continued

λ [Å] (1)	χ [eV] (2)	loggf (3)	HD030608 (4)	HD045415 (5)	HD050778 (6)	HD073017 (7)	HD099648 (8)	HD100920 (9)	HD115478 (10)	HD116976 (11)	HD117220 (12)
AlI											
6696.02	3.14	-1.481	67.8	76.1	98.7	...	71.8	70.0	108.2	115.6	30.6
6698.67	3.14	-1.782	45.0	51.9	82.0	31.2	50.2	40.0	88.8	81.5	14.9
SiI											
5488.98	5.61	-1.690	24.0	35.3	29.0	21.8	49.2	29.7	39.0	56.0	14.6
5701.10	4.93	-1.950	50.4	60.6	48.0	41.4	71.1	55.9	60.0	78.2	40.5
5772.15	5.08	-1.740	...	...	...	...	...	...	...	...	...
6142.48	5.62	-1.410	36.0	44.0	30.0	31.3	61.5	46.3	38.4	58.4	23.1
7235.33	5.62	-1.390	...	47.6	...	...	...	50.3	44.0	...	...
7235.82	5.62	-1.600	...	37.7	...	...	...	...	...	46.4	...
7250.63	5.62	-1.050	...	58.3	...	...	...	67.1	...	95.6	...
7423.50	5.62	-0.420	96.0	117.2	82.0	...	119.8	109.3	95.7	123.1	74.5
7800.00	6.18	-0.710	45.0	53.0	35.4	...	68.1	57.2	...	...	24.3
CaI											
5512.98	2.93	-0.464	108.0	119.4	141.0	93.9	124.1	112.1	144.6	134.7	74.7
5590.11	2.52	-0.571	119.5	124.9	152.5	103.1	130.1	120.1	159.0	134.5	85.1
5867.56	2.93	-1.570	52.9	56.8	83.0	36.3	52.9	48.6	87.5	73.4	18.7
6156.02	2.52	-2.420	26.9	35.3	62.5	17.8	37.4	28.3	63.9	44.8	7.6
6166.44	2.52	-1.142	101.9	112.0	138.9	86.1	113.5	103.7	140.7	126.9	65.1
6169.04	2.52	-0.797	123.5	134.5	167.0	105.7	138.7	125.6	173.0	158.4	85.5
6455.60	2.52	-1.340	94.0	106.2	127.2	78.0	102.3	93.0	131.0	122.5	49.7
6471.66	2.52	-0.686	126.8	136.4	174.5	116.3	146.5	128.0	166.5	158.9	84.9
6499.65	2.52	-0.818	124.3	132.8	170.0	107.0	138.3	125.1	160.5	152.5	80.8
TiI											
5020.03	0.84	-0.195	...	...	...	...	...	...	...	...	...
5024.84	0.82	-0.362	...	...	...	...	...	...	...	...	...
5210.39	0.05	-0.700	...	...	...	...	...	...	...	...	...
5453.64	1.44	-1.610	43.0	45.1	111.0	23.5	30.0	30.7	92.0	61.3	8.1
5460.47	0.05	-2.804	...	...	...	...	...	...	...	...	...
5648.57	2.50	-0.250	39.3	46.5	89.5	28.1	35.0	39.0	89.3	64.8	12.3
5739.46	2.25	-0.600	37.6	37.9	86.0	21.9	30.4	33.2	79.7	53.2	10.7
5913.71	0.02	-4.100	16.8	9.9	94.0	...	...	10.0	67.5	25.0	1.7
5918.54	1.07	-1.470	89.0	69.0	148.0	50.3	65.0	64.0	125.4	87.6	27.7
5944.65	0.00	-3.910	14.5	17.5	126.5	10.5	15.2	16.9	84.9	30.9	...
6092.80	1.89	-1.378	27.3	31.6	84.0	15.2	22.8	25.3	76.5	44.3	...
6258.10	1.44	-0.355	...	...	...	...	...	...	...	...	...
6261.10	1.43	-0.479	...	...	...	...	...	...	...	...	...
6273.39	0.02	-4.170	12.2	9.0	95.3	6.2	4.4	...	63.4	15.6	...
6706.29	1.50	-2.780	...	...	29.3	...	...	...	24.6	10.0	...
6716.71	2.49	-1.010	13.4	13.8	53.0	6.3	8.7	10.9	42.9	21.5	...
6746.31	1.89	-2.000	9.5	8.0	50.0	...	...	...	39.0	18.5	...
7138.08	1.43	-2.760	10.0	6.0	...	...	...	4.7	38.2	23.5	...
7352.16	2.49	-0.980	13.2	...	58.5	...	9.9	13.3	...	23.8	...
7391.52	1.50	-2.610	...	8.6	...	...	...	7.9	40.7	21.2	...

Table 14. Line list and measured equivalent widths given in mÅ

λ [Å] (1)	χ [eV] (2)	loggf (3)	HD117818 (4)	HD128188 (5)	HD132345 (6)	HD142948 (7)	HD171496 (8)	HD172223 (9)	HD174116 (10)	HD175219 (11)	HD186378 (12)
FeI											
5560.21	4.43	-1.120	69.4	23.3	...	49.2	48.2	99.1	77.1	66.5	85.1
5633.95	4.99	-0.180	81.0	30.7	119.9	57.4	61.4	...	87.7	84.2	105.0
5638.26	4.22	-0.800	97.3	49.1	141.0	76.5	79.3	130.7	115.3	94.6	123.4
5651.47	4.47	-1.850	31.2	6.4	70.2	15.0	16.1	58.3	43.7	30.0	53.6
5662.52	4.18	-0.573	112.6	64.9	161.9	95.0	96.9	151.1	129.0	112.1	136.4
5679.02	4.65	-0.810	75.0	31.2	102.3	55.6	52.9	98.0	80.4	68.4	90.2
5731.76	4.26	-1.110	78.9	29.2	121.8	59.2	60.3	115.1	93.9	77.7	100.7
5775.08	4.22	-1.230	80.4	31.4	122.3	60.2	59.4	116.0	93.7	80.2	102.3
5778.45	2.59	-3.430	62.0	19.3	110.4	35.7	...	103.5	...	59.1	...
5811.91	4.14	-2.440	21.9	...	53.6	10.1	11.5	46.7	34.3	21.2	41.2
5853.15	1.49	-5.260	38.6	12.3	94.6	24.0	17.0	85.2	80.0	38.5	71.1
5902.47	4.59	-1.880	18.8	...	61.5	9.1	...	51.6	...	...	44.4
5916.25	2.45	-2.994	101.7	53.1	149.3	75.7	80.5	148.1	137.8	97.5	124.7
5956.69	0.86	-4.608	111.5	67.9	167.9	...	82.9	165.7	173.5	116.3	142.5
6027.05	4.08	-1.089	90.8	43.3	129.6	68.9	69.7	123.1	107.6	92.5	112.2
6056.00	4.73	-0.480	88.9	38.5	122.2	70.5	68.7	112.6	93.9	89.7	108.9
6065.48	2.61	-1.530	...	...	...	...	135.0	...	...	...	...
6078.49	4.79	-0.400	90.0	35.9	131.1	68.2	70.7	118.7	97.3	89.2	112.7
6093.64	4.61	-1.430	47.7	11.2	73.5	28.1	26.8	77.5	55.8	45.4	65.3
6096.67	3.98	-1.900	63.0	16.8	95.6	43.3	38.5	86.1	75.1	61.9	81.4
6098.24	4.56	-1.810	...	...	66.3	16.5	...	61.6	44.7	33.5	52.0
6120.25	0.92	-5.970	33.0	7.4	...	...	13.3	81.9	86.8	34.7	67.3
6151.62	2.18	-3.299	93.0	...	143.6	70.8	69.6	...	132.6	96.4	120.3
6173.34	2.22	-2.880	112.5	66.4	174.2	...	89.3	167.4	156.3	115.0	147.8
6187.99	3.94	-1.690	76.9	...	112.7	48.1	50.0	103.9	89.4	72.7	98.5
6240.65	2.22	-3.320	91.8	43.4	147.4	67.3	68.1	142.9	132.0	97.5	123.3
6246.32	3.60	-0.877	...	...	...	...	113.8	...	...	...	...
6252.56	2.40	-1.687	...	...	...	...	140.1	...	...	...	...
6301.50	3.65	-0.718	140.7	91.5	...	111.2	106.7	185.1	150.2	139.0	161.5
6302.49	3.69	-1.310	110.8	...	153.9	...	86.7	148.5	123.8	110.4	131.0
6322.69	2.59	-2.426	116.2	64.9	169.2	...	92.6	162.3	152.0	117.8	149.4
6392.54	2.28	-4.070	53.1	16.8	107.5	28.7	27.1	97.4	90.6	54.5	83.3
6393.60	2.43	-1.580	...	...	...	...	145.7	...	...	...	...
6481.87	2.28	-2.984	119.1	65.5	174.3	90.9	86.0	158.8	153.8	115.9	150.6
6518.37	2.83	-2.570	96.7	46.5	148.5	74.3	...	146.5	124.6	97.7	126.0
6574.23	0.99	-5.004	93.9	39.0	152.5	...	56.0	143.5	151.8	89.4	126.3
6593.87	2.43	-2.422	135.5	83.7	201.3	110.6	109.0	191.7	178.8	135.7	172.5
6677.99	2.69	-1.418	...	...	...	...	...	...	...	...	...
6703.57	2.76	-3.080	75.7	27.7	128.6	49.7	48.7	114.1	106.7	77.2	104.4
6725.36	4.10	-2.260	33.0	7.3	71.5	15.7	16.7	67.4	46.3	32.7	57.0
6726.67	4.61	-1.140	63.0	19.5	101.1	40.8	40.0	100.9	70.7	61.3	84.0
6842.69	4.64	-1.200	56.1	...	99.2	...	36.7	83.0	65.7	57.9	79.4
6857.25	4.08	-2.190	39.7	...	82.1	23.7	20.4	74.9	52.3	43.5	64.6
6858.15	4.61	-0.930	69.3	...	113.5	49.5	47.4	101.3	76.7	72.7	92.4
7114.55	2.69	-4.070	27.4	5.21	72.0	12.5	13.1	65.5	52.9	32.3	53.0
7421.56	4.64	-1.680	35.0	...	65.5	15.1	16.0	49.8	36.0	26.9	46.3
7531.15	4.37	-0.590	111.7	58.4	161.6	78.1	86.8	161.5	124.0	108.0	142.7
7547.90	5.10	-1.080	...	...	73.0	...	...	60.8	...	36.6	...
7723.21	2.28	-3.617	...	38.2	147.4	67.0	...	142.0	...	87.8	...
FeII											
5264.81	3.23	-3.130	58.5	34.8	62.3	55.6	64.4	...	53.4	56.4	64.1
5425.26	3.20	-3.220	59.8	33.6	62.6	53.2	57.4	...	48.1	...	56.6
5435.26	3.20	-3.220	...	...	...	...	...	63.3	...	...	...
6247.56	3.89	-2.300	65.1	34.8	66.0	55.5	64.1	68.3	45.5	62.4	61.5
6369.46	2.89	-4.110	34.7	...	...	27.4	30.2	39.2	31.0	32.4	35.5
6432.68	2.89	-3.570	59.0	32.1	61.8	53.9	...	62.0	...	58.4	...
6456.38	3.90	-2.050	76.5	47.1	68.3	72.5	80.0	79.7	56.6	71.4	74.5
6516.08	2.89	-3.310	74.7	41.8	78.7	71.1	...	68.3	65.0	71.3	...
[O I]											
6300.30	0.00	-9.720	36.0	20.0	45.5	37.0	25.4	28.4	60.0	49.0	28.0
6363.78	0.02	-10.190	15.6	9.0	...	13.5	11.5	...	29.0	13.1	14.8
NaI											
5682.64	2.10	-0.706	...	...	...	...	...	...	...	...	...
5688.20	2.10	-0.406	137.6	73.1	218.5	110.7	104.2	188.9	174.8	141.2	180.7
6154.23	2.10	-1.547	58.2	11.9	161.8	31.9	27.0	137.4	102.7	59.6	111.8
6160.75	2.10	-1.246	80.7	22.3	170.8	48.3	42.5	146.3	123.4	82.6	131.4
MgI											
4702.99	4.35	-0.471	...	...	...	...	220.0	...	...	...	...
4730.03	4.35	-2.389	...	...	...	...	65.9	...	...	...	...
5528.40	4.35	-0.522	...	...	...	...	205.0	...	...	...	...
5711.09	4.34	-1.729	128.4	81.5	172.4	112.8	105.3	168.4	148.0	132.2	154.4
6318.72	5.11	-1.945	53.3	18.5	93.0	39.8	49.5	97.4	66.3	61.7	92.4
6319.24	5.11	-2.165	42.1	13.4	72.0	26.0	26.4	69.2	44.4	40.1	71.0
6765.45	5.75	-2.000	17.3	...	40.6	11.2	11.0	64.5	23.2	16.0	...
6894.92	5.75	-1.620	...	...	...	26.7	...	...	36.5	39.0	65.0
7387.69	5.75	-1.070	75.5	32.1	...	66.0	...	120.9	...	68.9	...

Table 14 – continued

λ [Å] (1)	χ [eV] (2)	$\log gf$ (3)	HD117818 (4)	HD128188 (5)	HD132345 (6)	HD142948 (7)	HD171496 (8)	HD172223 (9)	HD174116 (10)	HD175219 (11)	HD186378 (12)
AlI											
6696.02	3.14	-1.481	64.6	20.0	122.8	56.0	36.4	109.6	97.5	61.6	100.5
6698.67	3.14	-1.782	38.6	13.7	112.0	27.0	20.4	95.6	72.8	34.8	79.6
SiI											
5488.98	5.61	-1.690	30.3	5.8	...	20.9	22.2	44.3	26.4	29.2	42.6
5701.10	4.93	-1.950	51.4	19.4	76.6	40.8	38.5	69.0	50.6	56.3	65.7
5772.15	5.08	-1.740	...	...	...	...	50.6	...	...	...	...
6142.48	5.62	-1.410	42.8	14.8	53.6	34.5	31.0	48.2	32.3	39.4	52.5
7235.33	5.62	-1.390	...	...	...	...	...	46.6	...	...	...
7235.82	5.62	-1.600	...	...	...	...	...	37.7	...	...	...
7250.63	5.62	-1.050	71.0	24.2	74.4	56.0	...	...	...	62.3	...
7423.50	5.62	-0.420	110.5	58.4	120.8	96.1	96.0	...	90.0	109.2	114.4
7800.00	6.18	-0.710	43.5	...	70.0	40.4	41.0	...	34.6	51.6	63.4
CaI											
5512.98	2.93	-0.464	102.9	60.9	162.6	83.2	79.5	139.6	130.0	102.4	130.2
5590.11	2.52	-0.571	116.2	73.7	156.7	104.7	96.6	150.0	144.2	116.4	138.0
5867.56	2.93	-1.570	42.0	12.0	74.6	25.6	22.9	83.8	69.1	45.2	71.4
6156.02	2.52	-2.420	21.2	...	68.5	15.8	...	52.8	47.2	22.1	49.3
6166.44	2.52	-1.142	97.0	48.3	143.4	76.2	73.6	138.9	129.0	97.2	126.8
6169.04	2.52	-0.797	117.6	70.8	195.6	94.8	93.9	179.4	155.5	122.3	154.8
6455.60	2.52	-1.340	86.6	39.3	152.5	61.4	66.0	139.6	123.5	83.8	126.0
6471.66	2.52	-0.686	123.6	77.7	178.1	104.0	100.8	168.1	160.8	124.1	155.5
6499.65	2.52	-0.818	117.9	73.8	191.8	100.2	94.2	173.6	152.1	121.7	155.0
TiI											
5020.03	0.84	-0.195	...	...	...	...	103.0	...	...	...	...
5024.84	0.82	-0.362	...	...	...	...	91.5	...	...	...	...
5210.39	0.05	-0.700	...	...	...	...	128.6	...	...	...	...
5453.64	1.44	-1.610	24.6	5.9	89.9	14.9	11.0	82.8	85.8	28.5	63.9
5460.47	0.05	-2.804	...	...	...	...	31.7	...	...	...	...
5648.57	2.50	-0.250	31.8	6.4	92.3	16.7	14.7	85.7	72.5	32.1	64.6
5739.46	2.25	-0.600	27.1	7.3	82.8	16.3	12.5	69.3	69.3	26.8	57.2
5913.71	0.02	-4.100	7.7	...	64.6	2.6	...	44.4	69.7	11.0	28.1
5918.54	1.07	-1.470	59.5	25.8	124.4	36.8	31.7	111.1	120.7	60.6	93.0
5944.65	0.00	-3.910	10.6	...	73.0	6.9	...	54.8	75.3	...	36.0
6092.80	1.89	-1.378	19.9	4.7	78.7	...	...	58.0	63.7	20.4	45.7
6258.10	1.44	-0.355	...	...	...	...	72.8	...	...	...	...
6261.10	1.43	-0.479	...	...	...	...	70.0	...	...	...	...
6273.39	0.02	-4.170	5.8	...	52.0	...	...	43.4	59.2	7.2	22.6
6706.29	1.50	-2.780	2.1	...	20.0	...	...	18.6	13.8	3.9	7.0
6716.71	2.49	-1.010	8.4	...	44.5	...	...	34.3	30.8	7.5	24.4
6746.31	1.89	-2.000	5.5	...	40.4	...	...	32.9	24.3	8.5	17.5
7138.08	1.43	-2.760	2.6	...	30.9	...	...	26.1	25.0	4.7	12.0
7352.16	2.49	-0.980	9.2	...	15.1	7.2	...	42.7	32.5	...	26.2
7391.52	1.50	-2.610	...	...	39.2	...	...	22.6	...	...	...

Table 15. Line list and measured equivalent widths given in mÅ

λ [Å] (1)	χ [eV] (2)	$\log gf$ (3)	HD187195 (4)	HD211075 (5)	HD212320 (6)	HD214376 (7)	HD215030 (8)	HD221148 (9)
FeI								
5560.21	4.43	-1.120	89.6	74.0	70.0	84.4	61.3	82.9
5633.95	4.99	-0.180	107.3	85.4	88.2	99.5	72.1	90.9
5638.26	4.22	-0.800	121.2	109.8	103.3	121.8	87.7	...
5651.47	4.47	-1.850	58.7	40.0	32.0	51.0	24.5	51.7
5662.52	4.18	-0.573	139.2	123.2	117.9	135.0	98.1	139.4
5679.02	4.65	-0.810	87.9	79.6	74.9	89.8	62.4	89.9
5731.76	4.26	-1.110	103.5	89.0	86.8	101.6	70.1	95.7
5775.08	4.22	-1.230	104.6	90.1	...	100.2	67.6	94.7
5778.45	2.59	-3.430	91.4	78.4	...	87.1	47.7	83.1
5811.91	4.14	-2.440	41.8	30.5	...	40.4	19.5	42.3
5853.15	1.49	-5.260	74.8	67.0	30.0	67.8	35.9	63.5
5902.47	4.59	-1.880	...	28.2	21.4	41.8	16.8	44.3
5916.25	2.45	-2.994	131.4	121.6	91.2	130.2	90.8	112.0
5956.69	0.86	-4.608	147.7	155.1	...	143.6	104.7	121.1
6027.05	4.08	-1.089	112.7	100.4	94.0	111.3	81.3	...
6056.00	4.73	-0.480	107.8	89.3	91.0	108.0	76.3	104.5
6065.48	2.61	-1.530	...	...	...	...	...	...
6078.49	4.79	-0.400	112.2	92.7	96.9	110.1	75.8	105.2
6093.64	4.61	-1.430	68.0	53.1	49.7	63.4	39.7	64.0
6096.67	3.98	-1.900	79.5	73.4	59.8	81.5	52.0	81.1
6098.24	4.56	-1.810	...	42.4	...	50.2	25.2	51.9
6120.25	0.92	-5.970	76.9	71.9	27.7	69.6	30.6	61.6
6151.62	2.18	-3.299	127.5	121.4	...	117.6	84.1	105.2
6173.34	2.22	-2.880	154.2	140.4	115.9	149.3	102.7	121.9
6187.99	3.94	-1.690	99.3	84.6	78.1	96.5	62.7	96.3
6240.65	2.22	-3.320	122.8	119.3	93.0	122.1	77.9	109.6
6246.32	3.60	-0.877	...	...	...	...	...	...
6252.56	2.40	-1.687	...	...	...	...	...	...
6301.50	3.65	-0.718	174.6	...	...	...	...	...
6302.49	3.69	-1.310	134.2	121.6	...	134.8	92.3	...
6322.69	2.59	-2.426	150.7	142.0	118.1	153.7	107.1	143.0
6392.54	2.28	-4.070	84.7	78.2	50.9	81.9	48.5	75.6
6393.60	2.43	-1.580	...	...	...	...	...	...
6481.87	2.28	-2.984	143.4	133.2	107.9	132.1	104.8	123.8
6518.37	2.83	-2.570	126.6	114.6	94.5	118.6	85.4	107.7
6574.23	0.99	-5.004	127.8	131.0	82.9	123.2	81.7	107.1
6593.87	2.43	-2.422	175.5	163.4	135.9	165.6	118.1	145.7
6677.99	2.69	-1.418	...	...	...	...	...	...
6703.57	2.76	-3.080	105.6	93.5	...	99.4	68.1	90.5
6725.36	4.10	-2.260	60.1	42.9	33.0	56.0	25.3	55.0
6726.67	4.61	-1.140	83.3	69.8	61.6	84.8	52.4	84.0
6842.69	4.64	-1.200	81.8	66.1	60.7	78.8	...	74.4
6857.25	4.08	-2.190	68.4	47.8	41.1	62.3	...	61.2
6858.15	4.61	-0.930	93.2	73.8	82.4	89.7	...	86.7
7114.55	2.69	-4.070	57.3	...	27.7	...	...	...
7421.56	4.64	-1.680	...	...	30.2	...	...	...
7531.15	4.37	-0.590	145.8	...	114.3	...	...	...
7547.90	5.10	-1.080	60.4	...	35.6	...	...	...
7723.21	2.28	-3.617	128.1	...	82.9	...	...	...
FeII								
5264.81	3.23	-3.130	46.9	...	74.9	...	52.4	...
5425.26	3.20	-3.220	...	...	65.6	...	44.2	...
5435.26	3.20	-3.220	46.2	...	...	...	...	...
6247.56	3.89	-2.300	45.8	48.5	73.5	57.9	47.2	46.1
6369.46	2.89	-4.110	26.6	28.0	38.4	36.8	23.5	26.4
6432.68	2.89	-3.570	49.0	54.1	69.5	63.3	47.1	50.0
6456.38	3.90	-2.050	59.0	60.3	94.2	70.7	57.6	59.6
6516.08	2.89	-3.310	...	57.4	85.6	75.0	...	...
[O I]								
6300.30	0.00	-9.720	59.0	54.6	22.0	33.0	18.5	15.5
6363.78	0.02	-10.190	15.0	30.0	...	19.0	12.5	...
NaI								
5682.64	2.10	-0.706	...	127.0	142.2	132.4	119.2	152.6
5688.20	2.10	-0.406	185.6	149.3	148.7	173.7	122.2	204.2
6154.23	2.10	-1.547	132.9	79.6	74.6	78.7	53.6	117.6
6160.75	2.10	-1.246	144.6	99.3	92.2	120.0	73.7	154.5
MgI								
4702.99	4.35	-0.471	...	...	...	...	...	...
4730.03	4.35	-2.389	...	...	...	281.3	...	...
5711.09	4.34	-1.729	163.3	148.9	129.2	158.6	114.5	156.8
6318.72	5.11	-1.945	105.0	70.4	60.0	84.2	50.2	91.2
6319.24	5.11	-2.165	78.6	57.7	40.6	71.7	34.9	66.4
6765.45	5.75	-2.000	29.9	25.0	...	28.3	13.0	...
6894.92	5.75	-1.620	69.5	...	37.5	...	...	...
7387.69	5.75	-1.070	107.0	...	70.2	...	...	...
AlI								

Table 15 – continued

λ [Å] (1)	χ [eV] (2)	$\log gf$ (3)	HD187195 (4)	HD211075 (5)	HD212320 (6)	HD214376 (7)	HD215030 (8)	HD221148 (9)
6696.02	3.14	-1.481	113.1	91.0	51.7	98.9	53.4	116.4
6698.67	3.14	-1.782	98.9	63.2	40.3	72.8	34.7	88.1
SiI								
5488.98	5.61	-1.690	50.6	31.9	33.9	41.5	25.1	46.9
5701.10	4.93	-1.950	67.4	57.4	56.4	66.0	41.6	67.5
5772.15	5.08	-1.740	...	...	...	...	...	...
6142.48	5.62	-1.410	42.8	33.5	46.5	50.9	31.8	50.5
7235.33	5.62	-1.390	60.3	...	...	...	...	...
7235.82	5.62	-1.600	...	...	40.7	...	...	...
7250.63	5.62	-1.050	...	...	...	...	...	...
7423.50	5.62	-0.420	104.5	...	112.4	...	...	...
7800.00	6.18	-0.710	53.2	...	57.2	...	...	...
CaI								
5512.98	2.93	-0.464	142.2	120.7	111.4	132.7	97.3	142.4
5590.11	2.52	-0.571	145.4	136.4	113.4	133.2	108.8	136.0
5867.56	2.93	-1.570	80.1	63.1	35.0	65.4	38.7	78.2
6156.02	2.52	-2.420	61.3	42.4	18.3	45.1	20.5	54.2
6166.44	2.52	-1.142	134.3	123.2	101.3	123.8	89.3	131.8
6169.04	2.52	-0.797	174.8	145.7	124.2	155.4	107.9	158.2
6455.60	2.52	-1.340	131.5	111.3	93.2	123.4	79.7	...
6471.66	2.52	-0.686	163.4	147.0	120.9	149.8	113.2	155.4
6499.65	2.52	-0.818	162.7	141.1	124.3	152.7	106.6	159.1
TiI								
5020.03	0.84	-0.195	...	...	...	...	...	...
5024.84	0.82	-0.362	...	...	...	...	...	...
5210.39	0.05	-0.700	...	...	...	...	...	...
5453.64	1.44	-1.610	88.8	72.7	20.3	62.9	25.2	68.8
5460.47	0.05	-2.804	...	...	...	100.0	...	...
5648.57	2.50	-0.250	84.4	65.5	25.4	61.6	27.9	67.6
5739.46	2.25	-0.600	70.5	59.7	18.4	57.7	23.5	62.9
5913.71	0.02	-4.100	51.3	...	...	...	...	...
5918.54	1.07	-1.470	120.7	105.9	34.9	95.3	68.4	92.2
5944.65	0.00	-3.910	62.8	53.3	6.6	37.0	...	...
6092.80	1.89	-1.378	63.4	52.8	14.7	47.4	17.5	55.2
6258.10	1.44	-0.355	...	151.4	...	139.3	...	133.8
6261.10	1.43	-0.479	...	...	...	...	...	118.6
6273.39	0.02	-4.170	43.4	...	...	...	...	...
6706.29	1.50	-2.780	15.0	...	...	...	...	...
6716.71	2.49	-1.010	37.6	26.4	...	25.9	...	32.7
6746.31	1.89	-2.000	32.9	...	...	...	...	...
7138.08	1.43	-2.760	23.6	...	...	...	...	...
7352.16	2.49	-0.980	38.3	...	8.5	...	...	...
7391.52	1.50	-2.610	34.1	...	...	...	...	...